



MINISTRY OF EDUCATION & RESEARCH

National University of Science & Technology POLITEHNICA Bucharest

PhD School Biotechnical Engineering Systems

Eng. Andrei VASILE

ABSTRACT Ph.D. THESIS

Scientific Coordinator:

Prof. Habil. PhD Eng. Mihai BUGARU (NUSTPB)

2023

National University of Science & Technology POLITEHNICA Bucharest

PhD School Biotechnical Engineering Systems

ABSTRACT-Ph.D. Thesis

**THE INVESTIGATION OF THE DYNAMIC BEHAVIOR OF
THE AUTOMOTIVE DRIVESHAFTS**

Scientific Coordinator:

Prof. Habil. PhD Eng. Mihai BUGARU

Ph.D. Student:

Eng. Andrei VASILE

BUCHAREST

2023

Content

Chapter 1. State of Art for theoretical research concerning the dynamic behavior of automotive driveshafts	4
Chapter 2. Isometric Nonuniformity of Automotive Driveshafts.....	7
Chapter 3. Models of Forced Torsion Vibrations of Automotive Driveshafts.....	15
Chapter 4. Models of Forced Bending Vibrations of Automotive Driveshafts.....	27
Chapter 5. Chaotic manifestation of the automotive driveshaft’s forced bending vibrations.....	43
Chapter 6. Final conclusions. Contributions. Future directions of research.....	55
6.1 Final conclusions.....	55
6.2 Contributions.....	55
6.3 Future directions of research.....	56
References.....	57

Chapter 1. State of Art for theoretical research concerning the dynamic behavior of automotive driveshafts

The First Chapter investigates The State of Art for theoretical research concerning the automotive driveshaft's dynamic behavior based on the references [B.G.1- B.G.16], [B.C.1- B.C.14], dealing with the following aspects:

1. Defining the concept Constant Velocity Joints(CVJ) for the automotive driveshafts that are homokinetic-shafts,
2. kinematic of the automotive driveshaft's polypore
3. computation of the input automotive driveshafts.

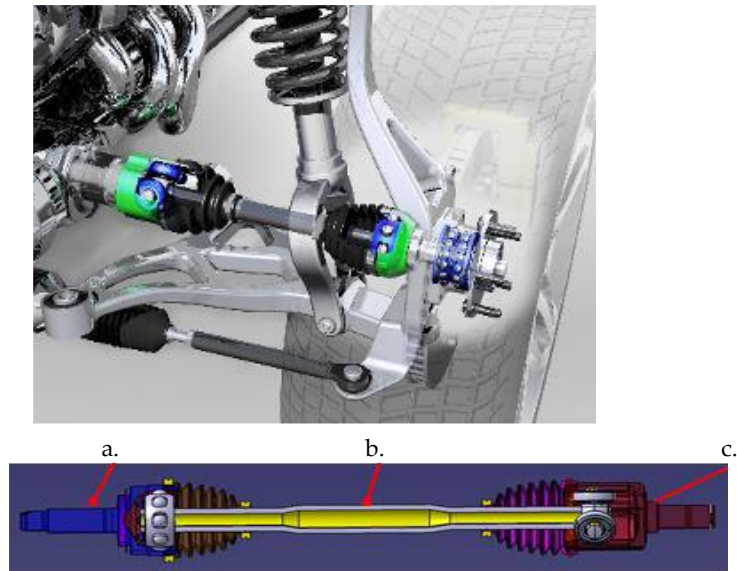


Fig. 1.1 An automotive driveshaft [R.C.1.1].

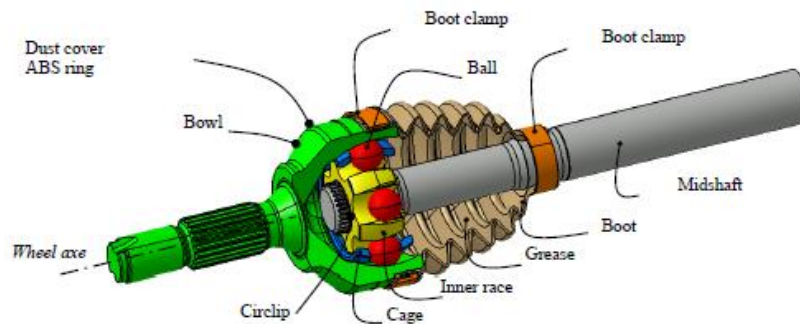


Fig. 1.2 Details of the bowl–balls (inner race of the midshaft) joint [R.C.1.1].

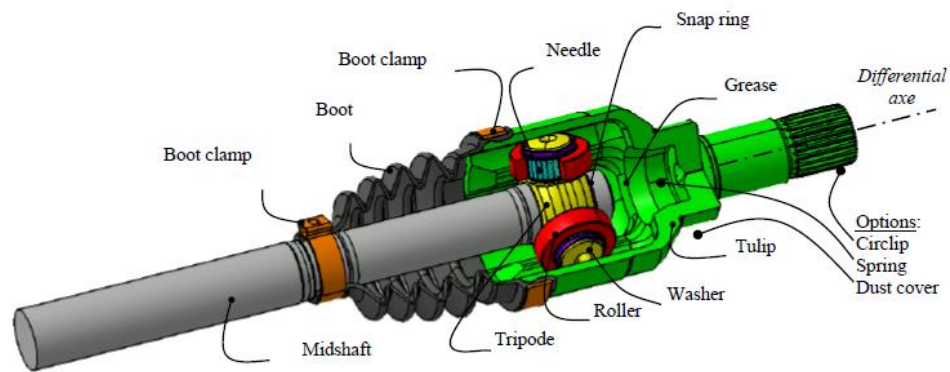


Fig. 1.3 Details of tulip–tripod (tripod of the midshaft) joint [R.C.1.1].

The Ph.D. thesis contains six chapters:

- Chapter 1. State of Art for theoretical research concerning the dynamic behavior of automotive driveshafts;
- Chapter 2. Isometric Nonuniformity of automotive;
- Chapter 3. Models of forced torsion vibrations of automotive driveshafts;
- Chapter 4. Models of forced bending vibrations of automotive driveshafts;
- Chapter 5. Chaotic manifestation of the automotive driveshaft’s forced bending vibrations;
- Chapter 6. Final conclusions. Contributions. Future directions of research.

Chapter 2 investigates the geometric and kinematic isometric nonuniformities of prezintă automotive driveshafts.

The aim of Chapter 3 is to design a physical consistent model for automotive driveshaft’s forced torsion vibrations that takes into account the next aspects:

- the harmonic excitation induced by the combustion through the geared system transmission,
- impulsive excitation induced by the road geometry,
- quasi-isometry of automotive driveshafts,
- nonuniformity of axial mass moments of inertia and axial geometric moments of inertia regarding the longitudinal axis of the tripod joint and the bowl-inner race joint,
- rigidity and damping of each joint.

Chapter 4 illustrates the use of the asymptotic method (AM) [B.C.4.1], to investigate the principal parametric resonance for forced bending vibrations of automotive driveshafts.

Chapter 5 investigates the chaotic manifestation of the automotive driveshaft’s forced bending vibrations. To detect the chaotic manifestation of the automotive driveshaft’s forced bending vibrations it was used the time-history analyses of the phase portraits for the automotive driveshaft’s forced bending vibrations in the region of the principal parametric resonance. To confirm this type of manifestation in the principal parametric resonance region it was used the Maximum Lyapunov Exponents (MLEM). To reconfirm the chaotic manifestation of the

automotive driveshaft's forced bending vibrations, was employed the Method Poincaré Maps, that is a qualitative method that certifies the deterministic chaos. In this way was created a powerful tool to investigate the chaotic vibrations generated by bending, in the principal parametric resonance area (PPRA).

Chapter 6 illustrates the Final conclusions, the original contributions, and the future directions of research.

Chapter 2. Isometric Nonuniformity of Automotive Driveshafts

The constant velocity joints (CVJs) for automotive driveshafts are special mechanisms that transmit the load torque by angular rotation from the gearbox to the wheels of a car as can be seen in Figure 1.1. For a better understanding, let us look inside the components of such a mechanism by looking at Figure 1.1, which consists of (a) the bowl-balls joint fixed assembled by the car wheel, (b) the midshaft axis; (c) the tulip–tripod joint that allows for axial plunging of the tripod in the tulip and the plunging assembled in the gearbox.

The first researchers who considered special phenomena for driveshafts were Mazzei and Scott, who enhanced the nonlinear parametric dynamic behavior of universal joints in [G.R.12]. The experimental evidence on the nonuniformity of CVJ driveshaft transmissions is presented and highlighted by Browne and Palazzolo in the paper [G.R.13]. But the most important experimental research on the nonuniformity of geometric and kinematic isometry of CVJ driveshafts was carried out by Steinwede during his PhD thesis [G.R.5] (pp. 68–97); thus, after 45 years, it was finally proven through experimental data that Dudita and Diaconescu were right, that CVJ driveshafts are quasi-homokinetic, and all the designed patents and design flow charts used in the automotive industry concerning CVJ driveshafts must be modified and corrected as already was mentioned in [G.R.5] (p. 78). This paper highlights this nonuniformity from the isometry of geometry and kinematics for CVJ automotive driveshafts.

The first to introduce the concept of a CVJ was Metzner, in 1967, who is mentioned in the literature [4] as the creator of the first indirect method (FIM) for proving constant velocity for special Hooke joints [G.R.7], based on the idea that “the generators of a constant velocity joint must be mirror images in space” [G.R.7] (p. 61). Figure 2.3 highlights the functioning through a flow chart of a CVJ automotive driveshaft.

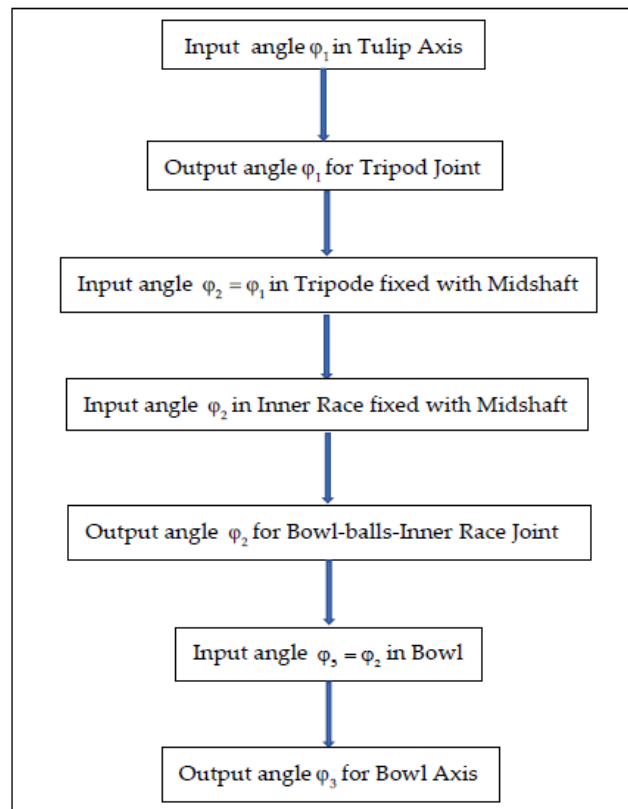


Fig. 2.3 Flow chart of a CVJ driveshaft [G.R.18].

Presented in detail in Figure 2.4 is a tripod that consists of three pods equally fixed inclined, with respect to the midshaft of the automotive driveshaft with the fixed angles, Ψ_i :

$$\Psi_i = \frac{2\pi(i-1)}{\delta}, i = 1, 2, 3 \quad (2.1)$$



Fig. 2.4. Tulip–tripode joint [G.R.18]

Figure 2.5, presents a schematic representation of an automotive drive shaft in three Cartesian systems with the coordinates X_1, Y_1, Z_1 attached to the tulip, X_2, Y_2, Z_2 attached to the midshaft, and X_3, Y_3, Z_3 attached to the bowl, having the next rigid movements:

- rotation with the angle φ_1 of the tulip with respect to the X_1 , $\varphi_1 = 0 \dots n_1\pi$,
- rotation with the angle φ_2 of the midshaft with respect to the X_2 , $\varphi_2 = 0 \dots n_2\pi$,
- rotation with the angle φ_3 of the bowl with respect to the X_3 , $\varphi_3 = 0 \dots n_3\pi$,
- relative rotation of the longitudinal axe of the midshaft (given by the direction of the axis X_2) with respect to the longitudinal direction of the tulip (given by the direction of the axis X_1), with β_1 (spatial angle between axis X_1 and X_2) with respect to the axis Z_1 , β_1 being the angle between longitudinal direction of the tulip and the longitudinal direction of the midshaft, $\beta_1 = 0^\circ \dots 15^\circ$,
- relative rotation of the longitudinal axis of the bowl (given by the direction of the axis X_3) with respect to the longitudinal direction of the midshaft (given by the direction of the axis X_2), with β_2 (spatial angle between axis X_2 and X_3) with respect to the axis Y_2 , β_2 being the angle between the longitudinal direction of the midshaft and the longitudinal direction of the bowl, $\beta_2 = 0^\circ \dots 47^\circ$.

Using all these notations, Orain proved, in 1976, using the second direct method [G.R.11] that the polypod joints, the tripod joints, are isometric joints from the kinematic and dynamic points of view, the kinematic point of view being expressed by the relations:

$$\tan\varphi_2 \cot\varphi_1 = 1 \quad (2.2)$$

$$\tan\varphi_2 = \tan\varphi_1 \quad (2.3)$$

$$\varphi_1 = \varphi_2 \quad (2.4)$$

It means the tripod joint that is a tulip–tripode joint is a CVJ, but, in 1975, Dudita and Diaconescu [G.R.1] proved that the tripod joint is quasi-isometric, a fact that was only recognized by researchers in the field [G.R.7] (p. 78) until 2006. At that time, in the nineteen-seventies, it was considered that a nonuniformity from a kinematic isometry of the tripod joints of 5–7% was acceptable; now, when an improvement of 1% is a huge gain in the automotive industry, and is

it is no longer acceptable. Thus, the homokinetic transmission of the driveshafts is, in fact, quasi-homokinetic; therefore, for the early stages of design in the automotive industry, it is necessary to express and evaluate the kinematic and geometric isometric nonuniformities of the driveshafts as well as their implications in the dynamic behavior of the transmission. In addition, the bowl-ball joint has not proven to be a CVJ.

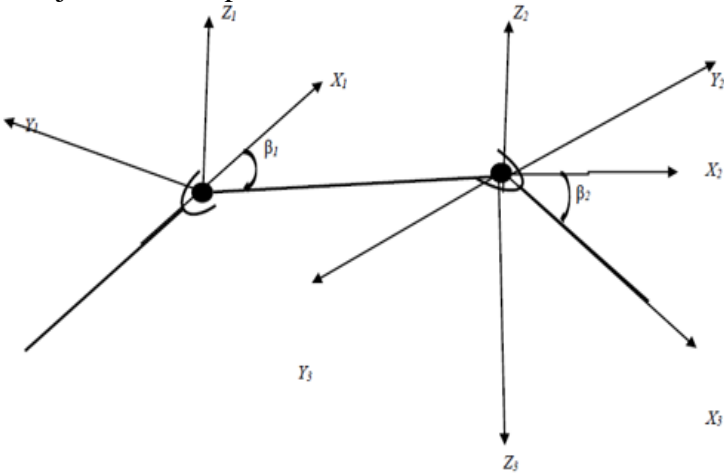


Fig. 2.5 - Schematic representation of an automotive driveshaft using 3 cartesian systems of coordinates [G.R.1].

Let us consider a general cross Hooke joint as presented in Figure 2.6, where the driving element is S_1 , having attached to the cartesian system $R_1(OX_1, Y_1, Z_1)$, the driven element is S_2 , having attached the cartesian system $R_2(OX_2, Y_2, Z_2)$; the cross joint is $A'OA-B'OB$, having the angle $\sphericalangle AOB = \delta$, the driving input angle is ϕ_1 , the driven output angle is ϕ_2 , and the angle between the longitudinal direction of the input element S_1 and the longitudinal direction of output element S_2 is θ .

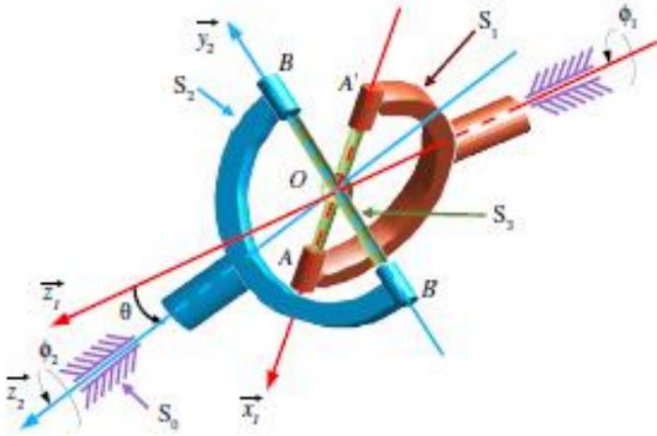


Fig. 2.6 A general cross Hooke joint [G.R.1]

We can consider three-unit vectors $\vec{e}_n, \vec{e}_v, \vec{e}_w$ so that we have the relations

$$\vec{e}_n \times \vec{e}_v = \vec{e}_{z_1} \tag{2.5}$$

$$\vec{e}_n \times \vec{e}_w = \vec{e}_{z_2} \tag{2.6}$$

that yield to express the unit vectors of \overline{OA} and \overline{OB} as:

:

$$\vec{e}_{x_1} = \cos \phi_1 \vec{e}_n + \sin \phi_1 \vec{e}_v, \quad (2.7)$$

$$\vec{e}_{y_2} = -\sin \phi_2 \vec{e}_n + \cos \phi_2 \vec{e}_w = -\sin \phi_2 \vec{e}_n + \cos \phi_2 (\cos \theta \vec{e}_v + \sin \theta \vec{e}_{z_1}). \quad (2.8)$$

Based on Equations (2.7) and (2.8) yields:

$$\vec{e}_{x_1} \cdot \vec{e}_{y_2} = \cos \delta \Rightarrow -\cos \phi_1 \sin \phi_2 + \sin \phi_1 \cos \phi_2 \cos \theta = \cos \delta \quad (2.9)$$

The most common number of balls for a bowl-balls joint is six, so using Equation (2.10) for the bowl-balls joint (see Figures 2.7 and 2.8), putting $\phi_2 = \phi_1$, $\phi_3 = \phi_2$, $\beta_2 = \theta$, and $\psi_i = \delta$,

$i = 1, 2, 3, \dots, i_{max}$ for Ψ_i given by the relation:

$$\psi_i = \frac{2\pi(i-1)}{i_{max}}, i = 1, 2, 3, \dots, i_{max} \quad (2.10)$$

where i_{max} is the numbers of balls of the bowl-balls joint that must be multiples of 3 (condition of homokinetic driveshaft joint).



Fig. 2.7 Picture of a bowl-balls joint [G.R.18]

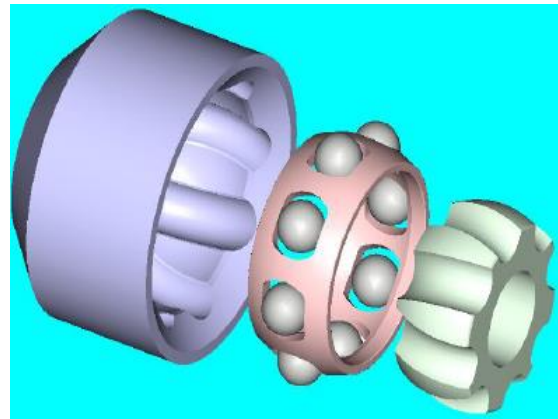


Fig. 2.8 Components of the bowl-balls joint [G.R.18]

The relations that express the nonuniformity of the kinematic isometry of driveshafts can be obtained from the general formulation found by Dudita and Diaconescu [G.R.1] for an input driving shaft with ϕ_1 rigid rotation angle and an output-driven shaft with a rigid rotation angle are

$$\phi_2 = \phi_1 + \frac{r}{2l} \tan \beta \tan^2 \frac{\beta}{2} \cos(3\phi_1), \quad (2.1)$$

where r is the radius of the joint, l is the length of the driven shaft, and β is the angle between the longitudinal directions of the two shafts. With the signification of the terms mentioned before yields:

- for the tulip–tripode joint:

$$\phi_2 = \phi_1 + \frac{r_1}{2l} \tan \beta_1 \tan^2 \frac{\beta_1}{2} \cos(3\phi_1), \quad (2.2)$$

- for the bowl-balls joint

$$\varphi_3 = \varphi_2 + \frac{r_2}{2l} \tan \beta_2 \tan^2 \frac{\beta_2}{2} \cos(3\varphi_2), \quad (2.3)$$

where r_1 is the tulip radius, r_2 is the bowl radius, and l is the length of the midshaft. After injecting the relation (2.20) in (2.21) yields:

$$\varphi_3 = \varphi_1 + \frac{r_1}{2l} \tan \beta_1 \tan^2 \frac{\beta_1}{2} \cos(3\varphi_1) + \frac{r_2}{2l} \tan \beta_2 \tan^2 \frac{\beta_2}{2} \cos \left(3\varphi_1 + 1.5 \frac{r_1}{l} \tan \beta_1 \tan^2 \frac{\beta_1}{2} \cos(3\varphi_1) \right) \quad (2.22)$$

And the dependance of the angular speed of the bowl with respect to the angular speed of the tulip is:

$$\dot{\varphi}_3 = \dot{\varphi}_1 - 1,5 \dot{\varphi}_1 \frac{r_1}{l} \tan \beta_1 \tan^2 \frac{\beta_1}{2} \sin(3\varphi_1) - 1,5 \dot{\varphi}_1 \frac{r_2}{2l} \tan \beta_2 \tan^2 \frac{\beta_2}{2} \sin \left(3\varphi_1 + 1,5 \frac{r_1}{l} \tan \beta_1 \tan^2 \frac{\beta_1}{2} \cos(3\varphi_1) \right) \cdot \left(3 - 4,5 \frac{r_1}{l} \tan \beta_1 \tan^2 \frac{\beta_1}{2} \sin(3\varphi_1) \right) \quad (2.23)$$

Figure 9 presents a flow chart of a quasi-isometric CVJ automotive driveshaft.

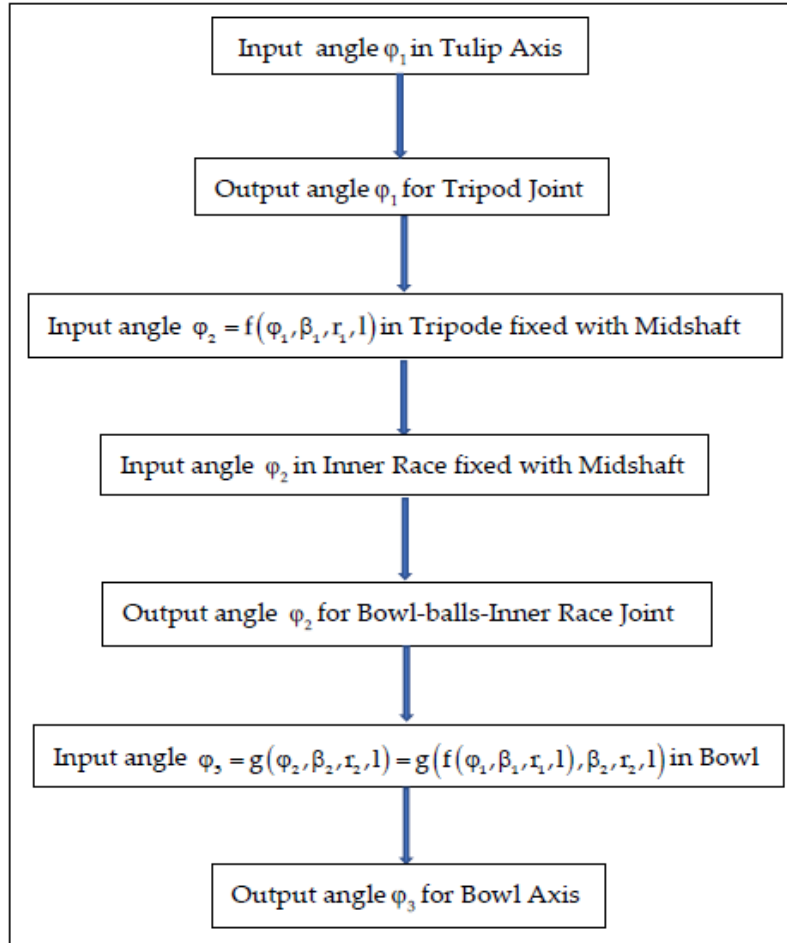


Fig. 2.9 Flow chart of a quasi-isometric CVJ automotive driveshaft [G.R.18]

Based on relation (2.22), the software in MATLAB was used to compute the geometric nonuniformity of the geometric isometry for the driveshaft $\Delta\varphi = \varphi_3 - \varphi_1 = \Gamma_1(\varphi_1, \beta_1, \beta_2)$ as a function of β_1 , β_2 and φ_1 as can be seen in Figures 2.10 and 2.11.

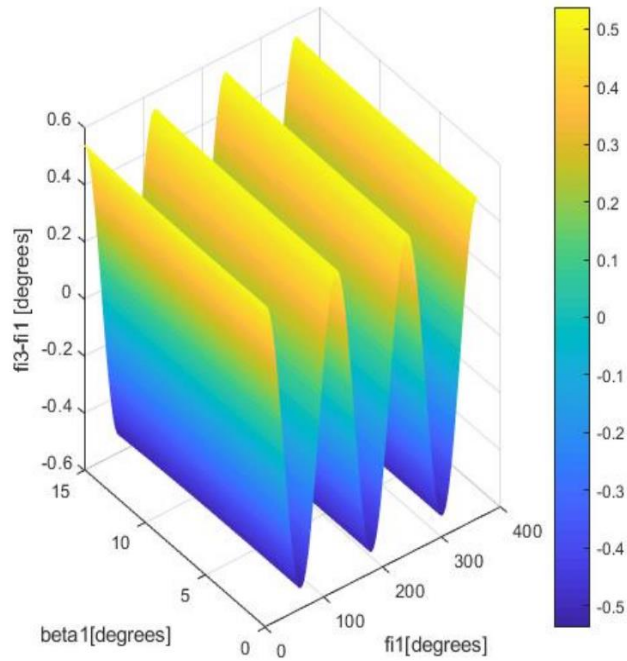


Fig. 2.10 Geometrical nonuniformity of isometry for automotive driveshaft for $r_1 / l = 0,11$, $r_2 / l = 0,09$, $\beta_1 = 0 \dots 15^\circ$ [G.R.18].

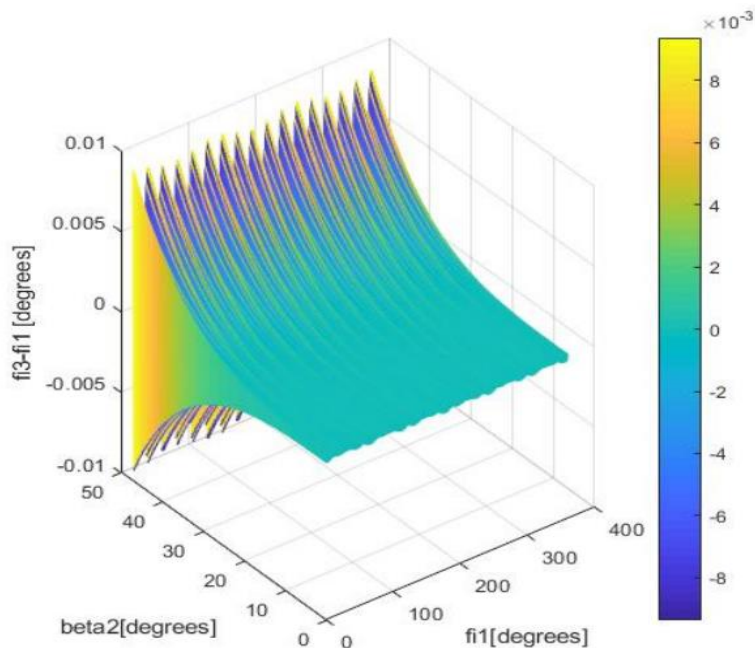


Fig. 2.11 Geometrical nonuniformity of isometry for automotive driveshaft for $r_1 / l = 0,11$, $r_2 / l = 0,09$, $\beta_2 = 0 \dots 47^\circ$ [G.R.18].

Analyzing these figures, it can be concluded that the geometric nonuniformity of isometry was in the range $\pm 0.009^\circ$ being maximum when β_2 has the maximum value of 47° . Comparing these results with the experimental data in the literature [G.R.4] (pp. 70–71), it can be remarked that it had close agreement. In addition, Steinwede in [G.R.4] (pp. 88–94) experimentally demonstrated that this geometric nonuniformity of isometry for a driveshaft is the principal cause of premature pitting on the flanks of the tripod, on the internal flanks of the tulip, on the balls of the bowl-inner race joint, and on the internal flanks of the bowl due to the insufficient

design for controlling Hertzian contact with respect to phenomena that involves geometric nonuniformity of isometry involving the driveshaft. Using relation (2.23), software in MATLAB was developed to compute the kinematic nonuniformity of isometry for the driveshaft $\dot{\varphi}_3 / \dot{\varphi}_1 = f(\varphi_1, \beta_1, \beta_2)$ as a function of β_1, β_2 , as can be seen in Figures 2.12 and 2.13.

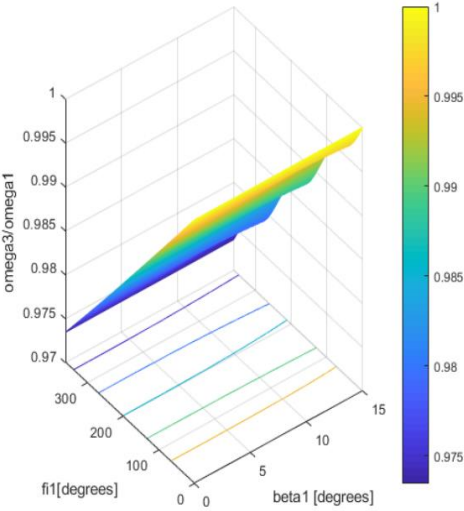


Fig. 2.12 Kinematic nonuniformity of isometry for automotive driveshaft for $r_1 / l = 0,11, r_2 / l = 0,09, \beta_1 = 0..15^\circ$ [G.R.18]

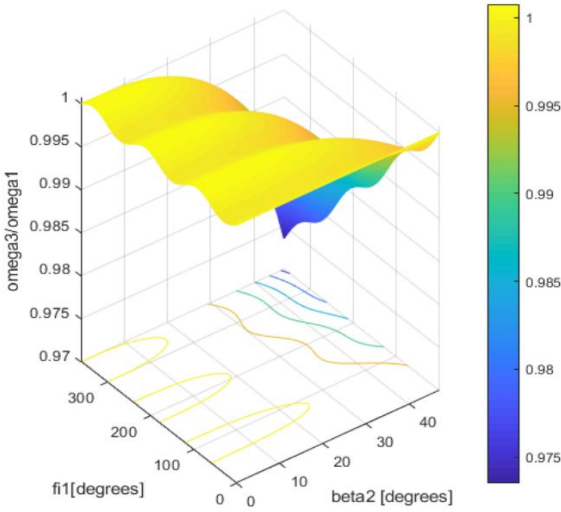


Fig. 2.13 Kinematic nonuniformity of isometry for automotive driveshaft for $r_1 / l = 0,11, r_2 / l = 0,09, \beta_2 = 0.. 47^\circ$ [G.R.18]

Analyzing Figure 2.12, it can be remarked that the kinematic nonuniformity of the isometry for the driveshaft, when $\beta_2 = 47^\circ$ and β_1 is in the range $0-15^\circ$, is in the range $(-0.027, 0)$, having maximum absolute values for $\varphi_1 = 93^\circ, 213^\circ,$ and 325° , while the minimum absolute values were obtained for $\varphi_1 = 33^\circ, 151^\circ,$ and 271° . Regarding Figure 2.13 it can be concluded that that the kinematic nonuniformity of the isometry for the driveshaft, when $\beta_1 = 15^\circ$ and β_2 is in the range $0-47^\circ$, was in the field $(-0.024, 0.001)$ having maximum value for $\varphi_1 = 76^\circ, 190^\circ,$ and 316° while the minimum values were obtained for $\varphi_1 = 31^\circ, 169^\circ,$ and 258° .

In Figure 2.14, the geometric nonuniformity isometry for the driveshaft $\Delta\varphi = \varphi_3 - \varphi_1 = g_1(\beta_1, \beta_2)$ as a function of β_1 and β_2 , being variables, and $\varphi_1 = 243^\circ$. As can be remarked from Figure 2.14, the geometric nonuniformity isometry for the driveshaft was maximum for $\beta_2 = 47^\circ$ regardless of the variation in β_1 in the range $0-15^\circ$. From the perspective of the last simulation concerning the geometric nonuniformity isometry for the driveshaft, it can be concluded a great sensitivity for the maximum angle β_2 of the longitudinal direction of the bowl with respect to the midshaft longitudinal direction. From the design point of view, this aspect involved a sensitivity to shocks received from the wheel of the driveshafts even if the value of nonuniformity was very small.

In addition, analyzing Figures 2.10–2.13, the harmonic fluctuation of the nonuniformity from the geometric and kinematic isometry of the automotive driveshaft can be highlighted. This is a challenge for the driveshaft’s designers because of the difficulty of predicting the supplementary quantities for the fatigue solicitations. Moreover, the harmonic fluctuation of the nonuniformity from geometric and kinematic isometry of the automotive driveshaft induces the nonlinear parametric dynamic behavior of a CVJ as mentioned in [G.R.12]. All these geometric and kinematic nonuniformities from the isometry of automotive driveshafts must be considered in the design patents for automotive driveshafts such as in [B.C.2.4 - B.C.2.7]. These aspects of considering the automotive driveshafts as quasi-isometric (isometry with nonuniformity) CVJ (homokinetic) transmissions allow for the development of future research in torsional forced vibrations and the bending–shearing vibrations of automotive driveshafts.

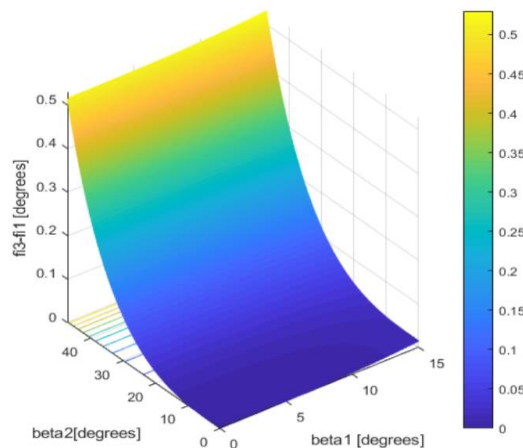


Fig. 2.14 Geometrical nonuniformity of isometry for automotive driveshaft for $r_1 / l = 0,11$, $r_2 / l = 0,09$, $\varphi_1 = \text{const.} = 243^\circ$ [G.R.18]

The prediction of geometric and kinematic isometry nonuniformity of the driveshaft represent a powerful tool for designers because it allows for prediction in the early design stages of the automotive driveshaft, the prediction of resonances such as super harmonic resonance, subharmonic resonance, principal parametric resonance, combination resonances, simultaneous resonances, and internal resonances. Also, this aspect allows the investigation of stability in these specific resonances ranges for the nonlinear parametric dynamic behavior of the automotive driveshaft as mentioned in [G.R.12].

Chapter 3. Models of Forced Torsion Vibrations of Automotive Driveshafts

The present chapter presents a consistent model to describe the forced torsional vibrations for an automotive driveshaft considering the next aspects: the joints of the driveshaft are quasi-isometric for the angular velocity[G.R.18], even if generally it is considered as CVJ (Constant Velocity Joint), the effect of induced torsional loads as the harmonic entry moment from the gear box[R.C.1](p. 360) and the impulsive reaction moment from the wheel[G.R. 17], the effect of nonuniformity for the axial moment of inertia of the joints that vary with the angle of twist of each element of the driveshaft and the effect of the torsional rigidity as well as the torsional damping for each joint of the driveshaft that vary with the angle of twist of each element of the driveshaft.

In literature [G.R.18] the nonuniformity of isometric properties for automotive driveshaft is already a recognized fact, being a reality demonstrated by experiments by Steinwede in his PhD thesis[G.R.,14](pp. 68-97) after half a century. This nonuniformity of isometric properties of the driveshaft is the main cause of nonlinear parametric vibrations of the driveshafts in the range (0.1 kHz...12 kHz) of the driveshafts as mentioned with no doubt by the experimental results in the literature [G.R.,14] (pp. 98-123). The first researchers who considered special phenomena for driveshafts were Mazzei and Scott, who enhanced the nonlinear parametric dynamic behavior of universal joints in [G.R.12]. The experimental evidence on the nonuniformity of CVJ driveshaft transmissions is presented and highlighted by Browne and Palazzolo in the paper [G.R.13].

The goal of the chapter is to establish a complete dynamic model for an automotive CVJ quasi-homokinetic driveshaft, that includes the elements that describe the nonlinear forced parametric dynamic behavior, a model that can be used in early design stages as well as in predicting the durability of the automotive driveshafts.

Figure 2.5 presents the schematical representation of an automotive drive shaft in three axis of Cartesians coordinates $X_1Y_1Z_1$ attach to the tulip, $X_2Y_2Z_2$ attach to the midshaft and $X_3Y_3Z_3$ attach to the bowl, having the next rigid movements:

- rotation with the angle φ_1 of the tulip with respect to the axis X_1 , $\varphi_1 = 0 \dots n1\pi$,
- rotation with the angle φ_2 of the mid shaft with respect to the axis X_2 , $\varphi_2 = 0 \dots n1\pi$,
- rotation with the angle φ_3 of the bowl with respect to the axis X_3 , $\varphi_3 = 0 \dots n1\pi$,
- relative rotation of the longitudinal axe of the midshaft (given by the direction of the axis X_2) with respect to the longitudinal direction of the tulip (given by the direction of the axis X_1), with β_1 (spatial angle between axis X_1 and X_2) with respect to the axis Z_1 , β_1 being the angle between longitudinal direction of the tulip and the longitudinal direction of the midshaft, $\beta_1 = 00 \dots 150$,
- relative rotation of the longitudinal axis of the bowl (given by the direction of the axis X_3) with respect to the longitudinal direction of the midshaft (given by the direction of the axis X_2), with β_2 (spatial angle between axis X_2 and X_3) with respect to the axe Y_2 , β_2 being the angle between the longitudinal direction of the midshaft and the longitudinal direction of the bowl, $\beta_2 = 00 \dots 470$.

In order to compute the equations of motions for the driveshaft, using the Variational Approach of the Hamilton Principle, it is necessary to reduce the axial mass moment of inertia of the cross-section and the geometric moment of inertia of the cross-section for the global tulip (tulip axis and tulip) with respect to the longitudinal axis of the midshaft X_2 in the centroid of the cross-section of tripod fixed on the midshaft as well as the axial mass moment of inertia of the cross-section and the axial geometric moment of inertia of the cross-section for the global bowl (bowl axis and bowl) with respect to the longitudinal axis of the midshaft X_2 in the centroid of the cross-section of the inner race fixed on the midshaft. The computations of these axial mass moments of inertia of the cross-section and axial geometric moments of inertia of the cross-section take into account: the

angle β_1 between X_1 and X_2 (see figure 3, rotation with respect to Z_1 parallel with Z_2), the distance from the mass center of the tulip axis to the centroid of the cross-section of tripod fixed on the midshaft, the distance from the mass center of the tulip to the centroid of the cross-section of tripod fixed on the midshaft (see figure 2.5), the angle β_2 between X_2 and X_3 (see figure 2.5, rotation with respect to Z_3 parallel with Z_2), the distance from the mass center of the bowl axis to the centroid of the cross-section of inner race fixed on the midshaft, the distance from the mass center of the bowl to the centroid of the cross section of inner race fixed on the midshaft (see figure 2.5). Thus, it is obtained the axial geometric moment of inertia of the cross-section for the global tulip J_{x_2GT} reduced to the longitudinal axis of the midshaft in the centroid of the cross-section of the tripod fixed on the midshaft, and the axial mass moment of inertia of the cross-section for the global tulip I_{x_2GT} reduced to the longitudinal axis of the midshaft in the centroid of the cross-section of tripod fixed on the midshaft, given by the equations:

$$J_{x_2GT} = J_{x_2T} + J_{x_2AT} \quad (3.1)$$

$$J_{x_2T} = 0,5(J_{1T} + J_{2T}) \left[1 + \cos^2 \beta_1 + X_{nT} \cos(2\varphi_1) \sin^2 \beta_1 \right] + S_T (d_{CT})^2 \quad (3.2)$$

$$X_{nT} = \frac{J_{1T} - J_{2T}}{J_{1T} + J_{2T}} \quad (3.3)$$

$$J_{x_2AT} = \frac{\pi d^4 AT}{64} (1 + \cos^2 \beta_1) + \frac{\pi d^2 AT}{4} (L_T + 0,5L_{AT})^2 \quad (3.4)$$

$$I_{x_2GT} = I_{x_2T} \rho L_T + I_{x_2AT} \rho L_{AT} \quad (3.5)$$

where J_{1T}, J_{2T} are the principal geometric moments of inertia with respect to the cross-section of the tulip in the center mass of the tulip, J_{x_2T}, J_{x_2AT} are the geometric moment of inertia of the tulip, and the geometric moment of inertia of the tulip axis reduced to the longitudinal axis of the midshaft in the centroid of the cross-section of tripod fixed on the midshaft, ρ is the volume mass density of the material of the driveshaft, d_{CT} is the distance between the center mass of the tulip and the centroid of the tripod, S_T is the area cross-section of the tulip, χ_{nT} is the nonuniformity of the geometric moments of inertia in the cross-section of the tulip, L_T is the length of the tulip, L_{AT} is the length of the tulip axis, d_{AT} is the diameter of the tulip axis and φ_1 is the angle of rotation of the tulip with respect to the axe X_1 . The global bowl consists by design in two major parts: bowl and bowl axis (wheel axis), having different geometry and therefore different mass moments of inertia and different geometric moments of inertia. In the same mathematical manner, it is obtained J_{x_2GB} the axial geometric moment of inertia of the cross-section for the global bowl reduced to the longitudinal axis of the midshaft in the centroid of the cross-section of the inner race fixed on the midshaft and I_{x_2GB} the axial mass moment of inertia of the cross-section for the global bowl reduced to the longitudinal axis of the midshaft in the centroid of the cross-section of inner race fixed on the midshaft, given by the equations:

$$J_{x_2GB} = J_{x_2B} + J_{x_2AB} \quad (3.6)$$

$$J_{x_2B} = 0,5(J_{1B} + J_{2B}) \left[1 + \cos^2 \beta_1 + X_{nB} \cos(2\varphi_3) \sin^2 \beta_1 \right] + S_B (d_{CB})^2 \quad (3.7)$$

$$X_{nB} = \frac{J_{1B} - J_{2B}}{J_{1B} + J_{2B}} \quad (3.8)$$

$$J_{x_2AB} = \frac{\pi d^4 AT}{64} (1 + \cos^2 \beta_1) + \frac{\pi d^2 AB}{4} (L_B + 0,5L_{AB})^2 \quad (3.9)$$

$$I_{x_2GB} = I_{x_2B} \rho L_B + I_{x_2AB} \rho L_{AB} \quad (3.10)$$

where J_{1B}, J_{2B} are the principal geometric moments of inertia with respect to the cross section of the bowl in the center mass of the bowl, J_{x_2B}, J_{x_2AB} are the geometric moment of inertia of the bowl and the geometric moment of inertia of the bowl axis reduced to the longitudinal axis of the midshaft in the centroid of the cross section of inner race fixed on the midshaft, ρ is the volume mass density of the material of the driveshaft, d_{CB} is the distance between the center mass of the bowl and the centroid of the inner race, S_B is the area cross-section of the bowl, χ_{nB} is the nonuniformity of the geometric moments of inertia in the cross-section of the bowl (see figure 4), L_B is the length of the bowl, L_{AB} is the length of the bowl axis, d_{AB} is the diameter of the bowl axis and φ_3 is the angle of rotation of the tulip with respect to the axe X_3 . As can be seen analyzing relations 1 to 10 the geometric axial moment of inertia of the cross section J_{x_2GT} , for the global tulip, and the geometric axial moment of inertia of the cross section J_{x_2GB} , for the global bowl, both of its reduced to the longitudinal midshaft axis X_2 , are functions that contains the effects of: twisting angle of tulip φ_1 as well as the twisting angle of bowl φ_3 , nonuniformity of the geometric moments of inertia of the cross section for both tulip and bowl χ_{nT} and χ_{nB} , the angle between longitudinal direction of the tulip and the longitudinal direction of the midshaft β_1 , the angle between the longitudinal direction of the midshaft and the longitudinal direction of the bowl β_2 , the length of the tulip and the length of the bowl, the position of the mass center of the tulip axis and tulip with respect to the centroid of the tripod, the position of the mass center of the bowl axis and bowl with respect to the centroid of the inner race, the principal geometric moments of inertia of the cross section for the tulip J_{1T}, J_{2T} , the principal geometric moments of inertia of the cross section for the bowl J_{1B}, J_{2B} , d_{AT} the diameter of the tulip axis and d_{AB} the diameter of the bowl axis. The physical model for the torsional vibrations of the driveshaft is presented in Figure 3.6. The present model (see Figure 3.6) considers that the tulip and the bowl have rigid body torsion movements through the twist angles φ_1 and φ_3 , that are functions of time $\varphi_1 = \varphi_1(t)$ and $\varphi_3 = \varphi_3(t)$, while the midshaft has a twist angle φ_2 that is a function $\varphi_2 = \varphi_2(x, t)$ of position (space) in the longitudinal direction of the midshaft, where $x \in [0, L_{Ms}]$, L_{Ms} being the length of the midshaft of the automotive driveshaft, and the time t .

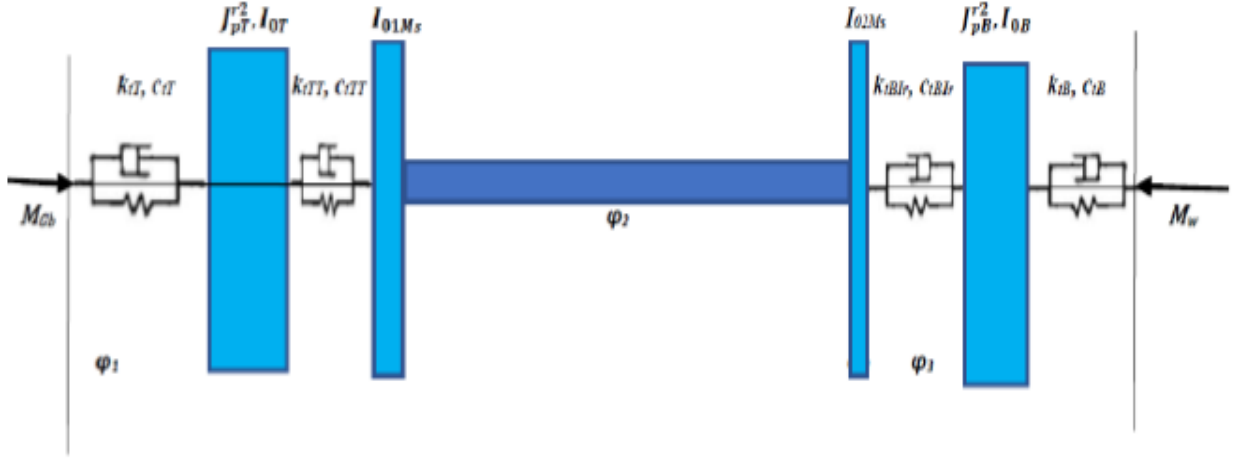


Fig. 3.6 The physical model for the torsional vibrations of the automotive driveshaft [G.R.26]

The effect of nonuniformity for the geometric and kinematic isometry of the driveshaft[G.R.1, G.R.18] is given by the equations:

$$\varphi_2(0,t) = \varphi_1(t) + \frac{R_{TTT}}{2L_{Ms}} \tan\beta_1 \tan^2 \frac{\beta_1}{2} \cos(3\varphi_1(t)) \quad (3.11)$$

$$\varphi_3(t) = \varphi_2(L_{Ms,t}) + \frac{R_{irB}}{2L_{Ms}} \tan\beta_2 \tan^2 \frac{\beta_2}{2} \cos(3\varphi_2(L_{Ms,t})) \quad (3.12)$$

where R_{TTT} is the tulip-tripode joint radius and R_{irB} is the inner race-bowl joint radius. By deriving the relations (3.11) and (3.12) with respect to time yields

$$\frac{\partial \varphi_2(0,t)}{\partial t} - \dot{\varphi}_1(t) = -1,5 \dot{\varphi}_1(t) \frac{R_{TTT}}{2L_{Ms}} \frac{R_{TTT}}{2L_{Ms}} \tan\beta_1 \tan^2 \frac{\beta_1}{2} \sin(3\varphi_1(t)) \quad (3.13)$$

$$\dot{\varphi}_3(t) - \frac{\partial \varphi_2(L_{Ms,t})}{\partial t} = -1,5 \dot{\varphi}_1(t) \frac{\partial \varphi_2(L_{Ms,t})}{\partial t} \frac{R_{irB}}{L_{Ms}} \tan\beta_2 \tan^2 \frac{\beta_2}{2} \sin(3\varphi_2(L_{Ms,t})) \quad (3.14)$$

Equations (3.11) - (3.14) introduce in this model the effect of nonuniformity for the geometric and kinematic isometry of the automotive driveshaft. The model presented consists of three different elements, tulip-midshaft-bowl, linked through two links the joint tulip-tripode (mounted on the midshaft, see Figure 3.6) and the joint bowl-balls-inner race (mounted at the other edge of the midshaft, see Figure 3.6), described in dynamic torsion as:

1. the tulip in torsional rigid body movement reduced to the torsional longitudinal axe of the midshaft, having a global torsional stiffness k_{iGT} , a global torsional damping coefficient c_{iGT} , an axial geometric moment of inertia of the cross section for the global tulip $J_{x_{2GT}}$ reduced to the longitudinal axis of the midshaft in the centroid of the cross section of tripod fixed on the midshaft (see equation 1), an axial mass moment of inertia of the cross section for the global tulip $I_{x_{2GT}}$ reduced to the longitudinal axis of the midshaft in the centroid of the cross section of tripod fixed on the midshaft (see equation 3.5), where k_{iGT} and c_{iGT} are given by the equations:

$$k_{iGT} = \frac{K_{iAT} K_{iT}}{K_{iAT} + K_{iT}}, K_{iAT} = \frac{GJ_{x_{2AT}}}{L_{AT}}, K_{iT} = \frac{GJ_{x_{2T}}}{L_T}, c_{iGT} = \frac{2\Delta_{GT}}{\sqrt{4\pi^2 + \Delta_{GT}^2}} \sqrt{k_{iGT} I_{x_{2GT}}} \quad (3.15)$$

where k_{tAT} is the stiffness rigidity of the tulip axis reduced to the longitudinal axis of the midshaft in the centroid of the cross section of tripode fixed on the midshaft, k_{tT} is the stiffness rigidity of the tulip reduced to the longitudinal axis of the midshaft in the centroid of the cross section of tripode fixed on the midshaft, L_T is the length of the tulip, L_{AT} is the length of the tulip axis, G is the shear modulus and Δ_{GT} is the logarithmic decrement of the free torsional vibrations of the global tulip ($\Delta_{GT} = 0.001 \dots 0.2$) [G.R.24, G.R.32],

2. the joint tulip-tripode in torsion that realizes the link between the tulip and the midshaft through the torsional stiffness k_{tTT} and the damping torsional coefficient c_{tTT} ,
3. the uniform midshaft in torsion having at $x = 0$ a tripode fixed on the midshaft with the axial mass moment of inertia of the cross section I_{01Ms} (midshaft axis included on the thickness of the tripode) and the geometric axial moment of inertia of the cross section of the tripode J_{x_2Tr} (midshaft axis included on the thickness of the tripode) and at $x = L_{Ms}$ an inner race fixed on the midshaft with the axial mass moment of inertia of the cross section I_{02Ms} (midshaft axis included on the thickness of the inner race) and the geometric axial moment of inertia of the cross section J_{x_2Ir} (midshaft axis included on the thickness of the inner race), given by the equations:

$$I_{01ms} = J_{x_2Tr} \rho L_{Tr} = (J_{1Tr} + J_{2Tr}) \rho L_{Tr} \quad (3.16)$$

$$I_{02ms} = J_{x_2Ir} \rho L_{Ir} = (J_{1Ir} + J_{2Ir}) \rho L_{Ir} \quad (3.17)$$

where J_{1Tr}, J_{2Tr} are the principal geometric moments of inertia in the cross section of the tripode, midshaft axis included on the thickness of the tripode, J_{1Ir}, J_{2Ir} are the principal geometric moments of inertia in the cross section of the inner race, midshaft axis included on the thickness of the inner race, J_{x_2Tr} is the geometric axial moment of inertia of the tripode (midshaft axis included on the thickness of the tripode), J_{x_2Ir} is the geometric axial moment of inertia of the inner race (midshaft axis included on the thickness of the inner race), L_{Tr} is the thickness of the tripode, L_{Ir} is the thickness of the inner race,

4. the joint bowl-balls-inner race in torsion that realizes the link between the bowl and the midshaft through the torsional stiffness k_{tBfR} and the damping torsional coefficient c_{tBfR} ,
5. the bowl in torsional rigid body movement reduced to the torsional longitudinal axe of the midshaft, having a global torsional stiffness k_{tGB} , a global torsional damping coefficient c_{tGB} , an axial geometric moment of inertia of the cross section reduced to the longitudinal axe of the midshaft J_{x_2GB} (see equation), an axial mass moment of inertia of the cross section reduced to the longitudinal axe of the midshaft I_{x_2GB} (see equation 10), where k_{tGB} and c_{tGB} are given by the equations:

$$k_{tGB} = \frac{K_{tAB} K_{tB}}{B + K_{tB}}; K_{tAT} = \frac{GJ_{x_2AB}}{L_{AB}}; K_{tT} = \frac{GJ_{x_2B}}{L_B}; c_{tGT} = \frac{2\Delta_{GB}}{\sqrt{4\pi^2 + \Delta_{GB}^2}} \sqrt{k_{tGBI_{x_2GB}}} \quad (3.18)$$

where k_{tAB} is the stiffness rigidity of the bowl axis reduced to the longitudinal axis of the midshaft in the centroid of the cross section of the inner race fixed on the midshaft, k_{tB} is the stiffness rigidity of the bowl reduced to the longitudinal axis of the midshaft in the centroid of the cross section of the inner race fixed on the midshaft, L_B is the length of the bowl, L_{AB} is the length of the bowl axis,

G is the shear modulus and Δ_{GB} the logarithmic decrement of the free torsional vibrations of the global bowl ($\Delta_{GB} = 0.001 \dots 0.15$)[G.R.24, G.R.32].

From the gearbox the driveshaft (see Figure 3.6) is receiving a torque from the engine that is given by the equation[R.C. 3.1](p. 361):

$$M_{GB} = \overline{M_e} \left[1 + X_e \cos(n\Omega_e t) \right], n \in N \quad (3.19)$$

$$\Omega_e = \frac{\pi n_e}{30} \quad (3.20)$$

where χ_e is the nonuniformity of the internal engine torque, being in the range 0.980...1.020 [R.C. 3.1](p. 363), $\overline{M_e}$ is the amplitude of the engine torque in Nm and n_e is the speed rotation (velocity angle) of the crank shaft of the engine in rot/min. The reactive torque induced by the wheel is a moderate impulsive type and can be considered of the mathematical form:

$$M_w = M_H \left[1 + q_3 t^{q_1} e^{-q_2 t} \right] \quad (3.21)$$

where M_H is the adhesion torque[G.R.5](p.130), $q_i, i = \overline{1, 3}, q_1 \gg q_2, q_3 \geq 1.1$ are experimental constants depending on the type of shock applied at the wheel by the road excitation[G.R.17].

For the model of the torsional vibrations of the automotive driveshaft presented in Figure 3.6, using the variational approach of the generalized Hamilton's principle [R.C.3.23](pp. 272-295), leads to the nonlinear system with partial derivatives of second degree:

$$\begin{aligned} Ix_{2GT}(\varphi_1) \ddot{\varphi}_2 + [c_{iGT} + 3c_{iTT} A_{TT_r} \sin(3\varphi_1)] \dot{\varphi}_1 + [K_{iGT} - K_{iTT} A_{TT_r} \cos(3\varphi_1)] \varphi_1 = \\ = \overline{M_e} \left[1 + X_e \cos(n\Omega_e t) \right] (1 - 3A_{TT_r} \sin(3\varphi_1)) \end{aligned} \quad (3.29)$$

$$\rho J x_2 M_s \frac{\partial^2 \varphi_2}{\partial t^2} = G J x_2 M_s \frac{\partial^2 \varphi_2}{\partial t^2} \quad (3.30)$$

$$\begin{aligned} Ix_{2GB}(\varphi_2) \ddot{\varphi}_3 + [c_{iGB} + 3c_{iTT} A_{TT_r} \sin(3\varphi_3)] \dot{\varphi}_3 + [K_{iGB} - K_{iTT} A_{TT_r} \cos(3\varphi_3)] \varphi_3 = \\ = M_H \left[1 + q_3 t^{q_1} e^{-q_2 t} \right] (1 - 3A_{Blr} \sin(3\varphi_3)) \end{aligned} \quad (3.31)$$

where the constants A_{TT_r} and A_{Blr} are given by the equations [G.R.1]:

$$A_{TT_r} = 0,5 \frac{R_{TT_r}}{L_{Ms}} \tan \beta_1 \tan^2 \frac{\beta_1}{2} \quad (3.32)$$

$$A_{Blr} = 0,5 \frac{R_{Blr}}{L_{Ms}} \tan \beta_1 \tan^2 \frac{\beta_1}{2} \quad (3.33)$$

and the boundary conditions are:

$$\begin{aligned} I_{01Ms} \frac{\partial^2 \varphi_2(0, t)}{\partial t^2} - 3c_{iTT} A_{TT_r} \sin(3\varphi_1) \varphi_1 + K_{iTT} A_{TT_r} \cos(3\varphi_1) \varphi_1 - \\ - G J x_2 M_s \frac{\partial^2 \varphi_2(0, t)}{\partial t^2} = 0, at x = 0 \end{aligned} \quad (3.34)$$

$$I_{02M_s} \frac{\partial^2 \varphi_2(L_{M_s}, t)}{\partial t^2} + 3c_{iBlr} A_{Blr} \sin(3\varphi_3) \varphi_3 - K_{iBlr} A_{Blr} \cos(3\varphi_3) \varphi_3 -$$

$$-GJx_2 M_s \frac{\partial^2 \varphi_2(L_{M_s}, t)}{\partial t^2} = 0, \text{ at } x = L_{M_s} \quad (3.35)$$

The system given by the equations (3.29) to (3.31) together with the boundary conditions (3.34) and (3.35) represent the nonlinear dynamic behavior of an automotive driveshaft in torsion under an input harmonic excitation, due to the modulation of the car engine and the nonuniformities of torque load transfer from the engine to the driveshaft through the automotive gearbox, and a reactive torque load of impulsive type induced to the wheel by the road excitations. Analyzing the equations (3.29) to (3.35) it can be remarked that equations (3.29) and (3.31) are the equations of forced parametric vibrations for the tulip and for the bowl in torsion that are generalized nonlinear forced Mathieu-Hill equation, equation (30) is an equation with partial derivatives for the torsional vibrations of a uniform shaft and the equations (3.34) and (3.35) represent the link between the torsional vibrations of the elements of the automotive driveshaft tulip-midshaft-bowl through the stiffness and the damping of the joints tulip-tripode-midshaft and bowl-balls-inner race-midshaft. Analyzing the joint tulip-tripode-midshaft and bowl-inner race-midshaft it is obvious that the midshaft is a fixed-fixed uniform shaft linked to the torsion of the tulip for $x = 0$ and at the bowl for $x = L_{M_s}$. Therefore, the general solution of equation (3.30) is [G.R.2] (p. 720)

$$\varphi_2(x, t) = \sum_n \Phi_{2n} \cos\left(\frac{\omega_n x}{c} - \Theta_{1n}\right) \cos(\omega_n t - \Theta_{2n}), c = \sqrt{\frac{G}{\rho}}, \omega_n = \frac{\pi n c}{L_{M_s}}, n = 1, 2, 3, \dots \quad (3.36)$$

Injecting (3.36) in the boundary conditions (3.34-3.35), and then in (3.29) and (3.31) yields

$$\ddot{\varphi}_1 + 2\zeta_1 \bar{\Omega}_1 \sqrt{\frac{1 + a_1 \cos 2\varphi_1}{(1 + a_2 \cos 2\varphi_1)(1 + x_{GTn} \cos 2\varphi_1)}} \dot{\varphi}_1 + \bar{\Omega}_1^2 \frac{1 + a_1 \cos 2\varphi_1}{(1 + a_2 \cos 2\varphi_1)(1 + x_{GTn} \cos 2\varphi_1)} \varphi_1 =$$

$$= \frac{\bar{M}_e}{Ix_{2GT}} \frac{1 + X_e \cos(n\Omega_e t)}{1 + X_{GTn} \cos \varphi_1} (1 - 3A_{Tr} \sin(3\varphi_1)) +$$

$$+ \sum_n \Phi_{2n} \left[\frac{I_{01M_s}}{Ix_{2GT}} \omega_n^2 \cos \Theta_{1n} + \frac{GJx_2 M_s}{Ix_{2GT}} \frac{\omega_n}{c} \sin \Theta_{1n} \right] \frac{\cos(\omega_n t - \Theta_{2n})}{(1 + x_{GTn} \cos 2\varphi_1)} \quad (3.40)$$

, $n=1, 2, 3, \dots$,

where χ_{GTn} is the global tulip nonuniformity, ζ_1 is the damping ratio of the global tulip, $\bar{\Omega}_1$ is the natural frequency in torsion of the global tulip, as function of the angle β_1 , given by the equation

$$\bar{\Omega}_1 = \frac{c}{L_T} \left[\frac{1 - \frac{Jx_{2AT} \rho L_{AT}}{Ix_{2GT}}}{1 + \left(\frac{L_{AT}}{L_T}\right)^2 \left(\overline{Ix_{2GT}} |Jx_{2AT} \rho L_{AT}\right) - 1} \right]^{\frac{1}{2}} \quad (3.41)$$

All the terms in the right hand side are excitations terms due to the phenomena: the joint tulip-tripode-midshaft of the driveshaft that is quasi-isometric for the angular velocity Φ_1 [R.G.1,

R.G.18], the effect of induced torsional loads as the harmonic entry moment from the gear box[R.C.3.1](p. 360), the effect of nonuniformity for the axial moment of inertia of the joint tulip-tripode-midshaft of the driveshaft that vary with the angle φ_1 , the effect of nonuniformity for the axial moment of inertia of the global tulip that vary with the angle φ_1 , the effect of the angle β_1 between the global tulip axis and the midshaft axis, and the effect of the torsional rigidity as well as the torsional damping for the joint tulip-tripode-midshaft of the driveshaft that are functions of the angle φ_1 . In a similar manner it yields for the bowl the equations

$$\begin{aligned} & \ddot{\varphi}_3 + 2\zeta_3 \bar{\Omega}_3 \sqrt{\frac{1 + a_3 \cos 2\varphi_3}{(1 + a_4 \cos 2\varphi_3)(1 + x_{GBn} \cos 2\varphi_3)}} \dot{\varphi}_3 + \bar{\Omega}_3^2 \frac{1 + a_3 \cos 2\varphi_3}{(1 + a_4 \cos 2\varphi_3)(1 + x_{GTn} \cos 2\varphi_3)} \varphi_3 = \\ & = \frac{M_H}{Ix_{2GB}} \left[\frac{1 + q_3 t^{q_1} e^{-q_2 t}}{(1 + x_{GBn} \cos 2\varphi_3)} (1 - 3A_{Br} \sin(3\varphi_3)) \right] + \\ & + \sum_n (-1)^n \Phi_{2n} \left[\frac{I_{01Ms}}{Ix_{2GT}} \omega_n^2 \cos \Theta_{1n} + \frac{GJx_2 M_s}{Ix_{2GT} c} \omega_n \sin \Theta_{1n} \right] \frac{\cos(\omega_n t - \Theta_{2n})}{(1 + x_{GTn} \cos 2\varphi_1)}, n = 1, 2, 3 \dots \end{aligned} \quad (3.43)$$

$$\bar{\Omega}_3 = \frac{c}{L_B} \left[\frac{1 - \frac{Jx_{2AB} \rho L_{AB}}{Ix_{2GT}}}{1 + \left(\frac{L_{AB}}{L_B} \right)^2 \left(\frac{Ix_{2GB}}{Ix_{2GT}} |Jx_{2AB} \rho L_{AB}| \right) - 1} \right]^{1/2}. \quad (3.44)$$

It was considered a tulip-tripod joint having the geometry characteristics, the geometric moment of inertia and the nonuniformity of the geometric moments of inertia presented in Table 3.1, for a driveshaft of a heavy-duty SUV with tulip, tulip-tripode joint, midshaft, bowl-balls-inner race joint, bowl.

Tabel 3.1. Geometry characteristics of a tulip-tripode joint.

L_T [m]	L_{AT} [m]	L_{Ms} [m]	R_{TTR} [m]	d_{AT} [m]	d_{CT} [m]	S_T [m ²]	$0.5(J_{1T} + J_{2T})$ [m ⁴]	X_{nT}
0.095	0.065	0.470	0.035	0.027	0.049	0.019	9.1531×10^{-7}	0.15

In Table 3.2 are presented the physical properties of the material of the tulip-tripode joint and global tulip as well as the amplitude of the maximum torque transmitted by the car engine, considering that the material is steel-iron cast. Comparing this presented material properties with those considered by Steinwede [B.G.14] (p. 112) it can be concluded that are in very close agreement.

Tabel 3.2. Material properties of a tulip-tripode joint and of the global tulip. Torque load.

ρ [kg/m ³]	G [GPa]	Torsional rigidity [Nm/rad]	Damping ratio ζ_1	Engine torque \bar{M}_e [Nm]
7850	77.3	1.11e+04	0.0016-0.0318	580

Using the data presented in Tables 3.1 and 3.2 in the equation (3.41) it was computed the variation of $\bar{\Omega}_1$, the natural frequency in torsion of the global tulip as function of the angle β_1 with a MATLAB software. The data are presented in Figures 3.7 and 3.8.

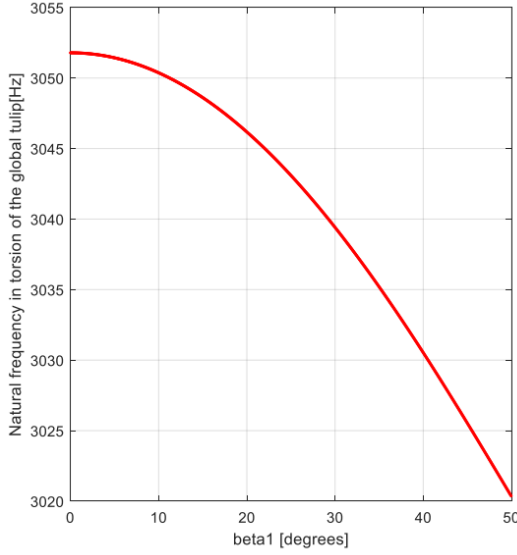


Fig. 3.7 Variation of $\bar{\Omega}_1 = \bar{\Omega}_1(\beta_1)$. [B.G.26]

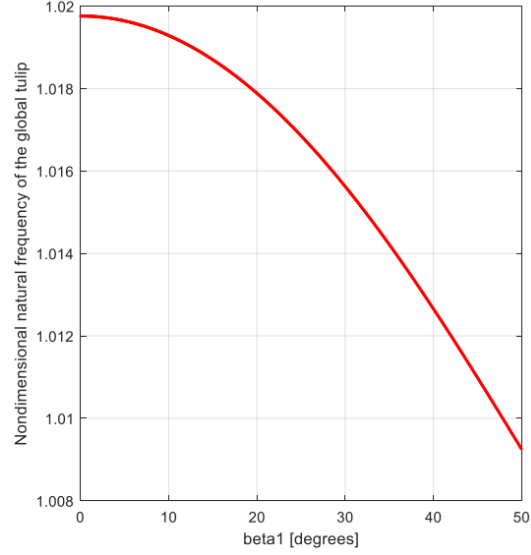


Fig. 3.8 Variation of $\frac{\bar{\Omega}_1}{\bar{\Omega}_1(0)} = \frac{\bar{\Omega}_1 \beta_1}{\bar{\Omega}_1(0)}$ [B.G.26]

To compute the amplitude of the torsional forced nonlinear parametric vibrations in the region of principal parametric resonance it was used the method of harmonic balance [R.C.3.3](p. 66) for the equation (3.40) yielding the equations

$$y = 1 - 2\Phi_1^2 \quad (3.50)$$

$$\begin{aligned} & \Gamma_1 \bar{\eta}^2 y^6 + \Gamma_2 \bar{\eta}^2 y^5 + \Gamma_3 \bar{\eta}^2 y^4 + [\Gamma_4 \bar{\eta}^2 + \Gamma_5 \bar{\eta}^2] y^3 + [\Gamma_6 \bar{\eta}^2 + \Gamma_7 \bar{\eta}^2 + \Gamma_8 \bar{\eta}^2] y^2 + \\ & + [\Gamma_9 \bar{\eta}^2 + \Gamma_{10} \bar{\eta}^2 + \Gamma_{11} \bar{\eta}^2] y + \Gamma_{12} \bar{\eta}^2 + \Gamma_{13} \bar{\eta}^2 + \Gamma_{14} \bar{\eta}^2 = 0 \end{aligned} \quad (3.53)$$

where y is a changing variable of the unknown amplitude $\Phi_1, \eta = \eta/2\bar{\Omega}_1$ is the nondimensional excitation frequency in the region of principal parametric resonance. Using the equation (3.53) it was developed a MATLAB software in order to compute the amplitude of the torsional forced nonlinear parametric vibrations in the region of principal parametric resonance for the global tulip for the steady-state torsional vibrations of the automotive driveshaft. In the same mathematical manner it can be computed the amplitude Φ_3 of the torsional forced nonlinear parametric vibrations

for the global bowl, as a function of nondimensional excitation frequency $\bar{\eta} = \frac{\eta}{2\bar{\Omega}_3}$, in the region of

principal parametric resonance $\eta \approx 2\bar{\Omega}_3$ for the steady-state torsional vibrations of the automotive driveshaft. Analysing Figure 3.7 and 3.8 it can be seen that the variation of the natural frequency in torsion of the global tulip is closed to the natural frequency in torsion of the midshaft being in the range 3052Hz...3020 Hz (see Figure 3.7) and the nondimensional natural frequency in torsion of the global tulip is in the range 1.009-1.0198. Unfortunately there are no published experiments

that investigate the natural free frequency in torsion only for the global tulip. In figures 3.9-3.14 is presented the variation of the nondimensional amplitude for torsional forced nonlinear parametric vibration in the region of principal parametric resonance for the global tulip, this being around 5.985 kHz. The nondimensional amplitude presented in the graphs 9 to 14 represents the normalized amplitude with respect to its maximum value for $\beta_1=5^0$, $\zeta_1=0.0016$, $\chi_{nT}=0.15$. Analysing figures 3.9-3.14 it can be remarked that for the cases we have a manifestation of “soft spring” with two branches for $\eta \leq 1.8\bar{\Omega}_1(0)$ that indicates the presence of interaction between principal parametric resonance and the primary resonance while for $\eta \geq 1.8\bar{\Omega}_1(0)$ it exists only one “hard spring” branch that indicates the manifestation of pure principal parametric resonance for the global tulip [R.C.3.5] (pp. 132-160). The aspects highlighted by figures 3.9-3.11 is that with the increase of the angle β_1 the maximum value of the nondimensional amplitude decreases from 1 to 0.35. This aspect agrees with the experimental data in the literature [G.R.14] (pp. 130-144). Figures 3.11-3.14 indicates that for an angle $\beta_1=15^0=\text{const.}$ the increase of the damping ratio ζ_1 in the range 0.008...0.0318 induces a decrease of the maximum nondimensional amplitude in the range 0.35...0.22 thus we can conclude that the model is much more sensitive to the geometry variation of the driveshaft than to the damping effects. Steinwede demonstrated by experiments that the nonlinear parametric dynamic behavior of automotive driveshafts is similar with the nonlinear parametric dynamic behavior of geared systems [G.R.14] (p. 117) and that is way we have similar pitting phenomena for inside the tulip and inside the bowl for the CVJ joints tulip-tripode and bowl-balls-inner race [G.R.14] (pp. 88-94). Also, it can be seen from the Figures 3.11-3.14, that the increase of damping ratio ζ_1 in the range 0.008...0.0318 induces an increase between the branches of the amplitude for both areas “soft spring” and “hard spring” being a manifestation of the multiple “jumps” between the amplitude branches knowing that usually the inferior branch is unstable while the superior branch is stable [G.R.16] (pp. 426-429), [R.C.3.5] (pp. 132-160). This aspect will “conduct” the dynamic behavior through a chaotic dynamic that has as practical effect an accelerating pitting phenomenon as mentioned by Steinwede [G.R.14] (pp. 88-94) or in the worst case the manifestation of cracks followed by the failure (broken) of the global tulip [G.R.14] (p. 89). Unfortunately, there are no published research analyzing in detail the dynamic behavior for each element of the automotive CVJ driveshaft: tulip, global tulip, bowl, global bowl, midshaft excepting work [5], all the research analyzing the global dynamic behavior of the automotive driveshaft. Even so there are huge confusion in the interpretation of experimental data due to the lack of understanding of specific global nonlinear phenomena such as in [G.R.22].

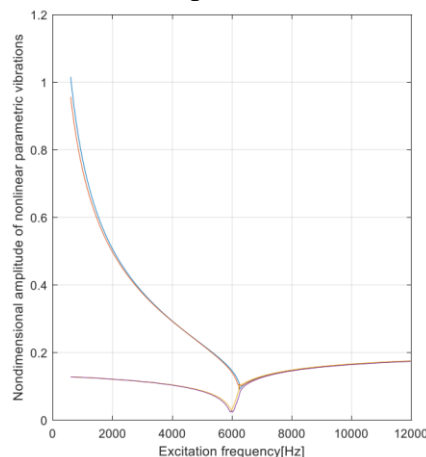


Fig. 3.9 Nondimensional amplitude for $\beta_1 = 5^0$, $\zeta_1 = 0,0016$, $\chi_{nT} = 0,15$. [G.R.26]

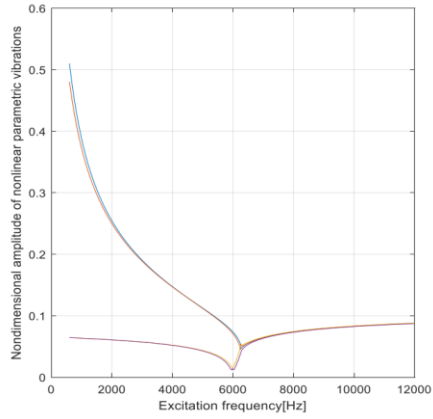


Fig. 3.10 Nondimensional amplitude for $\beta_1 = 10^\circ$, $\zeta_1 = 0,0016$, $\chi_{nT} = 0,15$. [G.R.26]

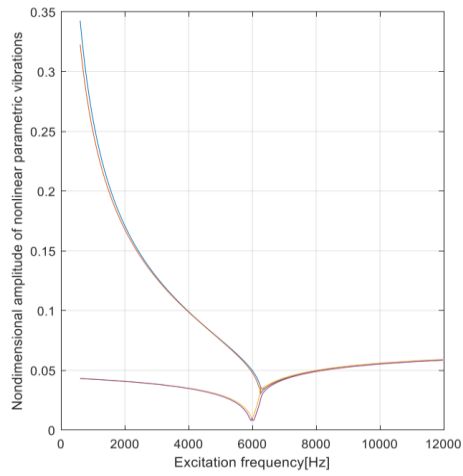


Fig. 3.11 Nondimensional amplitude for $\beta_1 = 15^\circ$, $\zeta_1 = 0,0016$, $\chi_{nT} = 0,15$. [G.R.26]

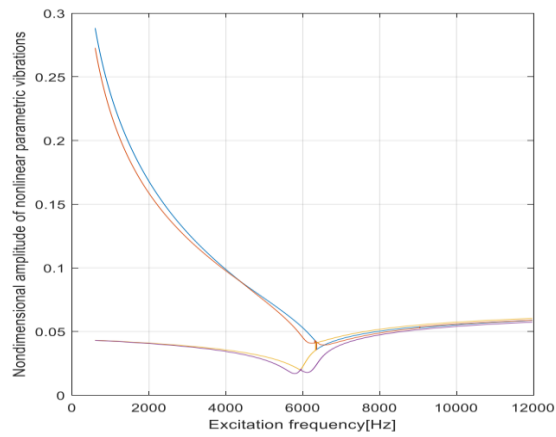


Fig. 3.12 Nondimensional amplitude for $\beta_1 = 15^\circ$, $\zeta_1 = 0,008$, $\chi_{nT} = 0,15$ [G.R.26]

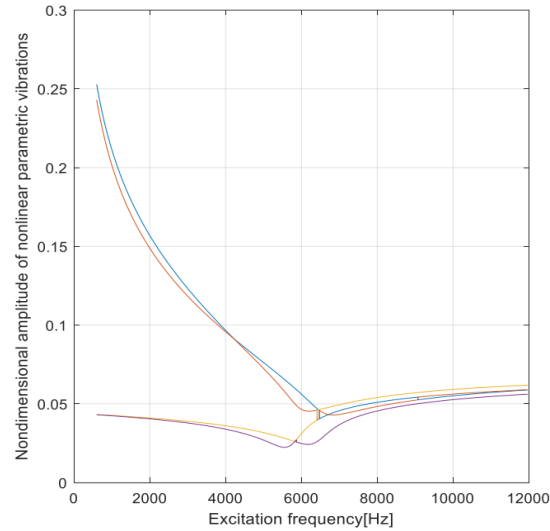


Fig. 3.13 Nondimensional amplitude for $\beta_1 = 15^\circ$, $\zeta_1 = 0,0159$, $\chi_{nT} = 0,15$ [G.R.26]

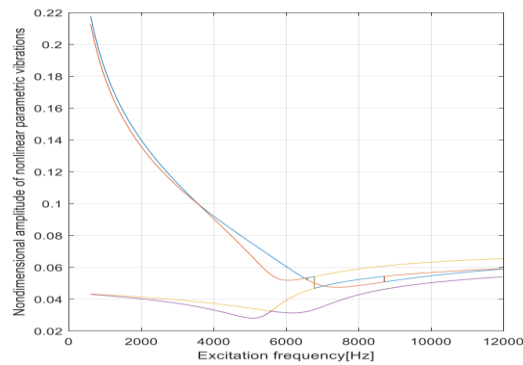


Fig. 3.14 Nondimensional amplitude for $\beta_1 = 15^\circ$, $\zeta_1 = 0,0318$, $\chi_{nT} = 0,15$ [G.R.26]

It can be concluded that the present investigation introduces a complex model for torsional vibrations of the automotive driveshaft, model that considers most of the phenomena remarked by the industrial practice and the exploitation of the cars such as:

- the nonuniformity of the geometric and kinematic isometry of the driveshaft,
- the nonuniformity of the geometric and mass moments of inertia of the cross section for the tulip, the tripod, the inner race and the bowl,
- the stiffness and the damping link of the joints of the driveshaft tulip-tripode-midshaft and midshaft-inner race-balls-bowl,
- harmonic excitation of the driveshaft due to the car engine,
- impulsive excitation of the driveshaft due to the road excitation.

Also, the model allows the development of future research directions for the investigation of primary resonances, superharmonic resonances, subharmonic resonances, principal parametric resonances, combination resonances, internal resonances, and simultaneous resonances as well as for the investigation of the stability for the steady-state motion as well as for the non-stationary motion. Therefore, this model of dynamic torsional behavior for the automotive driveshaft can be used in early design stages as well in predicting the durability of the automotive driveshafts. Also, the model must be added in the algorithm design of predicting the comfort elements of the automotive, because this kind of dynamic behavior induces excitations to the car structure as mentioned in literature[G.R.19].

Chapter 4. Models of Forced Bending Vibrations of Automotive Driveshafts

The present work presents a perturbation technique, namely the asymptotic method (AM)[R.C.4.1], to investigate the principal parametric resonance for the forced bending-shearing vibrations of an automotive driveshaft, the asymptotic method being a powerful tool for the investigation of vibrations induced by shocks (impulsive excitations) as mentioned by Webber in literature[R.C.4.2]. To investigate such a resonance region, it was designed a PCM (physically consistent model) of the bending vibrations for an automotive driveshaft, designed for heavy-duty SUVs, induced by impulsive excitations of the road, taking into account the next phenomena aspects: the joints of the driveshaft are quasi-isometric for the angular velocity[G.R.1], even in general it is considered as CVJ (Constant Velocity Joint), the effect of nonuniformity for the axial geometric moments of inertia and axial mass moments of inertia of the joints that vary with the angle of twist of each element of the driveshaft and the effect of the bending and shearing stiffness as well as the bending and shearing damping for each joint of the drive shaft. The excitations of the forced bending vibrations of the automotive driveshaft are due to the impulsive-shock excitations acting on the automotive wheel, being an excitation induced by the road[R.C.4.4]. In the literature [G.R.18], the nonuniformity in the isometric properties of automotive driveshafts has already a fact recognized for more than half a century, whose reality was demonstrated in experiments performed by Steinwede for his Ph.D. thesis [G.R.14](pp. 68-97). This non-uniformity in driveshaft isometric properties is undoubtedly the main cause of nonlinear parametric vibrations of driveshafts in the range 0.1–12 kHz, as established by experimental results documented in the literature [G.R.14] (pp. 98-123). Mazzei and Scott, the first researchers who considered the unique dynamic phenomena of driveshafts, enhanced the nonlinear parametric dynamic behavior of a universal joint in their paper [G.R.12]. The experimental evidence for the nonuniformity of CVJ driveshaft transmission is presented and highlighted by Browne and Palazzolo [G.R.13].

The chapter aims to investigate the dynamic stability in the region of principal parametric resonance based on the designed PCM of the automotive driveshaft for the forced bending vibrations induced by impulsive shock excitation of the road. It is envisaged that this model can be used in the early design stages and in predicting the durability of the automotive driveshafts. A driveshaft is a mechanism that transmits a torque load from the gearbox to the wheel. The general model of such automotive driveshaft, designed for heavy-duty SUVs, is shown in Figure 4.1. It consists of a) the bowl-balls joint fixed and assembled with the car wheel, (b) the midshaft axis, (c) the tulip-tripod joint that allows axial plunging of the tripod in the tulip and plunging assembled in the gearbox.

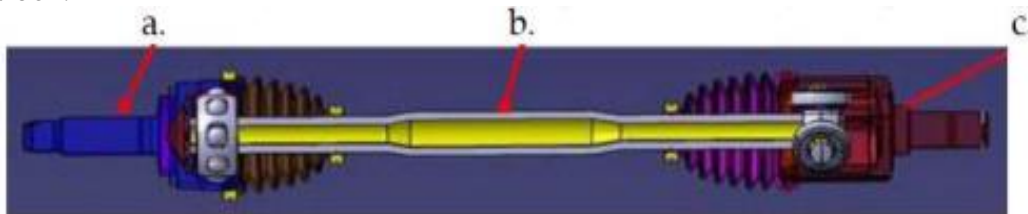


Fig. 4.1 Driveshaft in general detail [R.C.4.4]

Presented in Figure 4.2 are the schematical representation of an automotive driveshaft in the three axes of Cartesian coordinates $X_1Y_1Z_1$ attached to the tulip, $X_2Y_2Z_2$ attached to the midshaft, and $X_3Y_3Z_3$ attached to the bowl, which has the following rigid movements:

- rotation with the angle ϕ_1 of the tulip concerning the axis X_1 , $\phi_1 = 0 \dots n_1\pi$,
- rotation with the angle ϕ_2 of the midshaft concerning the axis X_2 , $\phi_2 = 0 \dots n_2\pi$,
- rotation with the angle ϕ_3 of the bowl concerning the axis X_3 , $\phi_3 = 0 \dots n_3\pi$,
- relative rotation of the longitudinal axis of the midshaft (given by the direction of the axis X_2) concerning the longitudinal direction of the tulip (provided by the direction of the axis X_1), with β_1 (spatial angle between axis X_1 and X_2) concerning the axis Z_1 , β_1 being the angle between longitudinal direction of the tulip and the longitudinal direction of the midshaft, $\beta_1 = 0^\circ \dots 15^\circ$,
- relative rotation of the longitudinal axis of the bowl (given by the direction of the axis X_3) concerning the longitudinal direction of the midshaft (provided by the direction of the axis X_2), with β_2 (spatial angle between axis X_2 and X_3) concerning the axis Y_2 , β_2 being the angle between the longitudinal direction of the midshaft and the longitudinal direction of the bowl, $\beta_2 = 0^\circ \dots 47^\circ$.

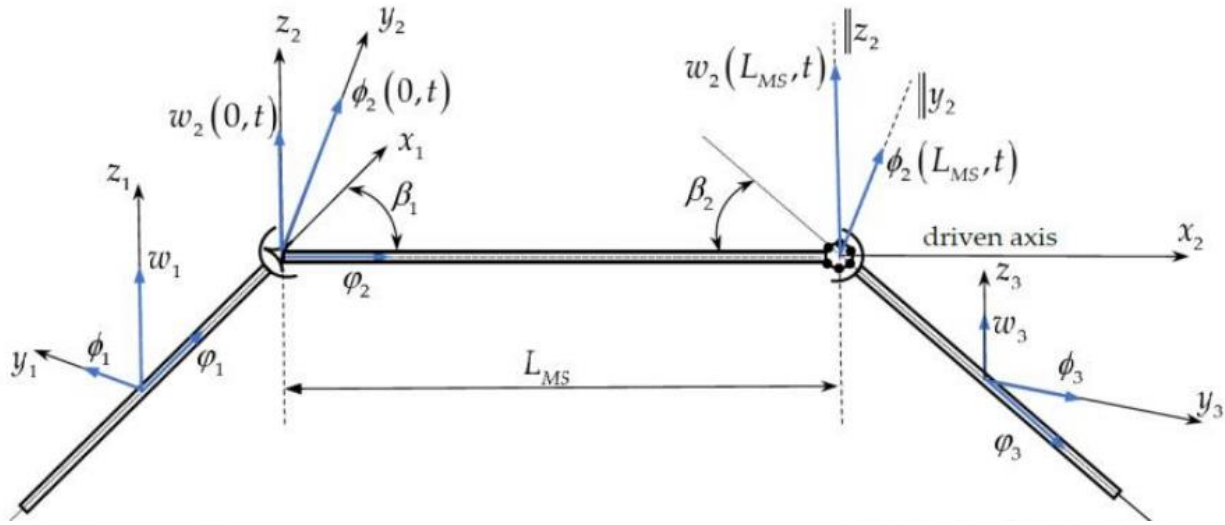


Fig. 4.2 Schematic representation of an automotive driveshaft [R.C.4.4]

To compute the equations of forced bending vibrations for the driveshaft, using the Variational Approach of the Hamilton Principle, it is necessary to reduce the axial mass moments of inertia of the cross-section and the axial geometric moments of inertia of the cross-section $J_{Y_{GT}}, J_{Z_{GT}}$ for the global tulip (tulip axis and tulip) concerning the longitudinal axis of the midshaft X_2 in the centroid of the cross-section of tripod fixed on the midshaft as well as the axial mass moments of inertia of the cross-section $I_{Y_{GB}}, I_{Z_{GB}}$ and the axial geometric moments of inertia of the cross-section $J_{Y_{GB}}, J_{Z_{GB}}$ for the global bowl (bowl axis and bowl) concerning the longitudinal axis of the midshaft X_2 in the centroid of the cross-section of the inner race fixed on the mid-shaft. In its design, the global tulip consists of two major parts, the tulip and tulip axis, which have different geometry and, therefore different mass and geometric moments of inertia. Thus, the computations of these axial mass moments of inertia of the cross-section and axial geometric moments of inertia of the cross-section are taken into account: the angle β_1 between X_1 and X_2 (see Figure 4.2, rotation concerning Z_1 parallel with Z_2), the distance from the mass center of the tulip axis to the centroid of the cross-section of tripod fixed on the midshaft, the distance from the mass center of the tulip to the centroid of the cross-section of tripod fixed on the midshaft, the angle β_2 between X_2 and X_3 (see Figure 4.2, rotation concerning Z_3 parallel with Z_2), the distance from the mass center of the bowl axis to the centroid of the cross-section of inner race fixed on the midshaft, the distance from

the mass center of the bowl to the centroid of the cross-section of inner race fixed on the mid-shaft. Thus, it is obtained the axial geometric moments of inertia of the cross-section for the global tulip J_{Y_2GT}, J_{Z_2GT} reduced to the Y_2, Z_2 axis of the midshaft in the centroid of the cross-section of the tripod fixed on the midshaft, and the axial mass moments of inertia of the cross-section for the global tulip I_{Y_2GT}, I_{Z_2GT} reduced to the Y_2, Z_2 axis of the midshaft in the centroid of the cross-section of the tripod fixed on the midshaft, given by the equations:

$$\begin{aligned} J_{Y_2GT} &= J_{Y_2T} + J_{Y_2AT}; J_{Z_2GT} = J_{Z_2T} + J_{Z_2AT}; I_{Y_2GT} = J_{Y_2T}\rho L_T + J_{Y_2AT}\rho L_{AT} \\ I_{Z_2GT} &= J_{Z_2T}\rho L_T + J_{Z_2AT}\rho L_{AT}; \chi_{nT} = \frac{J_{1T} - J_{2T}}{J_{1T} + J_{2T}} \end{aligned} \quad (4.1)$$

$$\begin{aligned} J_{Y_2T} &= 0.5(J_{1T} + J_{2T})\left[1 + \sin^2 \beta_1 + \chi_{nT} \cos^2 \beta_1\right] + \frac{S_T L_T^2}{12} \cos^2 \beta_1 + S_T (d_{CT})^2 \\ J_{Z_2T} &= 0.5(J_{1T} + J_{2T})\left[1 - \chi_{nT} \cos(\varphi_1)\right] + \frac{S_T L_T^2}{12} + S_T (d_{CT})^2 \end{aligned} \quad (4.2)$$

$$\begin{aligned} J_{Y_2AT} &= \frac{\pi d_{AT}^2}{64} (1 + \sin^2 \beta_1) + \frac{\pi d_{AT}^2}{4} \frac{L_{AT}^2}{12} \cos^2 \beta_1 + \frac{\pi d_{AT}^2}{4} (L_T + 0.5L_{AT})^2 \\ J_{Z_2AT} &= 0.5(J_{1T} + J_{2T})\left[1 - \chi_{nT} \cos(\varphi_1)\right] + \frac{S_T L_T^2}{12} + S_T (d_{CT})^2 \end{aligned} \quad (4.3)$$

where J_{1T}, J_{2T} are the principal geometric moments of inertia concerning the cross-section of the tulip in the center mass of the tulip, $J_{Y_2T}, J_{Y_2AT}, J_{Z_2T}, J_{Z_2AT}$ are the axial geometric moments of inertia of the tulip, and the axial geometric moments of inertia of the tulip axis reduced to the Y_2, Z_2 axis of the midshaft in the centroid of the cross-section of tripod fixed on the midshaft, ρ is the volume mass density of the material of the driveshaft, d_{CT} is the distance between the center mass of the tulip and the centroid of the tripod, S_T is the area cross-section of the tulip, χ_{nT} is the nonuniformity of the geometric moments of inertia in the cross-section of the tulip, L_T is the length of the tulip, L_{AT} is the length of the tulip axis, d_{AT} is the diameter of the tulip axis and φ_1 is the angle of rotation of the tulip concerning the axis X_1 . In its design, the global bowl consists of two major parts, the bowl and bowl axis (wheel axis), which have different geometry and therefore different mass and geometric moments of inertia. Thus, the computations were performed using the variation of the axial geometric moments of inertia concerning the concurrent axis and parallel axis (Steiner Theorem). In the same mathematical manner, it is obtained the axial geometric moments of inertia of the cross-section for the global bowl J_{Y_2GB}, J_{Z_2GB} reduced to the Y_2, Z_2 axis of the midshaft in the centroid of the cross-section of the inner race fixed on the midshaft and the axial mass moments of inertia of the cross-section for the global bowl I_{Y_2GB}, I_{Z_2GB} reduced to the Y_2, Z_2 axis of the midshaft in the centroid of the cross-section of the inner race fixed on the midshaft, given by the equations:

$$\begin{aligned} J_{Y_2GB} &= J_{Y_2B} + J_{Y_2AB}; J_{Z_2GB} = J_{Z_2B} + J_{Z_2AB}; I_{Y_2GB} = J_{Y_2B}\rho L_B + J_{Y_2AB}\rho L_{AB} \\ I_{Z_2GB} &= J_{Z_2B}\rho L_B + J_{Z_2AB}\rho L_{AB}; \chi_{nB} = \frac{J_{1B} - J_{2B}}{J_{1B} + J_{2B}} \end{aligned} \quad (4.4)$$

$$J_{Y_2B} = 0.5(J_{1B} + J_{2B}) \left[1 + \sin^2 \beta_1 + \chi_{nB} \cos^2 \beta_1 \right] + \frac{S_B L_B^2}{12} \cos^2 \beta_1 + S_B (d_{CB})^2$$

$$J_{Z_2B} = 0.5(J_{1B} + J_{2B}) \left[1 - \chi_{nB} \cos(\varphi_1) \right] + \frac{S_B L_B^2}{12} + S_B (d_{CB})^2 \quad (4.5)$$

$$J_{Y_2AB} = \frac{\pi d_{AB}^2}{64} (1 + \sin^2 \beta_1) + \frac{\pi d_{AB}^2}{4} \frac{L_{AB}^2}{12} \cos^2 \beta_1 + \frac{\pi d_{AB}^2}{4} (L_B + 0.5L_{AB})^2$$

$$J_{Z_2B} = 0.5(J_{1B} + J_{2B}) \left[1 - \chi_{nB} \cos(\varphi_1) \right] + \frac{S_B L_B^2}{12} + S_B (d_{CB})^2 \quad (4.6)$$

where $J_{Y_2B}, J_{Y_2AB}, J_{Z_2B}, J_{Z_2AB}$ are the axial geometric moments of inertia of the bowl and the axial geometric moments of inertia of the bowl axis reduced to the Y_2, Z_2 axis of the midshaft in the centroid of the cross-section of the inner race fixed on the midshaft, d_{CB} is the distance between the center mass of the bowl and the centroid of the inner race, S_B is the area cross-section of the bowl, χ_{nB} is the nonuniformity of the geometric moments of inertia in the cross-section of the tulip, L_B is the length of the bowl, L_{AB} is the length of the bowl axis, d_{AB} is the diameter of the bowl axis and φ_3 is the angle of rotation of the tulip concerning the axis X_3 .

As can be seen analyzing relations 4.1-4.6 the axial geometric moments of inertia of the cross section J_{Y_2CT}, J_{Z_2CT} , for the global tulip, and the axial geometric moments of inertia of the cross section J_{Y_2GB}, J_{Z_2GB} , for the global bowl, both of its reduced to the midshaft axis Y_2, Z_2 , are functions $\Gamma_1(\beta_1, \chi_{nT}, \varphi_1, S_T, d_{CT}, L_T, L_{AT}, d_{AT})$ respectively $\Gamma_2(\beta_2, \chi_{nB}, \varphi_3, S_B, d_{CB}, L_B, L_{AB}, d_{AB})$ that contains the effects of: twisting angle of tulip φ_1 as well as the twisting angle of bowl φ_3 , nonuniformity of the geometric moments of inertia of the cross section for both tulip and bowl χ_{nT} and χ_{nB} , the angle between longitudinal direction of the tulip and the longitudinal direction of the midshaft β_1 , the angle between the longitudinal direction of the midshaft and the longitudinal direction of the bowl β_2 , the length of the tulip and the length of the bowl, the position of the mass center of the tulip axis and tulip with respect to the centroid of the tripode, the position of the mass center of the bowl axis and bowl with respect to the centroid of the inner race, the principal geometric moments of inertia of the cross section for the tulip J_{1T}, J_{2T} , the principal geometric moments of inertia of the cross section for the bowl J_{1B}, J_{2B} , d_{AT} the diameter of the tulip axis and d_{AB} the diameter of the bowl axis.. The PCM is a dynamic model for the forced bending vibration (DMFFBV) movements of an AD's elements presented in Figure 4.3.

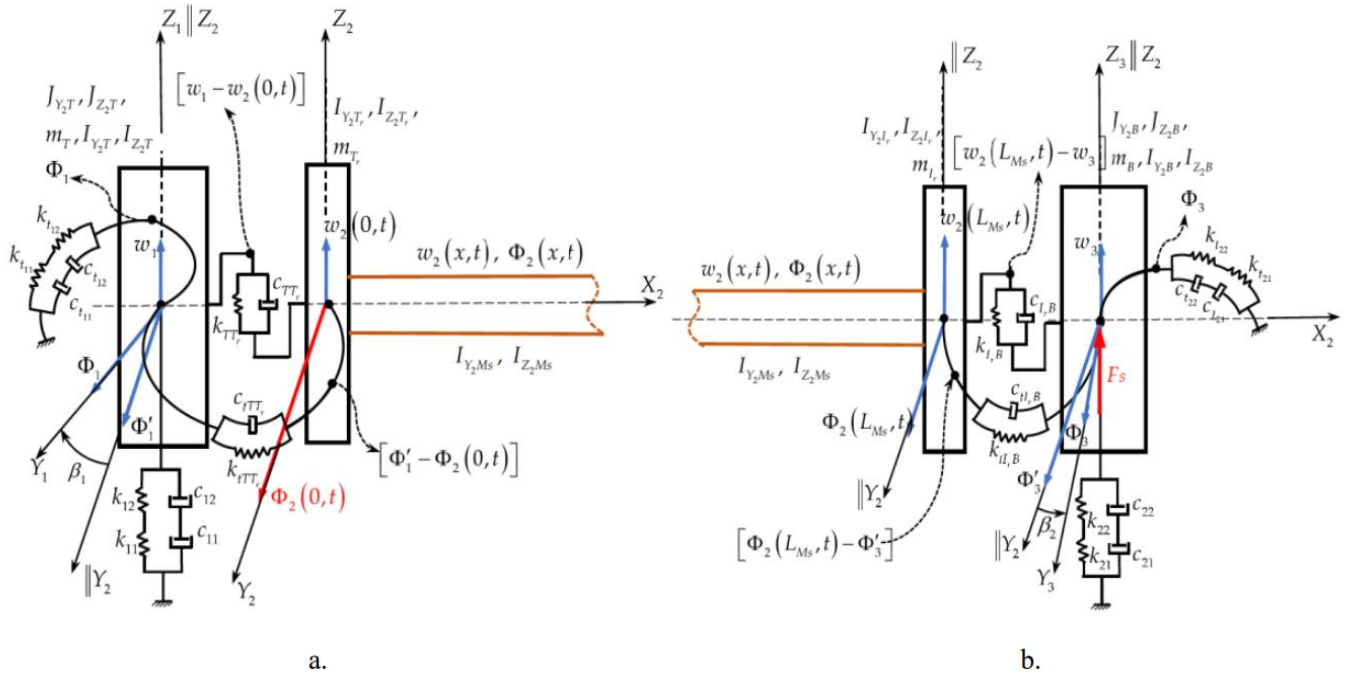


Fig. 4. 3. a. Tulip-Tripode joint Part of PCM: Global Tulip, the joint Tulip-Tripode, Midshaft
b. Bowl-Inner Race joint Part of PCM: Midshaft, the joint Bowl-Inner Race, Global bowl [B.C.4.4]

The DMFFBV movements, presented in Figure 4.3, have three elements: a tulip–midshaft–bowl linked through two joints, the tulip–tripod joint (mounted on the midshaft (see Figure 4.2)), and the bowl–inner race joint (mounted at the other edge of the midshaft (see Figure 4.2)). These have the following dynamic characteristics:

1. The tulip has a stiffness k_1 , given by the serial springs k_{11}, k_{12} (see figure 3.a), and damping c_1 , provided by the serial dampers c_{11}, c_{12} , for the bending vibration rigid movement of the tulip regarding the axis Z_2 and a stiffness k_{t1} , given by the serial springs k_{t1}, k_{t2} , as well as damping c_{t1} , provided by the serial dampers c_{t1}, c_{t2} , for the angular bending vibration rigid movement of the tulip regarding the axis Y_2 , given by the following relations:

$$\begin{aligned}
k_{11} &= \frac{3EJ_{Z_2TA}}{L_{TA}^3}; k_{12} = \frac{3EJ_{z_2TB}}{L_{TB}^3}; k_1 = \frac{k_{11}k_{12}}{k_{11} + k_{12}}; c_1 = 2\zeta\sqrt{k_1 m_T} \\
k_{t1} &= \frac{GJ_{Y_2TA}}{L_{TA}}; k_{t2} = \frac{GJ_{Y_2TB}}{L_{TA}}; k_{t1} = \frac{k_{t1}k_{t2}}{k_{t1} + k_{t2}}; c_{t1} = 2\zeta\sqrt{k_{t1} I_{Y_2T}}
\end{aligned} \quad (4.7)$$

where E is Young's modulus, G is the shearing modulus, m_T is the tulip's mass, and ξ is the damping ratio of the free bending vibrations of the tulip ($\xi = 0.0016-0.0318$) [G.R24,G.R.2];

2. The uniform midshaft (see Figures 4.3.a, 4.3.b) in continuous FBV movement is assimilated with a uniform Timoshenko beam simply supported at both ends by elastic supports (the tulip–tripod and inner race–bowl joints are elastic supports for the midshaft), having at $x = 0$ a tripod fixed on the midshaft through splines and elastically linked in the tulip–tripod joint with the tulip

and on the left-hand side at $x = L_{Ms}$ an inner race fixed on the midshaft through splines and elastically linked in the bowl–inner race joint with the bowl, with the inertial characteristics given by the relations below:

$$\begin{aligned}
J_{Y_2Tr} &= 0.5(J_{1Tr} + J_{2Tr})[1 + \chi_{nTr} \cos(\varphi_2)] \\
J_{Z_2Tr} &= 0.5(J_{1Tr} + J_{2Tr})[1 - \chi_{nTr} \cos(\varphi_2)] \\
J_{Y_2lr} &= 0.5(J_{1lr} + J_{2lr})[1 + \chi_{nlr} \cos(\varphi_2)] \\
J_{Z_2lr} &= 0.5(J_{1lr} + J_{2lr})[1 - \chi_{nlr} \cos(\varphi_2)]
\end{aligned} \tag{4.8}$$

where J_{1Tr}, J_{2Tr} are the principal geometric moments of inertia for the tripod, J_{1lr}, J_{2lr} are the principal geometric moments of inertia for the inner race, χ_{nTr} and χ_{nlr} are the geometric nonuniformities of the tripod and inner race, and $J_{Y_2Tr}, J_{Z_2Tr}, J_{Y_2lr}, J_{Z_2lr}$ are the geometric moments of inertia of the tripod and inner race concerning the axes Y_2, Z_2 ;

3. The bowl has a stiffness k_2 , given by the serial springs k_{21}, k_{22} (see figure 3.b), and damping c_2 , provided by the serial dampers c_{21}, c_{22} , for the bending vibration rigid movement of the bowl regarding the axis Z_2 and a stiffness k_{t2} , given by the serial springs k_{t21}, k_{t22} , as well as damping c_{t2} , provided by the serial dampers c_{t21}, c_{t22} , for the angular bending vibration rigid movement of the bowl regarding the axis Y_2 , provided by the following relations:

$$\begin{aligned}
k_{21} &= \frac{3EJ_{Z_2BA}}{L_{BA}^3}; k_{22} = \frac{3EJ_{z_2BB}}{L_{BB}^3}; k_2 = \frac{k_{21}k_{22}}{k_{21} + k_{22}}; c_2 = 2\zeta \sqrt{k_2 m_B} \\
kt_{21} &= \frac{GJ_{Y_2BA}}{L_{BA}}; kt_{22} = \frac{GJ_{y_2BA}}{L_{BA}}; kt_2 = \frac{kt_{21}kt_{22}}{kt_{21} + kt_{22}}; ct_2 = 2\zeta \sqrt{kt_2 I_{Y_2B}}
\end{aligned} \tag{4.9}$$

where m_B is the bowl's mass;

4. The tulip–tripod joint in FBV movement (see Figures 4.3.a and 4.3.b) realizes the elastic link between the tulip and the midshaft through the stiffness k_{tTr} and the damping c_{tTr} for the vibrating bending movements concerning the Z_2 axis and the angular stiffness k_{tTr} and angular damping c_{tTr} for the vibrating bending movements concerning Y_2 axis;

5. The bowl–inner race joint in FBV movement (see figures 3.a and 3.b) realizes the link between the bowl and the midshaft through the stiffness k_{lrB} and the damping c_{lrB} for the vibrating bending movements concerning the Z_2 axis and the angular stiffness k_{ttrB} and the angular damping c_{ttrB} for the vibrating bending movements relating to the Y_2 axis. The wheel induces excitations as a moderate impulsive shock force F_s acting in the Z_2 direction, and the excitation load can be expressed as

$$F_S = \bar{F}_S [1 + q_3 t^{q_1} e^{-q_2 t}] \tag{4.10}$$

where \bar{F}_S is the amplitude of the shock on the bowl's longitudinal axis X_3 transmitted from the wheel axis and $q_i, i = \overline{1,3}$, are experimental constants, depending on the type of shock applied at the wheel by the road excitation [G.R.14] (pp. 142–172).

For the DMFFBV movements of AD elements presented in Figures 4.3.a and 4.3.b, using Hamilton's principle [G.R.2] yields

$$\delta \int_{P_1, P_2} L(q_1, \dots, q_n, \dot{q}_1, \dots, \dot{q}_n, t) dt = 0 \quad (4.11)$$

where Lagrange's function $L(q_1, \dots, q_n, \dot{q}_1, \dots, \dot{q}_n, t)$ depends on the generalized coordinates q_1, \dots, q_n and the generalized velocities $\dot{q}_1, \dots, \dot{q}_n$, while P_1, P_2 are two points in the spatial configurations $(\overline{q_1, \dots, q_n}) = \Xi(q_1, \dots, q_n)$. The following equation gives the Lagrange's function:

$$L = T + \Pi \quad (4.12)$$

where the potential energy Π for the DMFFBV movements of AD elements (see Figures 4.3.a and 4.3.b) is given by the following generalized equation [G.R.2](pp. 371–376), [G.R.25](pp. 734–739).

$$\begin{aligned} \Pi = & \frac{1}{2} \int_0^{L_{Ms}} \left[EJ_{Y_2 Ms} \left(\frac{\partial \phi_2}{\partial x} \right) + kAG \left(\frac{\partial w_2}{\partial x} - \phi_2 \right)^2 \right] dx + \frac{1}{2} \left[c_1 \left(\dot{w}_1 \right)^2 + c_2 \left(\dot{w}_3 \right)^2 + c_{t1} \left(\dot{\phi}_1 \right)^2 + c_{t2} \left(\dot{\phi}_3 \right)^2 \right] + \\ & + \frac{1}{2} \left[c_{Tr} \left(\dot{w}_1 - \frac{\partial w_2}{\partial t}(0, t) \right)^2 \right] + c_{Tr} \left(\phi_1 \cos \beta_1 - \frac{\partial \phi_2}{\partial t}(0, t) \right)^2 + c_{IrB} \left(\frac{\partial w_2}{\partial t}(L_{Ms}, t) - \dot{w}_3 \right)^2 + c_{IrB} \left(\frac{\partial \phi_2}{\partial t}(L_{Ms}, t) - \dot{\phi}_3 \cos \beta_2 \right)^2 + \\ & + \frac{1}{2} \left[k_1 w_1^2 + k_2 w_3^2 + k_{t1} \phi_1^2 + k_{t2} \phi_3^2 \right] + \\ & + \frac{1}{2} \left[k_{Tr} \left(w_1 - w_2(0, t) \right)^2 + k_{Tr} \left(\phi_1 \cos \beta_1 - \phi_2(0, t) \right)^2 + \right. \\ & \left. + k_{IrB} \left(w_2(L_{Ms}, t) - w_3 \right)^2 + k_{IrB} \left(\phi_2(L_{Ms}, t) - \phi_3 \cos \beta_2 \right)^2 \right] \end{aligned} \quad (4.13)$$

where A is the cross-section area of the midshaft, $w_2(x, t)$ is the bending deflection (including the shear deformation) of the midshaft concerning the Z_2 axis, $\phi_2(x, t)$ is the rotation of the cross-section of the midshaft, and concerning the Y_2 axis, due only to the pure bending deflection, k is the shear correction factor, which in the literature [R.C.4.3] is in the range of 0.64–0.846, L_{Ms} is the length of the midshaft, and $J_{Y_2 Ms}$ is the geometric moment of inertia of the midshaft concerning the Y_2 direction given by the following equations:

$$J_{Y_2 Ms} = \frac{\pi d_{Ms}^4}{64}, J_{Y_2 Ms} = \frac{\pi(d_{eMs}^4 - d_{iMs}^4)}{64} \quad (4.14)$$

Energia cinetică a mișcărilor de încovoiere forțată sau bazată pe un model dinamic de mișcări ale elementelor arborilor planetari este dată de următoarea ecuație generalizată [G.R.2](p. 374), [G.R.25](p. 721):

$$\begin{aligned} T = & \frac{1}{2} m_T \dot{w}_1^2 + \frac{1}{2} m_{Tr} \left(\frac{\partial w_2}{\partial t}(0, t) \right)^2 + \frac{1}{2} m_B \dot{w}_3^2 + \frac{1}{2} m_{Ir} \left(\frac{\partial w_2}{\partial t}(L_{Ms}, t) \right)^2 + \frac{1}{2} I_{Y_2 T} \dot{\phi}_1^2 + \\ & + \frac{1}{2} I_{Y_2 Tr} \left(\frac{\partial w_2}{\partial t}(0, t) \right)^2 + \frac{1}{2} I_{Y_2 B} \dot{\phi}_3^2 + \frac{1}{2} I_{Y_2 Ir} \left(\frac{\partial \phi_2}{\partial t}(L_{Ms}, t) \right)^2 + \int_0^{L_{Ms}} \frac{1}{2} \left[\rho A \left(\frac{\partial w_2}{\partial t} \right)^2 + I_{Y_2 Ms} \left(\frac{\partial \phi_2}{\partial t} \right)^2 \right] dx \end{aligned} \quad (4.15)$$

where m_{Tr} is the mass of the tripod and m_{Ir} is the mass of the inner race (see Figures 4.3.a-4.3.b).

Several mathematical manipulations that include integration by parts of the nonlinear system of equations with partial derivatives of the second degree in the unknowns $w_1(t)$, $\Phi_1(t)$, $w_2(x, t)$, $\Phi_2(x, t)$, $w_3(t)$, $\Phi_3(t)$, yielding:

$$m_T \ddot{w}_1 + c_1 \dot{w}_1 + c_{TT} \left(\dot{w}_1 - \frac{\partial w_2}{\partial t}(0, t) \right) + k_1 w_1 + k_{TT} (w_1 - w_2(0, t)) = 0 \quad (4.16)$$

$$I_{Y_2T} \ddot{\phi}_1 + c_{t1} \dot{\phi}_1 + c_{tTr} \left(\dot{\phi}_1 \cos \beta_1 - \frac{\partial \phi_2}{\partial t}(0, t) \right) + k_{t1} \phi_1 + k_{tTr} (\phi_1 \cos \beta_1 - \phi_2(0, t)) = 0 \quad (4.17)$$

$$\rho A \frac{\partial^2 w_2}{\partial t^2} - kAG \left[\frac{\partial^2 w_2}{\partial x^2} - \frac{\partial \phi_2}{\partial x} \right] = 0$$

$$I_{Y_2Ms} \frac{\partial^2 \phi_2}{\partial t^2} - EJ_{Y_2Ms} \frac{\partial^2 \phi_2}{\partial t^2} - kAG \left(\frac{\partial w_2}{\partial x} - \phi_2 \right) = 0 \quad (4.18)$$

$$m_B \ddot{w}_3 + c_2 \dot{w}_3 + c_{tBr} \left(\dot{w}_3 - \frac{\partial w_2}{\partial t}(L_{Ms}, t) \right) + k_2 w_3 + k_{tBr} (w_3 - w_2(L_{Ms}, t)) = 0 \quad (4.19)$$

$$I_{Y_2B} \ddot{\phi}_3 + c_{t1} \dot{\phi}_3 + c_{tBr} \left(\dot{\phi}_3 \cos \beta_2 - \frac{\partial \phi_2}{\partial t}(L_{Ms}, t) \right) + k_{t2} \phi_3 + k_{tBr} (\phi_3 \cos \beta_2 - \phi_2(L_{Ms}, t)) = 0 \quad (4.20)$$

where the boundary conditions are

$$w_2(0, t) = 0, \frac{\partial \phi_2}{\partial x}(0, t) = 0, x = 0, w_2(L_{Ms}, t) = 0, \frac{\partial \phi_2}{\partial x}(L_{Ms}, t) = 0, x = L_{Ms} \quad (4.21)$$

$$c_{TT} \dot{w}_1 + k_{TT} w_1 - kAG \left(\frac{\partial w_2}{\partial x}(0, t) - \phi_2(0, t) \right) = 0$$

$$c_{tBr} \dot{w}_3 + k_{tBr} w_3 - kAG \left(\frac{\partial w_2}{\partial x}(L_{Ms}, t) - \phi_2(L_{Ms}, t) \right) = 0 \quad (4.22)$$

$$I_{Y_2Tr} \frac{\partial^2 \phi_2}{\partial t^2}(0, t) - c_{tTr} \left(\dot{\phi}_1 \cos \beta_1 - \frac{\partial \phi_2}{\partial t}(0, t) \right) - k_{tTr} (\phi_1 \cos \beta_1 - \phi_2(0, t)) = 0 \quad (4.23)$$

$$I_{Y_2Ir} \frac{\partial^2 \phi_2}{\partial t^2}(L_{Ms}, t) - c_{tBr} \left(\dot{\phi}_3 \cos \beta_2 - \frac{\partial \phi_2}{\partial t}(L_{Ms}, t) \right) - k_{tBr} (\phi_3 \cos \beta_2 - \phi_2(L_{Ms}, t)) = 0 \quad (4.24)$$

The system given by the equations (4.16–4.20) and the boundary conditions equations (4.21–4.24) represent the nonlinear dynamic behavior of the AD elements in FBV induced by shock force through the wheel by road excitations. Analyzing equation (4.18), it can be remarked that they represent a system of equations with partial derivatives for the bending-shearing vibrations of a uniform shaft that considers the effects of rotary inertia and shear deformation, with the midshaft being a Timoshenko beam. The boundary conditions are given by equations (4.21–4.24) and link the bending-shearing vibrations of the midshaft with the tulip and the bowl through the tulip–tripod and bowl–inner race joints, inducing the solutions of the system of equations (4.16–4.20) the following phenomena: the joints of the driveshaft are quasi-isometric [G.R.1, G.R.18], with the effect of geometric nonuniformity of the inertia characteristics of the joints that vary with the rigid

angle of rotation for each element of the driveshaft in the directions X_1, X_2, X_3 , the effects of the bending deflection and bending-twisting stiffness for the tulip and the bowl, the effects of the bending deflection and bending-twisting damping for each joint of the driveshaft, the rotary inertia effect in bending, and the shearing effect for the midshaft. The starting point to solve the system differential equations of the FBV movements (SDEOFBVM) (equations (4.16–4.20)) for the AD elements (ADEs) was to analyze the vibration mechanism of the midshaft as a Timoshenko beam simply supported at the ends (see Figure 4.4). For the midshaft element of the AD, it was considered that $f(x, t) = 0$.

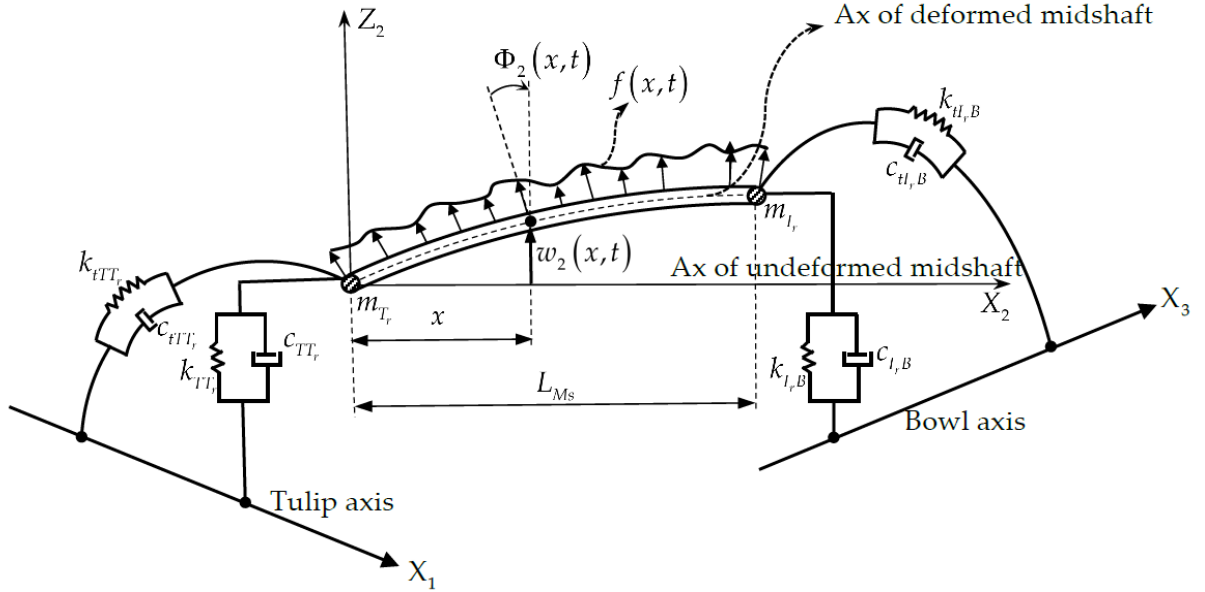


Fig. 4.4 The part of the DMFFBV for the midshaft [R.C.4.4]

The general solutions of equations (18) that satisfy the boundary conditions of equations (4.22) expressed in normalized bending deflection are [G.R.2] (p. 326–328).

$$w_2(\bar{x}, t) = \sin(n\pi\bar{x}) \left[0.1 \frac{F_s \Delta t_s}{\omega_{n1} L_{Ms} M} \sinh(\omega_{n1}, t) \right], \bar{x} = \frac{x}{L_{Ms}}, n = 1, 2, 3... \quad (4.25)$$

$$\phi_2(\bar{x}, t) = n\pi \cos(n\pi\bar{x}) \left(1 + \frac{\rho \omega_{n1}^2}{kG \left(\frac{n\pi}{L_{Ms}} \right)^2} \right) \left[0.1 \frac{F_s \Delta t_s}{\omega_{n1} L_{Ms} M} \sinh(\omega_{n1}, t) \right], \bar{x} = \frac{x}{L_{Ms}}, n = 1, 2, 3... \quad (4.26)$$

Injecting equations (4.25)-(4.26) in the boundary conditions (4.22) and the results in the equations (4.17) and (4.20), the equations (4.17) and (4.20) become the normalized differential equations in the time functions $w_1(t), w_3(t)$

$$\ddot{w}_1 + 2\xi_3 \Omega_3 \sqrt{\frac{1 - C_1 \cos(2\varphi_1)}{1 - C_2 \cos(2\varphi_1)}} \dot{w}_1 + \Omega_1^2 \frac{1 - C_1 \cos(2\varphi_1)}{1 - C_2 \cos(2\varphi_1)} w_1 = -\Gamma_1 w_1^3 - \Gamma_2 w_1^5 \quad (4.27)$$

$$\ddot{w}_3 + 2\xi_5 \Omega_3 \sqrt{\frac{1 - C_3 \cos(2\varphi_3)}{1 - C_4 \cos(2\varphi_3)}} \dot{w}_3 + \Omega_3^2 \frac{1 - C_3 \cos(2\varphi_3)}{1 - C_4 \cos(2\varphi_3)} w_3 = -\Gamma_3 w_3^3 - \Gamma_4 w_3^5 \quad (4.28)$$

where the natural frequency of the tulip in bending Ω_1 and the natural frequency of the bowl in bending Ω_3 are given by the following equations

$$\Omega_1 = \sqrt{\frac{3E}{m_T L_{TA}^3 \left(1 + \frac{b_1}{J_{Z_2TA}} (1 + a_1)\right)}}, a_1 = \frac{0.5(J_{1T} J_{2T})}{S_T \left[\frac{L_{TA}^2}{12} + d_{CT}^2\right]}, b_1 = S_T \left[\frac{L_{TA}^2}{12} + d_{CT}^2\right] \quad (4.29)$$

$$\Omega_3 = \sqrt{\frac{3E}{m_B L_{BA}^3 \left(1 + \frac{b_2}{J_{Z_2BA}} (1 + a_2)\right)}}, a_2 = \frac{0.5(J_{1B} J_{2B})}{S_B \left[\frac{L_{BA}^2}{12} + d_{CB}^2\right]}, b_2 = S_B \left[\frac{L_{BA}^2}{12} + d_{CB}^2\right] \quad (4.30)$$

The other terms in equations (4.27)-(4.28) are given by the expressions

$$C_1 = \frac{a_1}{1 + a_1} \chi_{nT}, C_2 = \frac{a_1 b_1}{J_{Z_2TA} (1 + a_1)} \chi_{nT}, C_3 = \frac{a_2}{1 + a_2} \chi_{nB}, C_4 = \frac{a_2 b_2}{J_{Z_2BA} b_2 (1 + a_2)} \chi_{nB} \quad (4.31)$$

$$\Gamma_1 = \frac{0.2\rho A \bar{F}_s \Delta t_s}{\pi 3! M m_T} \Omega_1, \Gamma_2 = \frac{0.2\rho A \bar{F}_s \Delta t_s}{\pi 5! M m_T} \Omega_1, \Gamma_3 = \frac{0.2\rho A \bar{F}_s \Delta t_s}{\pi 3! M m_B} \Omega_3, \Gamma_4 = \frac{0.2\rho A \bar{F}_s \Delta t_s}{\pi 5! M m_B} \Omega_3. \quad (4.32)$$

The authors used the AMA (asymptotic method approach) in the first-order approximation. This would allow the investigation of the nonlinear parametric dynamic stability for the FBV movement of the tulip and the bowl in the PPR region for both the stationary and nonstationary cases. The principal parametric resonance (PPR), defined by the excitation frequency $\eta \approx 2\Omega$ (almost twice the natural frequency of the system) is the most important resonance region, as mentioned in [G.R.16](p. 425). To compute the solutions of equations (4.27)-(4.28), it was assumed that the slowing time was $\tau = \varepsilon t$, where ε is a small positive parameter [R.C.4.1] (p. 299). To introduce the slowing time, equations (4.27)-(4.28) needed to be transformed to be used in the AMA. The coefficients of the second and third terms of equations (4.27)-(4.28) on the left side can be expressed as

$$\frac{1 - C_1 \cos(2\varphi_1)}{1 - C_2 \cos(2\varphi_1)} \approx 1 - 2 \cos(\theta_1), \sqrt{\frac{1 - C_1 \cos(2\varphi_1)}{1 - C_2 \cos(2\varphi_1)}} \approx 1 + \mu \cos(\theta_1), \mu = \frac{1}{2}(C_2 - C_1) \quad (4.33)$$

cu frecvențele de excitație η_1, η_3 , pentru lăua și bol în regiunea rezonanței parametrice principale (PPR) date de expresiile:

$$\eta_1 = 2\Omega_1 \approx \frac{d\theta_1}{dt} = \frac{d\varphi_1}{dt} \approx \omega_{n1}, \eta_3 = 2\Omega_3 \approx \frac{d\theta_3}{dt} = \frac{d\varphi_3}{dt} \approx \omega_{n1} \quad (4.34)$$

and $\frac{d\varphi_1}{dt}$ is the excitation induced in the FBV movement (equation (4.27)) by the rigid twisting angle of the tulip concerning the X_1 axis, and $\frac{d\varphi_3}{dt}$ is the excitation induced in the FBV movement (equation (4.28)) by the rigid twisting angle of the bowl concerning the X_3 axis. The assumption that the damping ratio ξ , the excitation coefficient μ , and the coefficients of cubic and quintic nonlinearity $\Gamma_1, \Gamma_2, \Gamma_3, \Gamma_4$ are small is incorporated in the analysis by representing these quantities in the following form:

$$\xi = \varepsilon \xi, \mu = \varepsilon \mu, \varepsilon \Gamma_1, \Gamma_2 = \varepsilon \Gamma_2, \Gamma_3 = \varepsilon \Gamma_3, \Gamma_4 = \varepsilon \Gamma_4, \quad (4.35)$$

where ε is the same small positive parameter used to obtain the slowing time. It is also assumed that the excitation frequency and the excitation parameter μ vary slowly with time, such that $\frac{d\theta_1}{dt} = \eta_1(\tau), \frac{d\theta_3}{dt} = \eta_3(\tau), \mu = \mu(\tau)$. Equations (4.26)-(4.27) become the following after neglecting the terms in ε^2 :

$$\begin{aligned} \ddot{w}_1 + \Omega_1^2 w_1 &= \varepsilon \left[-2\xi \Omega_1 \dot{w}_1 + 2\mu \Omega_1^2 \cos(\theta_1) w_1 - \Gamma_1 w_1^3 - \Gamma_2 w_1^5 \right], \\ \ddot{w}_3 + \Omega_3^2 w_3 &= \varepsilon \left[-2\xi \Omega_3 \dot{w}_3 + 2\mu \Omega_3^2 \cos(\theta_3) w_3 - \Gamma_3 w_3^3 - \Gamma_3 w_3^5 \right] \end{aligned} \quad (4.36)$$

Regarding equations (4.36), the right-hand side represent a perturbation of the mathematical form $H_1(w_1, \theta_1), H_3(w_3, \theta_3)$ being periodic functions in θ_1, θ_3 with period 2π , while the left-hand side of the equation is a linear oscillator. By considering all these physical considerations and confining our attention to the investigation of the PPR region, a solution for equations (4.36) is sought after in the following form to the first-order approximation in ε :

$$w_1 = w_1 \cos\left(\frac{1}{2}\theta_1 + \psi_1\right), w_3 = w_3 \cos\left(\frac{1}{2}\theta_3 + \psi_3\right), \quad (4.37)$$

where and W_1, W_3, Ψ_1, Ψ_3 are functions of time defined by the systems of differential equations

$$\left. \begin{aligned} \left\{ \begin{aligned} \frac{dW_1}{dt} &= \varepsilon A_1(\tau, W_1, \psi_1) \\ \frac{d\psi_1}{dt} &= \Omega_1 - \frac{1}{2}\eta_1(t) + \varepsilon \beta_1(\tau, W_1, \psi_1) \end{aligned} \right\} \left\{ \begin{aligned} \frac{dW_3}{dt} &= \varepsilon A_3(\tau, W_3, \psi_3) \\ \frac{d\psi_3}{dt} &= \Omega_3 - \frac{1}{2}\eta_3(t) + \varepsilon \beta_3(\tau, W_3, \psi_3) \end{aligned} \right\} \end{aligned} \right\} \quad (4.38)$$

Using equations (4.37) and (4.38) in the primary form of equations (36), equating the terms of the form $\varepsilon \cos\left(\frac{1}{2}\theta_j + \psi_j\right), \varepsilon \sin\left(\frac{1}{2}\theta_j + \psi_j\right), j=1,3$ from the left-hand side of equations (36) with the same terms from the right-hand side of the same equation and neglecting the overtones yields the solutions of the systems (38)

$$\left. \begin{aligned} \left\{ \begin{aligned} \frac{dW_1}{dt} &= -\frac{\mu \Omega_1^2}{\eta_1} \sin 2\psi_1 - \xi \Omega_1 W_1 \\ \frac{d\psi_1}{dt} &= \Omega_1 - \frac{1}{2}\eta_1 - \frac{\mu \Omega_1^2}{\eta_1} \cos 2\psi_1 + \frac{3}{8} \frac{\Gamma_1 W_1^2}{\Omega_1} + \frac{5}{16} \frac{\Gamma_2 W_1^4}{\Omega_1} \end{aligned} \right\}, \\ \left\{ \begin{aligned} \frac{dW_3}{dt} &= -\frac{\mu \Omega_3^2}{\eta_3} \sin 2\psi_3 - \xi \Omega_3 W_3 \\ \frac{d\psi_3}{dt} &= \Omega_3 - \frac{1}{2}\eta_3 - \frac{\mu \Omega_3^2}{\eta_3} \cos 2\psi_3 + \frac{3}{8} \frac{\Gamma_1 W_3^2}{\Omega_3} + \frac{5}{16} \frac{\Gamma_2 W_3^4}{\Omega_3} \end{aligned} \right\} \end{aligned} \right\} \quad (4.39)$$

The investigation of the dynamic instability of the FBV movement for the tulip and bowl represents the computation of the boundaries of the principal parametric region of instability. The base width of the stationary response is the only region in which vibrations may typically initiate. Setting to

zero the amplitudes in the systems of equations (4.39) yields the following equations:

$$\begin{aligned} \left(\frac{\eta_1}{2\Omega_1}\right)^2 - 2\left(\frac{\eta_1}{2\Omega_1}\right)^3 + (1 + \xi^2)\left(\frac{\eta_1}{2\Omega_1}\right)^2 - \frac{\mu^2}{4} &= 0 \\ \left(\frac{\eta_3}{2\Omega_3}\right)^4 - 2\left(\frac{\eta_3}{2\Omega_3}\right)^3 + (1 + \xi^2)\left(\frac{\eta_3}{2\Omega_3}\right)^2 - \frac{\mu^2}{4} &= 0 \end{aligned} \quad (4.40)$$

Equations (4.40) give the boundaries of the principal parametric region of stationary dynamic instability in the space $\left(\frac{\eta_1}{2\Omega_1}, \xi, \mu\right)$ for the tulip and in the space $\left(\frac{\eta_3}{2\Omega_3}, \xi, \mu\right)$. This is the investigation of

the stationary FBV movement of the tulip and the bowl. For the nonstationary FBV movement of the tulip and the bowl, the analysis of the dynamic instability consisted of analyzing the graphed representation in the configuration space of the “speed” nonstationary amplitudes versus the nonstationary amplitudes $\left(\frac{dW_1}{dt}, W_1\right), \left(\frac{dW_3}{dt}, W_3\right)$, that is the evidence of the transition of FBV

movement for the tulip and the bowl through the chaotic movement in the PPR region, and the results are presented in the next paragraph.

Figure 4.5a,b illustrates the stationary dynamic instability region of the tulip in the space (η_1, ξ, μ) using equations (4.40). When analyzing Figure 4.5a,b, it can be noticed that the two folded surfaces obtained were symmetrical concerning the plan given by (η_1, ξ) for the excitation frequency and the damping ratio. In contrast, the excitation coefficient μ could be positive or negative. The folded surface of the dynamic instability “kept” inside the two branches the region where it manifested the stationary instability. It can also be seen that increasing the damping ratio had a stabilizing effect on the dynamics of the tulip, as expected. Figure 4.6a,b illustrates the stationary dynamic instability region of the bowl in the space (η_3, ξ, μ) using equations (4.40).

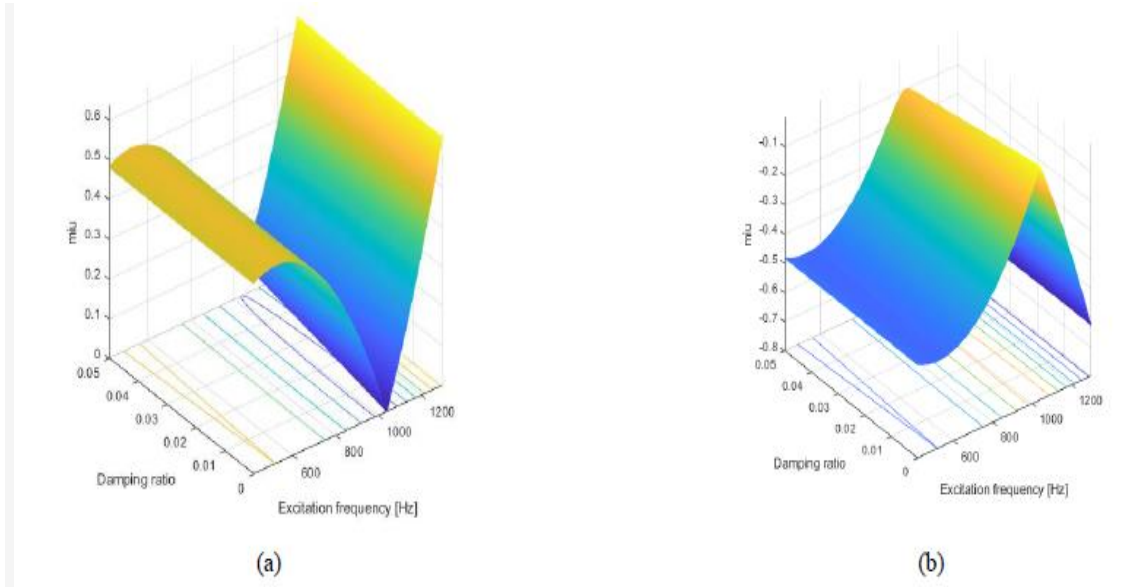


Fig. 4.5. Stationary dynamic instability surface frontier for the tulip.a. $\mu > 0$, b. $\mu < 0$ [R.C.4.4]

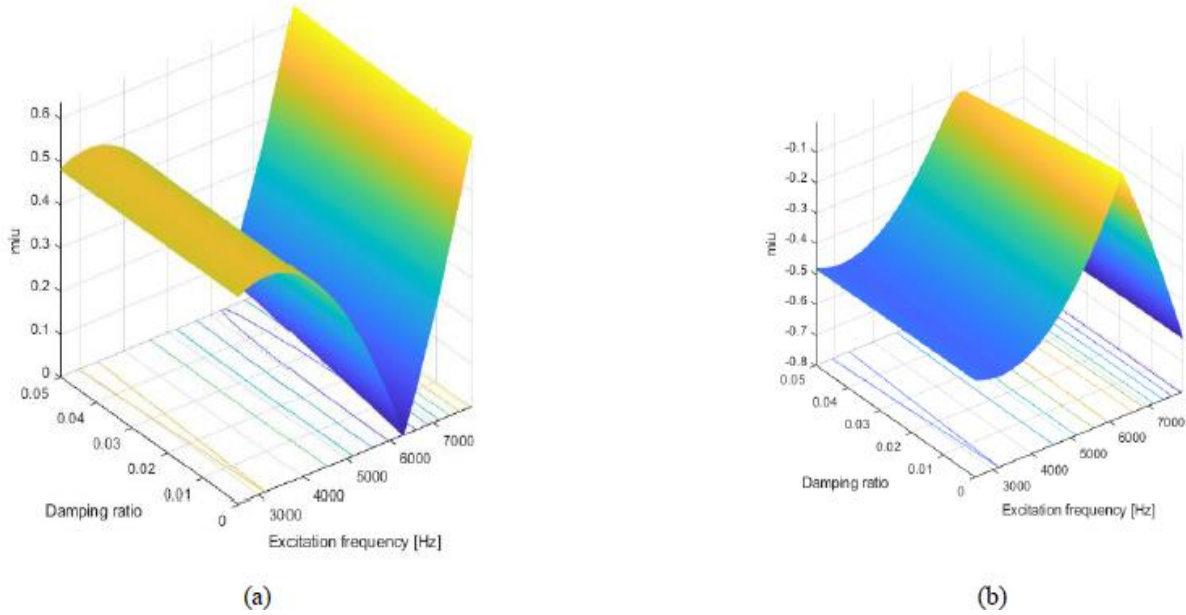


Fig. 4.6. Stationary dynamic instability surface frontier for the bowl. a. $\mu > 0$, b. $\mu < 0$ [R.C.4.4]

By analyzing Figure 4.6a,b, it can be noticed that the two folded surfaces obtained were symmetrical concerning the plan given by (η_3, ξ) for the excitation frequency and the damping ratio, while the excitation coefficient μ could be positive or negative. The folded surface of the dynamic instability “kept” inside the two branches the region where it manifested the stationary instability for the bowl. It can also be seen that increasing the damping ratio had a stabilizing effect on the dynamic of the bowl, as expected. The only difference between these phenomena for the bowl was that the manifestation was in another range frequency than that of the tulip: the range frequency given by the natural frequency of the bowl in bending. Figure 4.7 illustrates the graphs of the phase space $\left(w_1, \frac{dw_1}{dt} \right)$ for the nonstationary FBV movements of the tulip in the PPR region.

Figure 4.8 shows the charts of the phase space $\left(w_3, \frac{dw_3}{dt} \right)$ for the nonstationary FBV movements of the bowl in the PPR region. By analyzing the graphs in Figure 4.7, a transition to chaotic behavior for the FBVM (FBV movements) of the tulip due to the presence of limit cycles or even of strange attractors can be seen, but this last conclusion needs to be certified by detailed analysis using the methods of chaotic movements. One evident aspect is that the transition through the PPR region for the tulip was an unstable one. When analyzing the graphs in Figure 4.8, the same manifestation for the bowl as for the tulip (see Figure 4.7) can be seen, that being a transition to chaotic behavior for the FBVM of the bowl due to the presence of limit cycles or even strange attractors. However, this last conclusion needs to be certified by detailed analysis using the methods of chaotic movements. This manifestation is valid only in the damping ratio range of 0.0016–0.0096. One aspect that is evident is how the transition through the PPR region for the bowl was also an unstable one. Unfortunately, no published studies analyze in detail the dynamic behavior of each element of the AD for the FBVM (the tulip, bowl, and midshaft) apart from [G.R.14], as all the studies analyzed the global dynamic behavior of the automotive driveshaft.

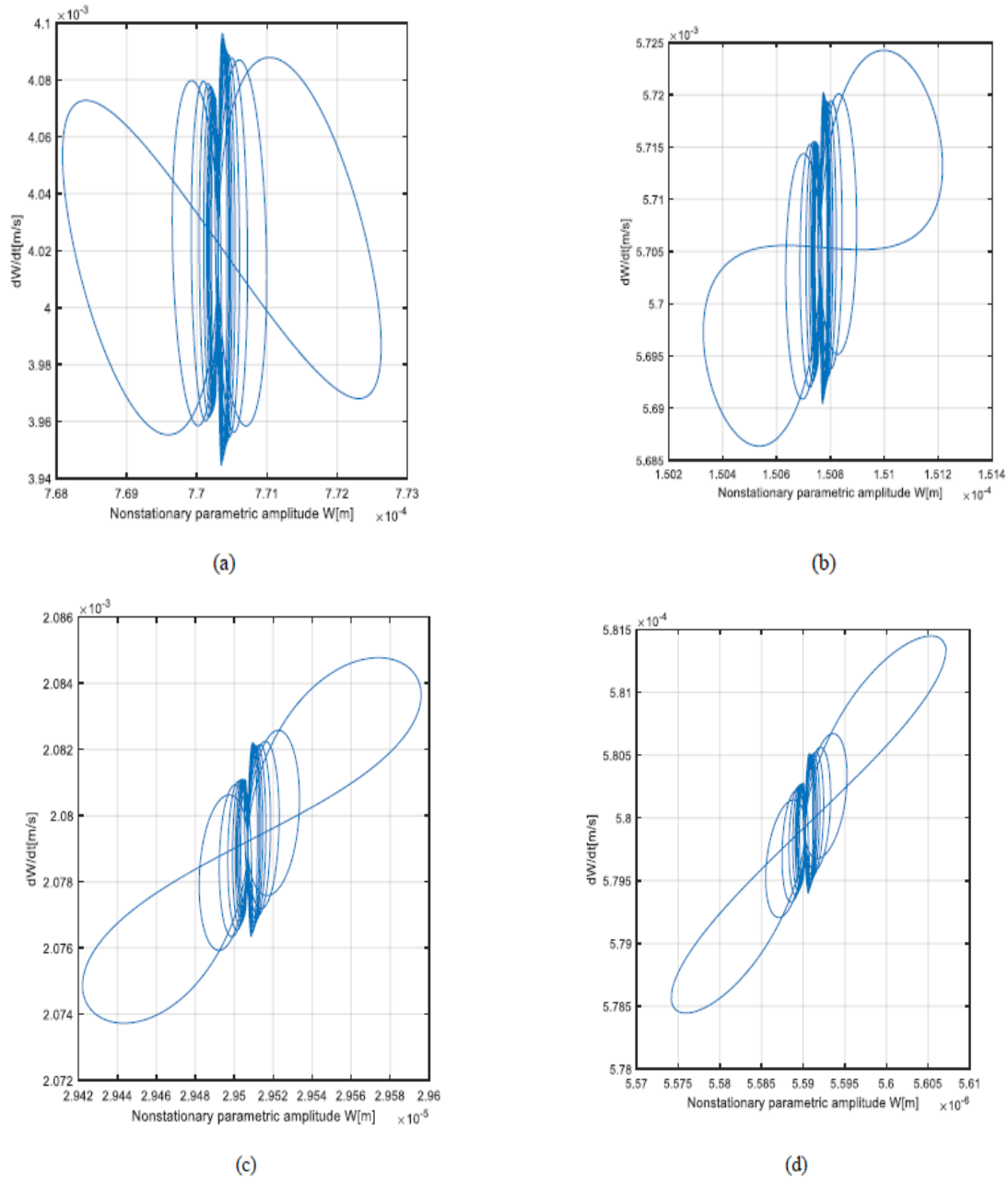


Fig. 4.7. Phase space of the tulip for $\mu = 0,623 \times 10^{-4}$. (a) $\zeta = 0,0016$. (b) $\zeta = 0,0116$. (c) $\zeta = 0,0216$. (d) $\zeta = 0,0318$. [R.C.4.4]

As can be seen from this chapter, the use of AMA coupled with Hamilton's principle allowed the investigation of the stationary motion for the FBV movements of an AD's tulip and bowl in the PPR region by computing the dynamic instability frontiers (see Figures 4.5-4.6) in the PPR region. In the meantime, the use of the AMA coupled with Hamilton's principle allowed the investigation of the nonstationary motion for the FBV movements of an AD's tulip and bowl in the transition through a PPR region by computing the velocity amplitude versus the amplitude in the phase space (see Figures 4.7-4.8). Figures 4.7-4.8 allowed the investigation of the dynamic instability in the transition through the PPR region. As is noted in Figures 4.7-4.8, the transition to the PPR region

had an aspect of chaotic manifestation. To check whether this nonstationary dynamic behavior is deterministic chaos or a stochastic process, it would be necessary to use Lyapunov's exponents method coupled with the Poincare map method.

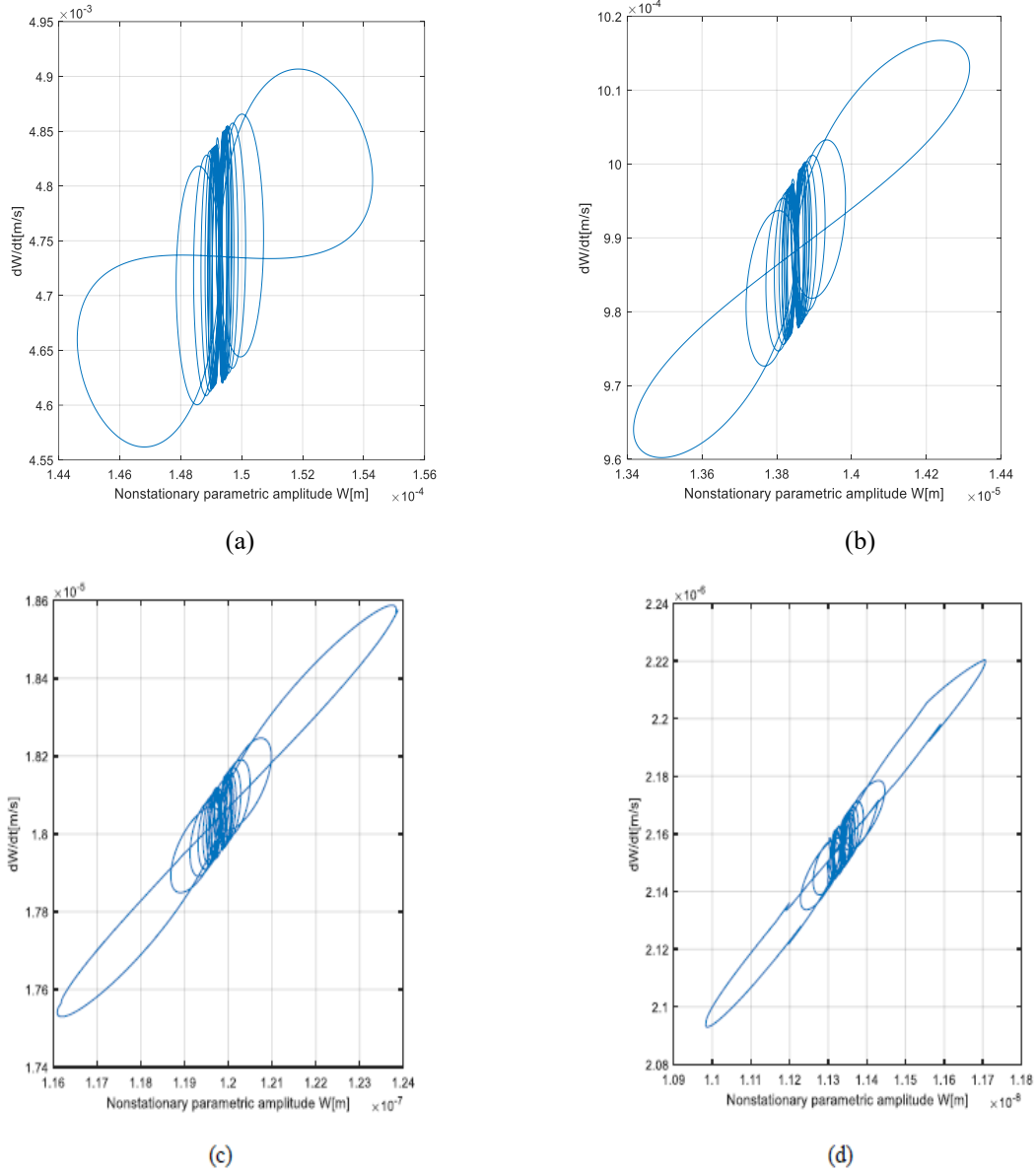


Fig. 4.8. Phase space of the bowl for $\mu = 0,754 \times 10^{-4}$. (a) $\zeta = 0,0016$. (b) $\zeta = 0,0036$. (c) $\zeta = 0,0076$. (d) $\zeta = 0,0096$. [R.C.4.4]

The present chapter introduces a newly designed DMFFBVM for the AD, with the following phenomena being included for the first time: nonuniformity of the inertial characteristics of the AD's elements, serial stiffness and damping for the tulip and bowl, shock excitation due to the road geometry, and nonuniformity of the kinematic isometry. Based on this newly designed DMFFBVM, using Hamilton's principle coupled with the first-order approximation of the AMA, the stationary and nonstationary dynamic instability behavior of the AD elements were investigated in detail by computing the following: the dynamic instability frontiers were determined for the first

time for the stationary FBV movements of the tulip and bowl in the parametric spaces (η_1, ξ, μ) , (η_3, ξ, μ) , in addition, for the first time, the velocity amplitude versus the amplitude was determined for the nonstationary FBV movements of the tulip and bowl in transition through the PPR region. Agreements were found with the numerical and experimental data in the literature concerning the natural free frequency in bending and the manifestation of beating effects that conduct pitting and micro-cracking effects. Therefore, this DMFFBVM of the AD elements coupled with Hamilton's principle and first-order approximation of the AMA can predict an AD's durability in the early design stages. Moreover, the DMFFBVM must be added to the design algorithm for predicting the comfort elements of automobiles.

Chapter 5. Chaotic manifestation of the automotive driveshaft's forced bending vibrations

To investigate the chaotic forced bending vibrations of the automotive driveshaft it is necessary first to adopt an appropriate dynamic model that describes such dynamic behavior. Such a dynamic model was already realized in previous works by the authors, and therefore, based on the dynamic equations already obtained it was used a complex method developed by the authors based on two elements: chaos manifestation detection, and chaos manifestation confirmation. The chaotic manifestation detection consists of using the time-history graphs in a specific resonance region namely the principal parametric region. For the same region was applied the Maximum Lyapunov Exponents Method (MLEM) was coupled with the contraction criterion for the sum of Lyapunov exponents that certifies the chaos. In addition, was applied the Poincaré Map as a qualitative method to reconfirm chaos manifestation. Thus, a powerful analytical tool was created to investigate the chaotic forced bending vibrations for specific conditions in the principal parametric resonance's area (PPRA). The chapter represents a development of previous research carried out by the authors [G.R.18, G.R.26, G.R.28] concerning the dynamic behavior of automotive driveshafts. The automotive driveshafts are homokinetic transmission elements for cars from gearboxes or differential boxes to the wheels, being important elements of the automotive's driveline. The author has already shown that geometric and kinematic isometry of the automotive driveshafts have nonuniformities [G.R.18] and therefore, all the dynamic models must consider this aspect [G.R.26], [G.R.28]. The present chapter considers the same dynamic model for the forced bending vibrations of the automotive driveshaft, as in Chapter 4 (see Figure 4.2), involving the following physical aspects:

- a. geometric and kinematic nonuniformities from the isometry property of the tulip, bowl, and midshaft as elements of the driveshaft,
- b. due to the rigidity imposed by technical demands the tulip and the bowl have rigid body deflections and rotations ($w_1 / w_3, \phi_1 / \phi_3, \varphi_1 / \varphi_3$ -tulip/bowl deflections and rotations, as shown in Figure 4.2, while the midshaft is considered as a continuum media namely as a simply supported Timoshenko beam with mass, springs, and dampers at both ends having continuous functions w_2, ϕ_2, φ_2 respectively midshaft deflections and rotations;
- c. the excitations are induced by the impact road shocks transmitted through automotive wheels generated by road nonuniformities [G.R.17].

Based on Hamilton's principle[G.R.28], it was derived the forced bending vibrations equations using the previous assumptions. Starting from this point the present paper's analysis is devoted to detecting and certifying chaotic FBV (forced bending vibrations) for the automotive driveshaft elements in the PPRA (principle parametric resonance's area). Mazzei and Scott analyze in [R.C.5.2] the nonlinear dynamic behavior of automotive driveshaft elements in the PPRA. The experimental confirmation that one of the most important resonance areas for the FBV of automotive driveshafts is the PPRA was done by Steinwede in [G.R.14]. The detection of chaotic FBV in the PPRA will be performed using the general equations of FBV for a heavy-duty automotive driveshaft designed for an SUV (sports utility vehicle) having a permanent 4-WD (four-wheeler drive). This will imply the determination of the phase portraits for the tulip and the bowl in the PPRA. The certification of chaotic FBV manifestation in the PPRA implies the computation of Lyapunov exponents, namely the use of the Maximum Lyapunov Exponents Method (MLEM) for a modified system of equations for FBV of the automotive driveshaft elements (tulip and bowl)

followed using the contraction criterion: *the sum of all Lyapunov exponents is negative* for tulip/bowl, as stated in [G.R.29]. As a supplementary confirmation of chaotic FBV manifestation for the tulip/bowl in the PPRA, it was computed Poincaré Maps for the tulip/bowl in the PPRA so that the pictures of Poincaré Maps have the property of *the system's auto-similarity*, also mentioned in [G.R.29] as a qualitative method for chaos manifestation.

To calculate the equations of FBV for the tulip/bowl of the automotive driveshaft it is mandatory to reduce the mass inertial moments and the geometric inertial moments of the tulip/bowl to the cartesian system of reference (CSR) $X_2Y_2Z_2$ of the midshaft as in [G.R.28]. All the inertial characteristics of the tulip and the bowl, respecting the schematic representation shown in Figure 4.2, are presented in Chapter 4, as described in the paper [G.R.28]. The dynamic model of FBV for the tulip is presented in Chapter 4 (see Figure 4.3.a), while the dynamic model of FBV for the bowl is also presented in Chapter 4 (see Figure 4.3.b), being adopted with those stated in the paper [G.R.28]. The equation of the FBV in normalized bending deflection for the tulip is [G.R.28](pp. 13, 14)

$$\ddot{w}_1 + 2\xi\Omega_1 \sqrt{\frac{1-C_1 \cos(2\varphi_1)}{1-C_2 \cos(2\varphi_1)}} \dot{w}_1 + \Omega_1^2 \frac{1-C_1 \cos(2\varphi_1)}{1-C_2 \cos(2\varphi_1)} w_1 = -\Gamma_1 w_1^3 - \Gamma_2 w_1^5 \quad (5.1)$$

while the equation of the FBV in normalized bending deflection for the bowl is [G.R.28](pp. 13, 14)

$$\ddot{w}_3 + 2\xi\Omega_3 \sqrt{\frac{1-C_3 \cos(2\varphi_3)}{1-C_4 \cos(2\varphi_3)}} \dot{w}_3 + \Omega_3^2 \frac{1-C_3 \cos(2\varphi_3)}{1-C_4 \cos(2\varphi_3)} w_3 = -\Gamma_3 w_3^3 - \Gamma_4 w_3^5. \quad (5.2)$$

The constants C_i , Γ_i and the natural frequencies for the tulip in bending Ω_1 and for the bowl in bending Ω_3 are expressed in Chapter 4 as stated in the paper [G.R.28]. The terms that induce the forced excitations in the PPRA contain for the tulip Ω_1 , $\cos(2\varphi_1)$ and for the bowl Ω_3 , $\cos(2\varphi_3)$ and must satisfy the equations [G.R.16](pp. 199, 425)

$$\eta_1 = 2\Omega_1 = \frac{2d\varphi_1}{dt}, \eta_3 = 2\Omega_3 = \frac{2d\varphi_3}{dt} \quad (5.3)$$

where η_1 is the tulip's excitation frequency and η_3 is the bowl's excitation frequency. To use equations (5.1) and (5.2) it is mandatory to compute the tulip's geometry characteristics J_{1T}, J_{2T} , and the bowl's geometry characteristics J_{1B}, J_{2B} based on their general geometry. This was done using the AUTOCAD software, and the results presented in Table 1 are like the data in [G.R.28](pp. 15,19).

Tabel 5.1. Tulip's/Bowl's geometry characteristics and material properties & shock's amplitude/time

$0.5(J_{1T}+J_{2T})$ [m ⁴]	$0.5(J_{1B}+J_{2B})$ [m ⁴]	χ_{nT}/χ_{nB}	ρ [kg/m ³]	E/G [GPa]	ξ	$F_s/\Delta t_s$
9.1531×10^{-7}	10.560×10^{-7}	0.25/0.10	7850	200/77.3	(16-318)10 ⁻⁴	0.5/1...10

Tabel 5.1 illustrates the material properties of the tulip/bowl as well as the values of the shock's amplitude and the shock's duration. Comparing the data in Table 1 with those used by

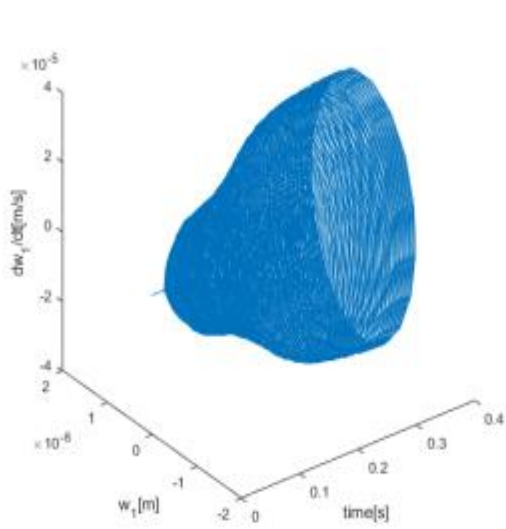
Steinwede in his experiments [G.R.14](p. 111) it can be remarked the agreements. For the tulip, the PPRA is defined by a range around the value 1038.38 Hz, the natural bending frequency being $v_1 = 519,19$ Hz[G.R.28](p. 19-20). For the bowl, the bowl's PPRA is defined by a range around the value 6306.6 Hz, the natural bending frequency being $v_3 = 3153,3$ Hz [G.R.28](p. 19-20).

To determine the time phase portraits for the tulip and the bowl in FBV is mandatory to modify the equations (5.1) and (5.2), which become the systems

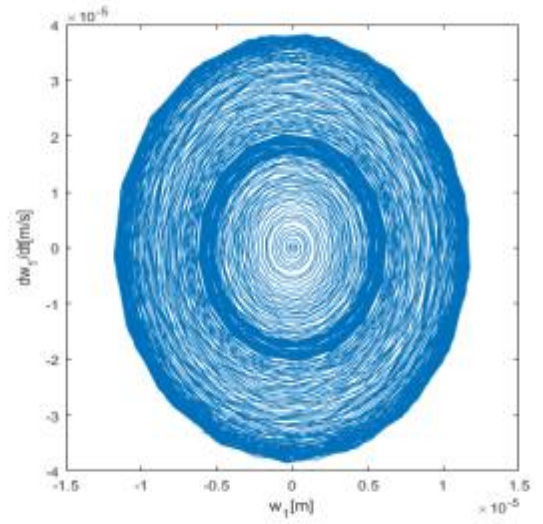
$$\begin{cases} \frac{dw_1}{dt} = V_{w_1}, \\ \frac{d\Theta_1}{dt} = \frac{d\theta_1}{dt} = \eta_1, \Theta_1 = d\theta_1, \\ \frac{dV_{w_1}}{dt} = -2\xi\Omega_1 \sqrt{\frac{1-C_1 \cos(\Theta_1)}{1-C_2 \cos(\Theta_1)}} V_{w_1} - \Omega_1^2 \frac{1-C_1 \cos(\Theta_1)}{1-C_2 \cos(\Theta_1)} w_1 - \Gamma_1 w_1^3 - \Gamma_2 w_1^5 \end{cases} \quad (5.4)$$

$$\begin{cases} \frac{dw_3}{dt} = V_{w_3}, \\ \frac{d\Theta_3}{dt} = \frac{d\theta_3}{dt} = \eta_3, \Theta_3 = d\theta_3, \\ \frac{dV_{w_3}}{dt} = -2\xi\Omega_3 \sqrt{\frac{1-C_3 \cos(\Theta_3)}{1-C_4 \cos(\Theta_4)}} V_{w_4} - \Omega_3^2 \frac{1-C_3 \cos(\Theta_3)}{1-C_4 \cos(\Theta_3)} w_3 - \Gamma_3 w_3^3 - \Gamma_4 w_3^5 \end{cases} \quad (5.5)$$

Using the MATLAB software, it was computed the time phase portraits of the tulip's FBV and the bowl's FBV in the PPRA are presented in Figures 5.1-5.4. Analyzing the phase portraits of the tulip's FBV (see Fig. 5.1.b, Fig. 5.2.b) it can be concluded that a chaotic FBV for the tulip is manifested in the range $\xi = 0.0016 - 0.0216$ of the damping ratio, while the increase with 0.02 of the damping ratio induces a decrease of the tulip's bending deflection w_1 more than ten times. Also, the same increase of the damping ratio induces a decrease of the tulip's velocity bending deflection $\frac{dw_1}{dt}$ more than six times. Analyzing the time history of the tulip's phase portraits in the PPRA(see Fig. 5.1.a and 5.2.a) it is obvious the manifestations of beating effects specific to chaos[G.R.30], [R.C.5.3]. Analyzing the phase portraits of the bowl's FBV (see Fig. 5.3.b, Fig. 5.4.b) it can be concluded that a chaotic FBV for the bowl is manifested in the same range $\xi = 0.0016 - 0.0216$ of the damping ratio, while the increase with 0.02 of the damping ratio induces a decrease of the bowl's bending deflection w_3 more than ten times. Also, the same increase of the damping ratio induces a decrease of the bowl's velocity bending deflection $\frac{dw_3}{dt}$ more than six times. Analyzing the time history of the bowl's phase portraits in the PPRA (see Fig. 5.3.a and 5.4.a) it is obvious the manifestations of beating effects specific to chaos[R.G.27].

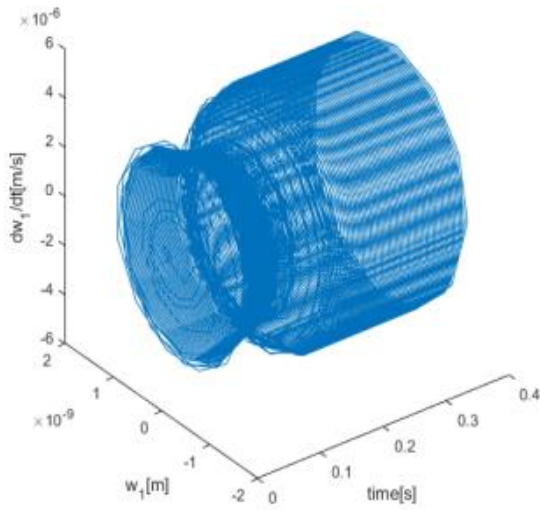


a.

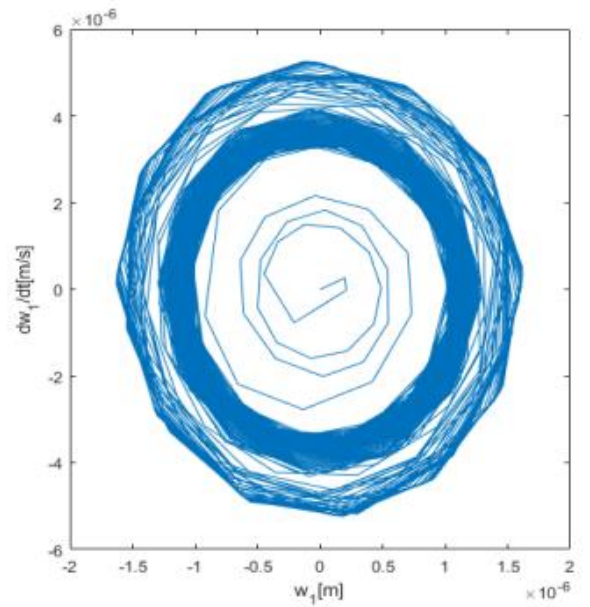


b.

Fig. 5.1 Time-history (phase portraits) of the tulip's FBV $\chi_{nT}=0,25$; $\xi=0,0016$ [G.R.30]

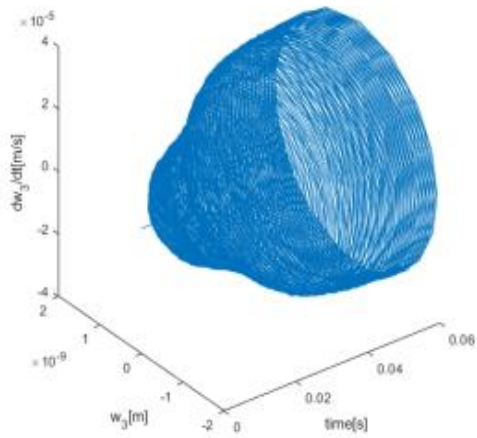


a.

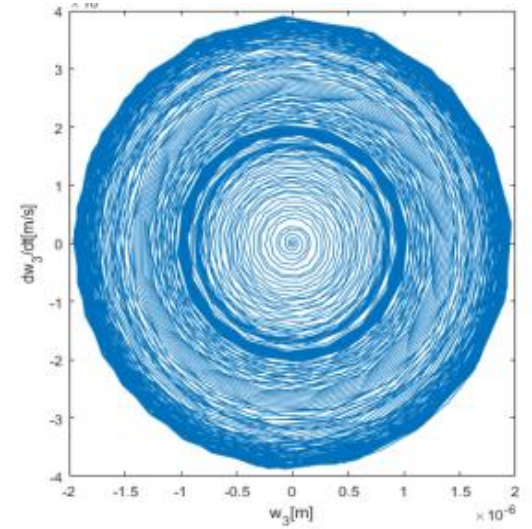


b.

Fig. 5.2 Time-history (phase portraits) of the tulip's FBV $\chi_{nT}=0,25$; $\xi=0,0216$ [G.R.30].

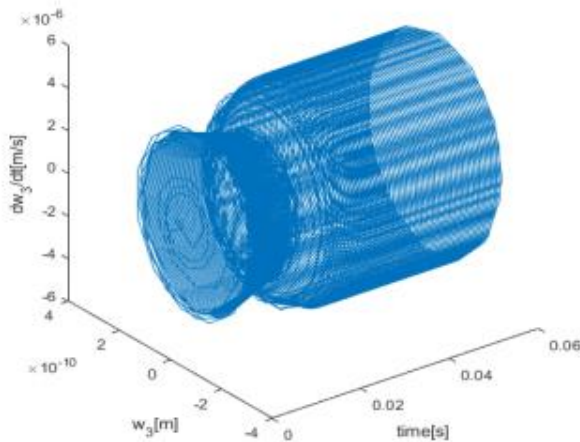


a.

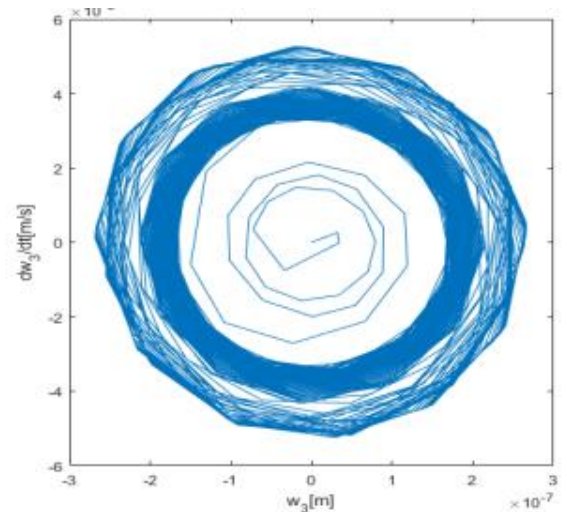


b.

Fig. 5.3 Time-history (phase portraits) of the bowl's FBV $\chi_{nT}= 0,25$; $\xi= 0,0016$ [G.R.30]



a.



b.

Fig. 5.4 Time-history (phase portraits) of the bowl's FBV $\chi_{nT}= 0,25$; $\xi= 0,0216$ [G.R.30]

If we compare the results illustrated in Figures 5.1 and 5.2 for the tulip's FBV with those illustrated in Figures 5.3 and 5.4 for the bowl's FBV it can be remarked an accentuation of the beating effects for the bowl for the damping ratio around the value 0.0016 (see Fig. 5.1.b and Fig. 5.3.b) and a similar manifestation of time-history for the tulip's FBV and the bowl's FBV for the damping ratio around the value 0.0216 (see Fig. 5.2.a and Fig.5.4.a) [G.R.30], [B.C.5.3].

The Lyapunov exponents computed based on the system (4), that describes the tulip's FBV in the tulip's PPRA (the excitation frequency of the tulip is in the range around 1038.38 Hz[G.R.28]) are given by the equations [G.R.12](p. 306-307)

$$\begin{aligned}
L_{11} &= \frac{1}{T_f} \sum_{i=1}^N \log_{10} \frac{|(w_1 - w_1^p)^{T_i}|}{\left\| (w_1, V_{w_1}, \Theta_1)^{T_i} - (w_1^p, V_{w_1}^p, \Theta_1^p)^{T_f} \right\|} \\
L_{21} &= \frac{1}{T_f} \sum_{i=1}^N \log_{10} \frac{|(V_{w_1} - V_{w_1}^p)^{T_i}|}{\left\| (w_1, V_{w_1}, \Theta_1)^{T_f} - (w_1^p, V_{w_1}^p, \Theta_1^p)^{T_f} \right\|} \\
L_{31} &= \frac{1}{T_f} \sum_{i=1}^N \log_{10} \frac{|(\Theta_1 - \Theta_1^p)^{T_i}|}{\left\| (w_1, V_{w_1}, \Theta_1)^{T_f} - (w_1^p, V_{w_1}^p, \Theta_1^p)^{T_f} \right\|}
\end{aligned} \tag{5.6}$$

where the superscript p indicates the perturbed solution on an interval break (T_i, T_{i+1}) , T_f is the final time of integration and N is the number of intervals contained in the time range $(0, T_f)$. The Lyapunov exponents computed based on the system (5.5), that describes the bowl's FBV in the bowl's PPRA (the excitation frequency of the bowl is in the range around 6306.6 Hz[G.R.28]) are given by the similar equations, with the same signification of the superscripts previously described,

$$\begin{aligned}
L_{13} &= \frac{1}{T_f} \sum_{i=1}^N \log_{10} \frac{|(w_3 - w_3^p)^{T_i}|}{\left\| (w_3, V_{w_3}, \Theta_3)^{T_f} - (w_3^p, V_{w_3}^p, \Theta_3^p)^{T_f} \right\|} \\
L_{23} &= \frac{1}{T_f} \sum_{i=1}^N \log_{10} \frac{|(V_{w_3} - V_{w_3}^p)^{T_i}|}{\left\| (w_3, V_{w_3}, \Theta_3)^{T_f} - (w_3^p, V_{w_3}^p, \Theta_3^p)^{T_f} \right\|} \\
L_{33} &= \frac{1}{T_f} \sum_{i=1}^N \log_{10} \frac{|(\Theta_3 - \Theta_3^p)^{T_i}|}{\left\| (w_3, V_{w_3}, \Theta_3)^{T_f} - (w_3^p, V_{w_3}^p, \Theta_3^p)^{T_f} \right\|}
\end{aligned} \tag{5.7}$$

To certify the chaos is necessary to apply two criteria respectively the Maximum Lyapunov Exponents Method (MLEM) coupled with the contraction criterion of the sum of all Lyapunov exponents that imposes the next mathematical proposition to be true [G.R.12](pp. 306-307)

$$\exists i \in \{1, 2, 3\}, \max(L_{ij}) > 0, \exists L_{ij} \approx 0, \sum_1^3 L_{ij} < 0, j \in \{1, 2, 3\} \tag{5.8}$$

Figures 5.5 and 5.6 are illustrated the Lyapunov exponents for two values of the damping ratio 0.0016 and 0.011 in the tulip's PPRA, with excitation frequency in the vicinity of 1038.38 Hz. As can be remarked from Figures 5.5 and 5.6 the proposition (5.8) is true only for the damping ratio in the range 0.0016-0.011. Analyzing Figure 5.5 it can be concluded that chaos manifestation is confirmed in the excitation frequency range (950-1150) Hz for the damping ratio of 0.0016, while in Figure 5.6 the chaos manifestation is confirmed in the excitation frequency range (1100-1150) Hz for the damping ratio of 0.011 even if from chaos detection (see Fig. 5.2) it indicates the maximum value of damping ratio 0.0216. Figures 5.7 and 5.8 illustrate the Lyapunov exponents for two values of the damping ratio 0.0016 and 0.0125 in the bowl's PPRA, with excitation frequency in the vicinity of 6306.6 Hz.

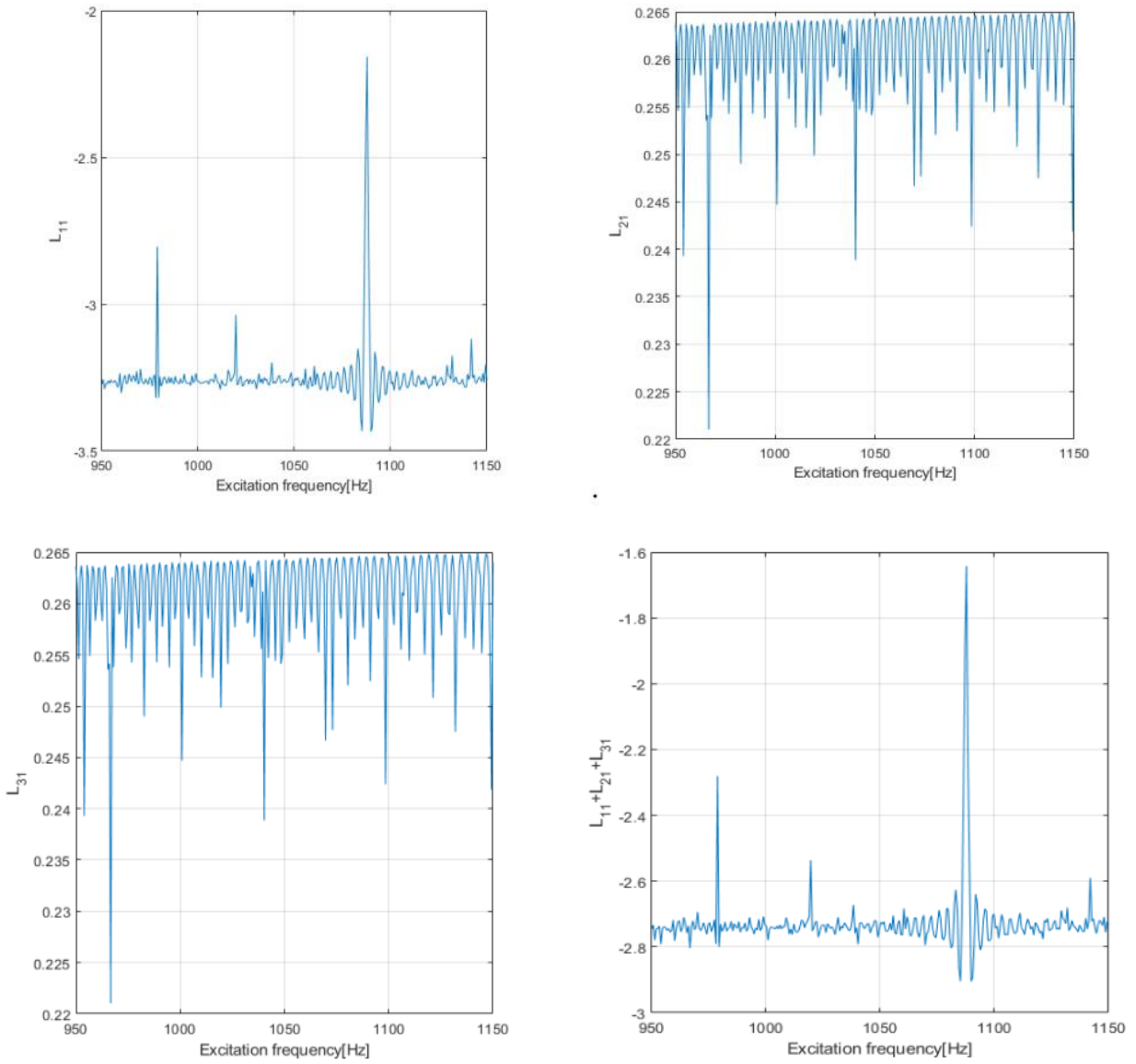


Fig. 5.5 Tulip's Lyapunov exponents of FBV in the PPRA (1038,38 Hz), $\nu_1=519.19\text{Hz}$, $\xi=1.6 \cdot 10^3$ [G.R.30]

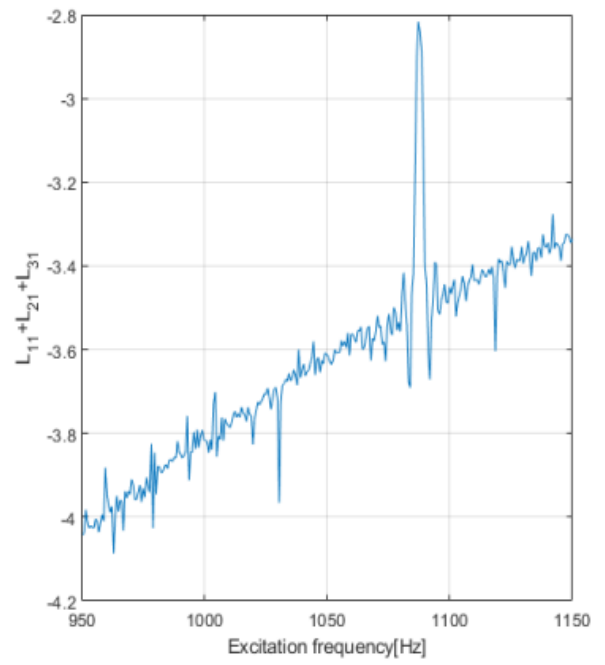
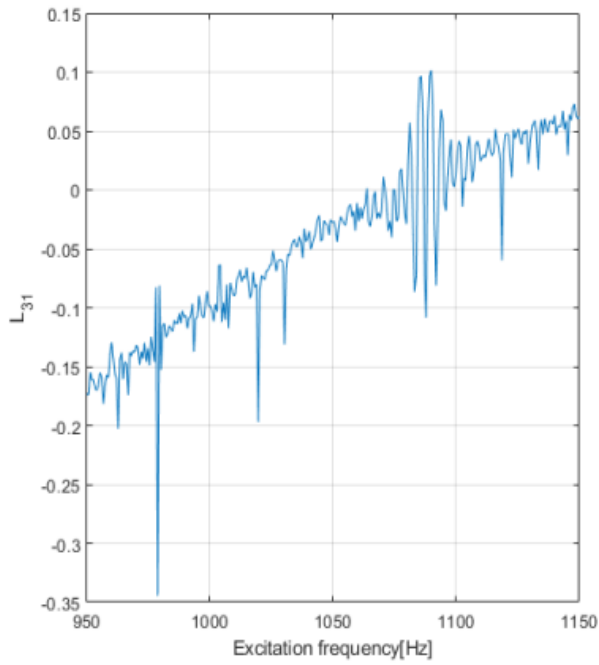
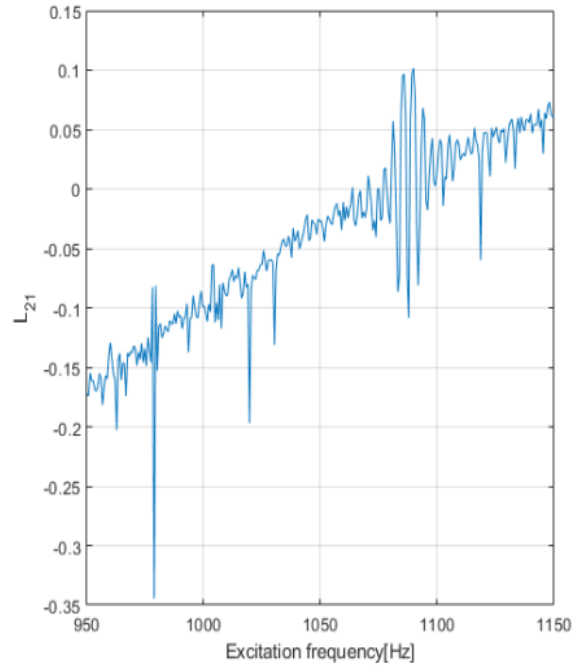
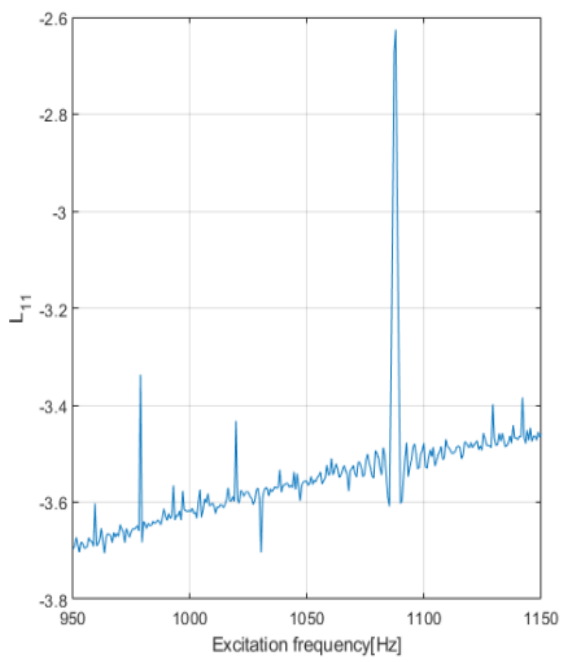


Fig. 5.6 Tulip's Lyapunov exponents of FBV in the PPRA (1038,38 Hz), $v_1=519$ 19Hz , $\xi= 11 \cdot 10^3$ [G.R.30]

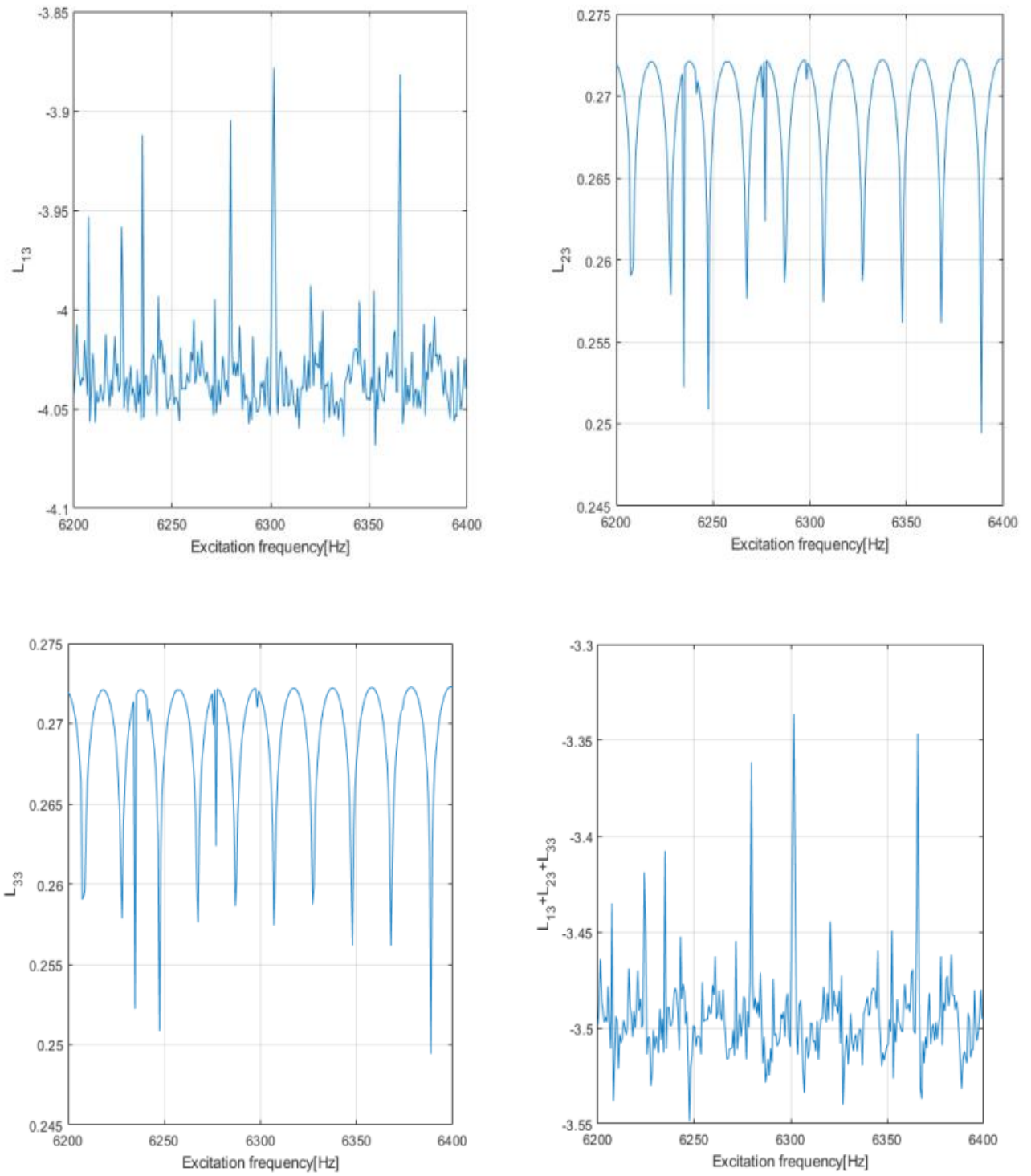


Fig. 5.7 Bowl's Lyapunov exponents of FBV in the PPRA (1038,38 Hz), $v_3=519.19\text{Hz}$, $\xi=1.6 \cdot 10^3$ [G.R.30]

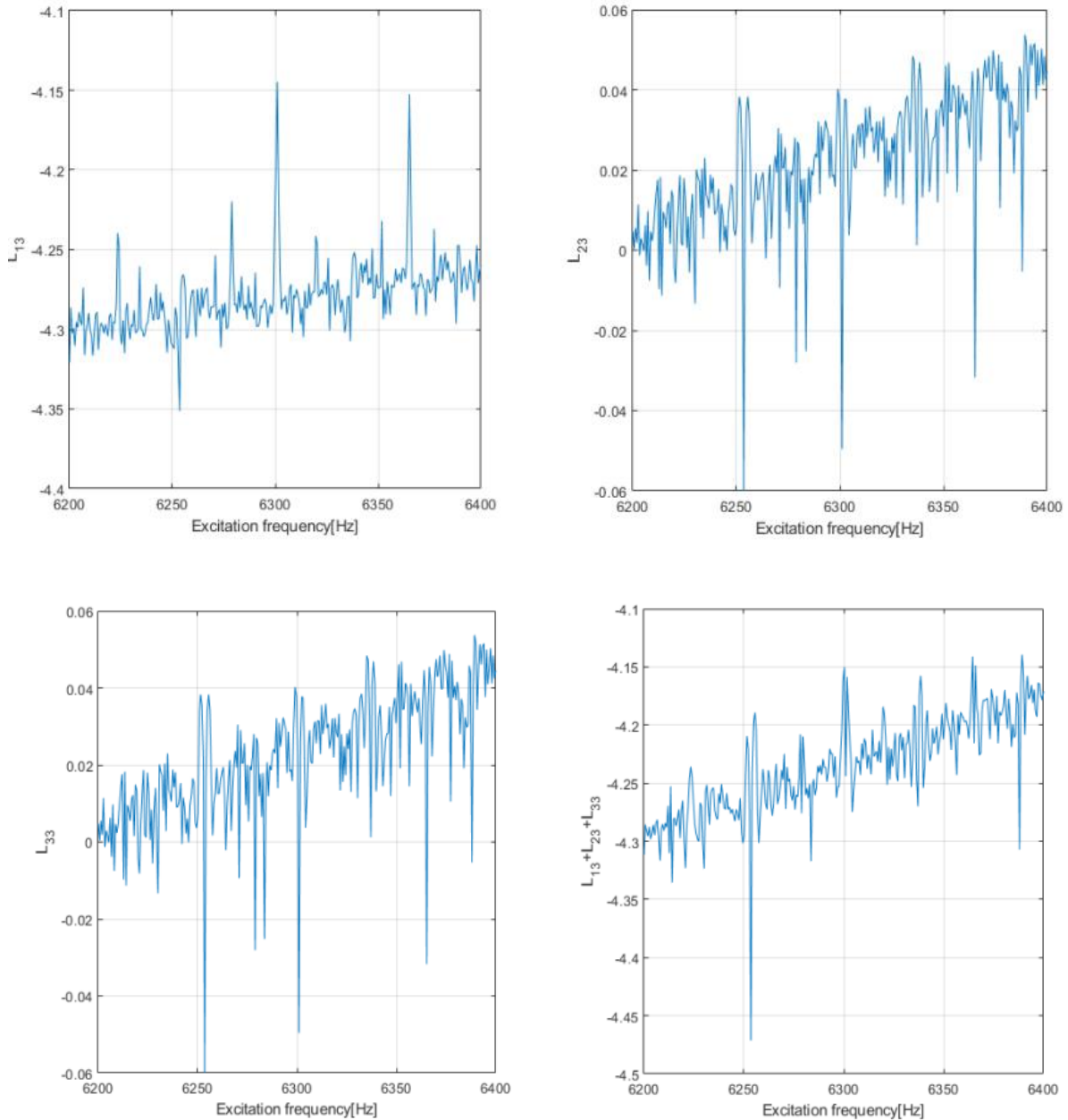


Fig. 5.8 Bowl's Lyapunov exponents of FBV in the PPRA (1038,38 Hz), $v_3=519$ 19Hz , $\xi= 12,5 \cdot 10^{-3}$ [G.R.30]

As can be remarked from Figures 5.7 and 5.8 the proposition (5.8) is true only for the damping ratio in the range of 0.0016-0.0125. Analyzing Figure 5.7 it can be concluded that chaos manifestation is confirmed in the excitation frequency range (6200-6400) Hz for the damping ratio of 0.0016, while in Figure 5.8 the chaos manifestation is confirmed in the excitation frequency ranges (6300-6365) Hz and (6368-6400)Hz for the damping ratio of 0.0125 even if from chaos detection (see Fig. 5.4) it indicates the maximum value of damping ratio 0.0216. Accordingly, to the latest developments in the theory of chaos if two Lyapunov exponents are positive and all the Lyapunov exponents respect the proposition (8) the dynamic system is considered to be a hyperchaotic system [R.C.5.1]. Analyzing Figures 5.5-5.8 it can be concluded that the automotive driveshaft is a hyperchaotic system for a damping ratio in the range of 0.0016-0.011 and excitation

frequency in the range (1100-1150)Hz for the tulip in FBV, while for the bowl in FBV the hyper chaos manifestation is valid for a damping ratio in the range of 0.0016-0.0125 and excitation frequency in the ranges (6300-6365) Hz and (6368-6400)Hz. To reconfirm the chaotic manifestation of tulip's FBV and bowl's FBV in the PPRA it was computed, using in MATLAB software based on systems (5.4) and (5.5), the Poincaré Maps (PM) that represents the intersection of the orbits in the phase portraits with an orthogonal surface at equal periods (N number of points), using the mathematical procedure presented in [G.R.12] (p. 194). If the tulip's FBV or the bowl's FBV are periodic or quasi-periodic the PM represents saddle points or saddle separatrices pictures. For an excitation frequency range in the vicinity of 1038.38 Hz and for a damping ratio $\xi = 1.6 \cdot 10^{-3}$ Figure 5.9 illustrates the Poincaré Map for the tulip's FBV in the PPRA using $N = 100,000$ orthogonal surface sections to the orbits for the phase portraits $(w_1, dw_1 / dt)$.

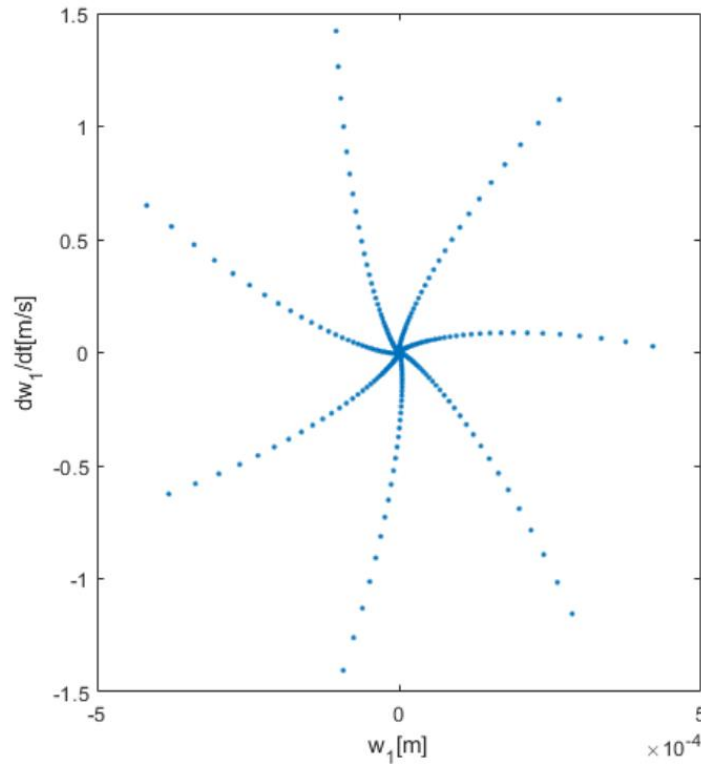


Fig. 5.9 Poincaré Map for the tulip's FBV in the PPRA (1038.38Hz), $N=100,000$ $\xi = 1,6 \cdot 10^{-3}$ [G.R.30]

As can be remarked from Figure 5.9 the picture has the properties of strange attractors respectively auto-similarity and a diffuse structure of points having a different density of pixels per image's unit area. For an excitation frequency range in the vicinity of 6306.6 Hz and for a damping ratio $\xi = 1.6 \cdot 10^{-3}$ Figure 5.10 illustrates the Poincaré Map for the bowl's FBV in the PPRA using $N = 100,000$ orthogonal surface sections to the orbits for the phase portraits $(w_3, dw_3 / dt)$. As can be remarked from Figure 5.10 the picture has the properties of strange attractors respectively auto-similarity and a diffuse structure of points having a different density of pixels per image's unit area.

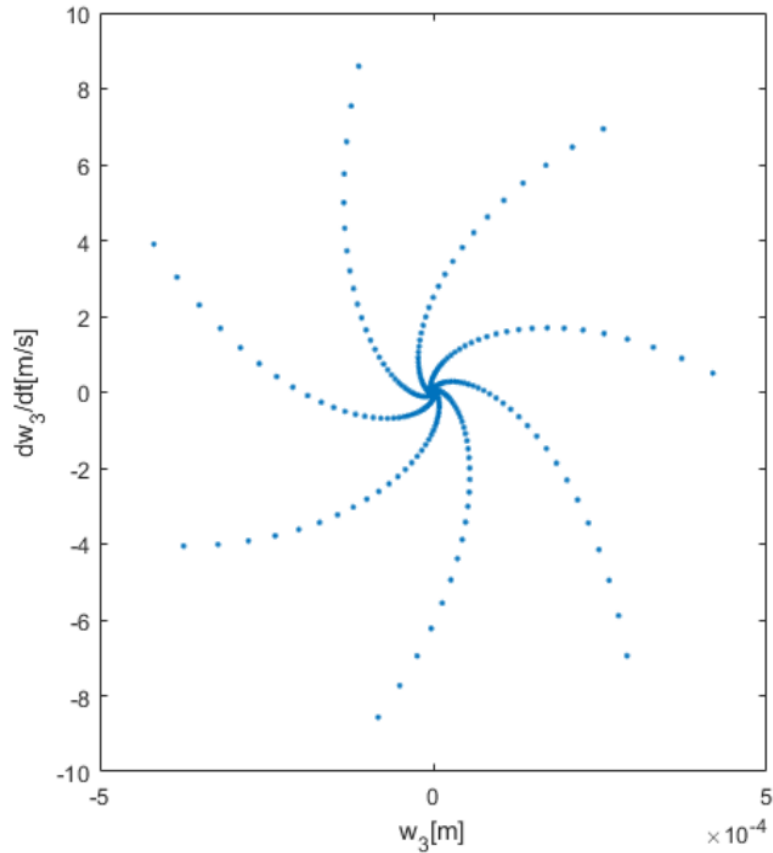


Figura 5.10 Poincaré Map for the bowl's FBV in the PPRA (1038.38Hz), $N=100,000$ $\xi=1,6 \cdot 10^{-3}$ [G.R.30]

The reconfirmation of chaotic manifestation of the tulip's and bowl's FBV through Poincaré Maps respectively the strange attractors. Such dynamic behavior is considered by Steinwede [G.R.14](pp. 88-94) to be the cause of the internal pitting of the bells of the tulip and the bowl as well as the micro-cracks on the tripod axes. Also, Steinwede assimilated the mechanism of the chaotic FBV and chaotic forced torsional vibration of the automotive driveshafts with a similar mechanism for the nonlinear dynamic behavior of the geared systems transmissions, mechanisms already investigated by the first author of the exposed paper in [R.C.5.2]. As can be remarked the increase of the damping ratio has a benefic effect avoiding the chaotic behavior of FBV for the automotive driveshafts but it induces thermal stress.

Finally, the paper highlighted the mechanism of hyperchaotic nonlinear dynamic behavior for the homokinetic transmission [R.C.5.2]. This new method may be used as a powerful tool by the designers of automotive driveshafts as well as the designers of the FBV's dynamic absorbers for the automotive driveshafts [G.R.30, R.C.5.3].

Chapter 6. Final conclusions. Contributions. Future directions of research

6.1 Final conclusions

Finally, it can be concluded that the nonuniformity of geometric and kinematic isometry must be considered for automotive driveshafts. This challenge as well as the harmonic variation of the nonuniformity of geometric and kinematic isometry for the automotive driveshafts induce nonlinear parametric behavior of the homokinetic joints, increasing the stress manifested in this kind of transmission.

The prediction of the automotive driveshaft's geometric and kinematic isometry nonuniformity is a key element in the early stages of the design because it allows the prediction of resonances such as:

- subharmonic resonance,
- super-harmonic resonance,
- principal parametric resonance,
- simultaneous resonance,
- combination resonance,
- internal resonance.

These aspects permit the investigations concerning the stationary and non-stationary stability in all the resonance ranges mentioned previously. These phenomena have a huge importance in the determination of the dynamic behavior of the transmission from the gearbox to the wheel.

The phenomena considered are:

- the nonuniformity of geometric and kinematic isometry of the automotive driveshafts,
- the nonuniformity of axial mass moments of inertia, and axial geometric moments of inertia for tulip, bowl, tripod, inner race,
- rigidity and damping of the joints tulip-tripod and bowl-inner race,
- harmonic excitation due to the internal combustion engine,
- moderate impulsive shocks induced by the road geometry.

The thesis responds to all the goals established in the Paragraph 1.4 in the First Chapter.

6.2 Contributions

The investigations allow the publication of eight research articles: two articles WOS indexed (Q2), one article Scopus indexed and six articles presented at International Conferences.

The original contributions highlighted by this Ph.D. thesis:

- the determination of the nonuniformity of geometric and kinematic isometry of the automotive driveshafts,
- the computation of the nonuniformity of axial mass moments of inertia, and axial geometric moments of inertia for tulip, bowl, tripod, inner race,
- the computation of the rigidity and the damping for the joint's tulip-tripod and bowl-inner race,
- the detection of possible chaotic manifestation for the FTV of the automotive driveshafts in the PPR,
- the investigation of chaotic manifestation for the FBV of the automotive driveshafts in the PPR using MLEM and Poincaré Maps,

- the determination of the stationary instability frontiers for the FBV of the automotive driveshafts in the PPR.
- the determination of the strange attractors for the FBV of the automotive driveshafts in the PPR.

The obtained theoretical data confirmed for the first time the manifestation of hyper chaos for FBV of the automotive driveshafts in a similar manner to the chaotic manifestation of the geared systems transmissions.

The theoretical data agree with the experimental ones obtained by Steinwede [G.R.14] explaining by this behavior the pitting, the micro-cracks inside the tulip and the bowl [G.R.14] (pp. 88–94).

6.3 Future directions of research

The future directions of research are:

1. investigations of the hyperchaotic manifestations of the FTV of the automotive driveshafts;
2. investigations of the nonlinear dynamic behavior of the automotive driveshafts in the regions of specific resonance such as:
 - subharmonic resonance,
 - super-harmonic resonance,
 - principal parametric resonance,
 - simultaneous resonance,
 - combination resonance,
 - internal resonance,
3. the design and development of models for the FTV and FBV of the automotive driveshafts,
4. the investigations of hyperchaotic manifestations of the FTV and the FBV of the automotive driveshafts in the resonance regions mentioned at point 2,
5. the design and development of software to predict the dynamic behavior of homokinetic transmissions.

References

General References

1. Duditzka, F. D. (1975). Zur Kinematik und Dynamik von Tripode-Gelenkgetrieben (The kinematics and dynamics of tripod jointed drivelines) *Konstruktion* 27 p. 335–341.
https://www.academia.edu/22098406/Kinematic_and_dynamic_analyses_of_the_tripode_joint
2. Rao, S.S. (2007), *Vibration of Continuous Systems*, John Wiley & Sons, Hoboken, New Jersey, USA, ISBN: 978-0-471-77171-5. <https://wp.kntu.ac.ir/hrahmani/Adv-Vibrations-Books/Continuous-Vibrations-Rao.pdf>
3. Schmelz, F.: Count Seherr-Thoß, H. Ch.: Die Entwicklung der Gleichlaufgelenke für den Frontantrieb (Development of constant velocity joints for front wheel drive). VDI-Report 418 (1981) 197–207 https://link.springer.com/chapter/10.1007/978-3-662-02746-2_2
4. Orain, M.: Die Gleichlaufgelenke, allgemeine Theorie und experimenteller Forschung (Constant velocity joints, general theory and experimental research). German translation by H. W. Günther. Paris: Glaenzer-Spicer 1976
https://link.springer.com/chapter/10.1007/3-540-30170-4_2
5. Seherr-Thoss, H.C.; Schmelz, F.; Aucktor, E. Theory of Constant Velocity Joints (CVJ). In *Universal Joints and Driveshafts*, 2nd ed.; Springer: Berlin, Germany, 2006; pp. 53–80. <https://download.e-bookshelf.de/download/0000/0101/78/L-G-0000010178-0002343465.pdf>
6. Shao, K.; Zheng, J.; Huang, K.; Qiu, M.; Sun, Z. Robust model referenced control for vehicle rollover prevention with time-varying speed. *Int. J. Veh. Des.* 2021, 85, 48–68. Available online: <https://www.inderscienceonline.com/doi/abs/10.1504/IJVD.2021.117154> (accessed on 7 December 2021).
https://www.researchgate.net/publication/354041363_Robust_model_referenced_control_for_vehicle_rollover_prevention_with_time-varying_speed
7. Deng, B.; Zhao, H.; Shao, K.; Li, W.; Yin, A. Hierarchical Synchronization Control Strategy of Active Rear Axle Independent Steering System. *Appl. Sci.* 2020, 10, 3537. https://www.researchgate.net/publication/341518394_Hierarchical_Synchronization_Control_Strategy_of_Active_Rear_Axle_Independent_Steering_System
8. Tiberiu-Petrescu, F.I.T.; Petrescu, R.V.V. The structure, geometry, and kinematics of a universal joint. *Indep. J. Man ana Prod.* 2019, 10, 1713–1724.
https://www.researchgate.net/publication/336966355_The_structure_geometry_and_kinematics_of_a_universal_joint
9. Ertürka, A.T.; Karabayb, S.; Baynalç, K.; Korkutd, T. Vibration Noise Harshness of a Light Truck Driveshaft, Analysis and Improvement with Six Sigma Approach. *ACTA Phys. Pol. A* 2017, 131, 477–480.
https://www.researchgate.net/publication/316437150_Vibration_Noise_Harshness_of_a_Light_Truck_Driveshaft_Analysis_and_Improvement_with_Six_Sigma_Approach

10. Kamalakkannan, B. Modelling and Simulation of Vehicle Kinematics and Dynamics. Master's Thesis, Halmstad University, Halmstad, Sweden, 13 January 2017
<https://hh.diva-portal.org/smash/get/diva2:1115795/FULLTEXT02.pdf>
11. Kishore, M.; Keerthi, J.; Kumar, V. Design and Analysis of Drive Shaft of an Automobile. *Int. J. Eng. Trends Technol.* 2016, 38, 291–296.
https://www.researchgate.net/publication/309329869_Design_and_Analysis_of_Drive_Shaft_of_an_Automobile
12. Mazzei, A.J.; Scott, R.A. Principal Parametric Resonance Zones of a Rotating Rigid Shaft Driven through a Universal Joint. *J. Sound Vib.* 2001, 244, 555–562.
https://www.researchgate.net/publication/243365524_Principal_parametric_resonance_zones_of_a_rotating_rigid_shaft_driven_through_a_universal_joint
13. Browne, M.; Palazzolo, A. Super harmonic nonlinear lateral vibrations of a segmented driveline incorporating a tuned damper excited by a non-constant velocity joints. *J. Sound Vib.* 2008, 323, 334–351.
<https://vcel.tamu.edu/Other%20Contents/Publications/Super%20harmonic%20nonlinear%20lateral%20vibrations%20of%20a%20segmented%20driveline%20incorporating%20a%20tuned%20damper%20excited%20by%20non-constant%20velocity%20joints.pdf>
14. Steinwede, J. Design of a Homokinetic Joint for Use in Bent Axis Axial Piston Motors. Ph.D. Thesis, Aachen University, Aachen, Germany, 25 November 2020. Available online: <https://www.google.com/search?client=firefox-b-d&q=%E2%80%9DDESIGN+OF+A+HOMOKINETIC+JOINT+FOR+USE+IN+BENT+AXIS+AXIAL+PISTON+MOTORS%E2%80%9D+J.+Steinwede+>
15. Feng, H.; Rakheja, S.; Shanguan, W.B. Analysis and optimization for generated axial force of a driveshaft system with interval of uncertainty. *Struct. Multidiscip. Optim.* 2021, 63, 197–210. <https://dl.acm.org/doi/abs/10.1007/s00158-020-02679-0>
16. Nayfeh, A.H.; Mook, D.T. *Nonlinear Oscillations*; John Wiley & Sons: New York, NY, USA, 1979 <https://www.wiley.com/en-gb/Nonlinear+Oscillations-p-9780471121428>
17. Sireteanu, T.; Gündisch, O.; Paraian, S. *Random Vibrations of Automotive*; Technical Publishing House: Bucharest, Romania, 1981.
https://www.researchgate.net/publication/226119372_Simulation_Results_Using_Shock_Absorbers_with_Primary_Intelligence-VZN
18. Bugaru, M., **Vasile, A.**, Nonuniformity of Isometric Properties of Automotive Driveshafts, *MDPI-Computation*, e-ISSN 2079-3197, **2021**, Vol 9, 9(12)-145, **WOS: 000735922400001**, DOI: 10.3390/computation9120145, **FI=2.2,Q2(indexat WOS 2022)**
<https://doi.org/10.3390/computation9120145>,
<https://www.webofscience.com/wos/woscc/fullrecord/WOS:000735922400001?SID=EUW1ED0BAEcWoqNMuNgqJY88vtNwz>
19. Farshidianfar, A., Ebrahimi, M., Rahnejat, H., Menday, M.T., Moavenian, M.(2002), “Optimization of the high-frequency torsional vibration of vehicle driveline systems using genetic algorithms.”, *Proc. Inst. Mech. Eng. Part K J. Multi-Body Dyn.*, Vol. 216, pp. 249–262. <https://doi.org/10.1177/146441930221600305>.
20. Komorska, I., Puchalski, A.(2013), “On-board diagnostics of mechanical defects of the vehicle drive system based on the vibration signal reference model.”, *J. Vibroeng.*, Vol.

15, pp. 450–458, ISSN 1392-8716.

https://www.academia.edu/95840440/On_board_diagnostics_of_mechanical_defects_of_the_vehicle_drive_system_based_on_the_vibration_signal_reference_model

21. Alugongo, A.A. Parametric Vibration of a Cardan Shaft and Sensitivity Analysis. In Proceedings of the World Congress on Engineering and Computer Science 2018 Vol II WCECS, San Francisco, CA, USA, 23–25 October 2018. Available online: <https://www.google.com/search?client=firefox-b-d&q=Parametric+Vibration+of+a+Cardan+Shaft+and+Sensitivity+Analysis+Alfayo+A.+Alugong>
22. Xu, J., Zhu, J., Xia, F.(2020), “Modeling and Analysis of Amplitude-Frequency Characteristics of Torsional Vibration for Automotive Powertrain. Hindawi Shock Vib. 2020, 2020. <https://www.hindawi.com/journals/sv/2020/6403413/>
23. Idehara, S.J.; Flach, F.L.; Lemes, D. Modeling of nonlinear torsional vibration of automotive powertrain. J. Vib. Control. 2018, 24, 1774–1786. https://www.researchgate.net/publication/308132759_Modeling_of_nonlinear_torsional_vibration_of_the_automotive_powertrain
24. Bugaru, M.; Chereches, T.; Trana, E.; Gheorghian, S.; Homotescu, T.N. Theoretical model of the dynamic interaction between wagon train and continuous rail. WSEAS Trans. Math. 2006, 5, 374–378. Available online: https://scholar.google.com/citations?view_op=view_citation&hl=en&user=tYI6MzwAAAAJ&citation_for_view=tYI6MzwAAAAJ:FxGoFyzp5QC
25. Rao, S.S. Mechanical Vibrations, 5th ed.; Prentice Hall: Upper Saddle River, NJ, USA, 2011; ISBN 978-0-13-212819-3. https://www.researchgate.net/profile/V-T-T-Nguyen/publication/273330566_Basic_Mechanical_Vibrations/links/54fecf170cf2741b69f164f2/Basic-Mechanical-Vibrations.pdf
26. Bugaru, M., Vasile, A., A Physically Consistent Model for Forced Torsional Vibrations of Automotive Driveshafts, MDPI-Computation, e-ISSN 2079-3197, **2022**, Vol 10, 10(1), **WOS: 000747629800001**, DOI: 10.3390/computation10010010, **FI=2.2,Q2(indexat WOS 2022)** <https://doi.org/10.3390/computation10010010>, <https://www.webofscience.com/wos/woscc/fullrecord/WOS:000747629800001?SID=EUW1ED0BAEcWoqNMuNgqJY88v>
27. Bugaru, M., Vasile, O., Vasile, A., Investigation of Nonlinear Dynamic Parametric Stability for Forced Bending Vibration of an Automotive Driveshaft Using Asymptotic Method, *Proceedings of the 10th IC-SCCE, 10th International Conference from Scientific Computing to Computational Engineering*, 6-9 July **2022**, Athens, Greece, ISSN 2241-8865, ISBN 978-618-84028-4-3, pp. 104-117 <https://www.mdpi.com/2079-3197/9/12/145>
28. Bugaru, M., Vasile, O., Modeling and Analysis of FBV Movements for Automotive Driveshafts in the PPR Region, *MDPI-Applied Sciences*, e-ISSN 2076-3417, **2022**, Vol. 12(7), 3237, **WOS: 000781051300001**, DOI: 10.3390/app12073237, **IF=2,838 (2021)--Q2**, <https://www.webofscience.com/wos/woscc/full-record/WOS:000781051300001?SID=EUW1ED0EABncEBOWBgpRp8kZOQOcJ>

29. Deciu, E.; Bugaru, M.; Dragomirescu, C. Nonlinear Vibrations with Applications in Mechanical Engineering; Romanian Academy Publishing House: Bucharest, Romania, 2002; ISBN 973-27-0911-1. [file:///C:/Users/py12774/Downloads/applsci-12-03237-v3%20\(2\).pdf](file:///C:/Users/py12774/Downloads/applsci-12-03237-v3%20(2).pdf)
30. M. Bugaru, **A. Vasile**, Investigation of chaotic forced bending vibrations of the automotive driveshaft, U.P.B. Sci. Bull., Series D, Vol. 85, Issue 3, pp. 93-110, Indexat Scopus 30/08/2023 2023 ISSN 1454-2358 <https://0d10e8nla-y-https-www-scopus-com.z-e-nformation.ro/record/display.uri?eid=2-s2.0-85168542524&origin=resultslist&sort=plf-f>

References Chapter 1

1. Glaenger Spicer, Specialiste mondial de la transmission, 1988. <https://docplayer.fr/66116946-Joints-homocinetiques.html>
2. Reuleaux, F.: Theoretische Kinematik (Theoretical Kinematics). Vol. I, Brunswick: Vieweg 1875, p. 179 onwards <https://www.qbbooks.com/pages/books/71547/f-reuleaux-franz-reuleaux/lehrbuch-der-kinematik-textbook-of-kinematics-volumes-i-and-ii-2-volume-set-all-published>
3. Reuleaux, F.: Der Konstrukteur (The Designer). 3rd edition Brunswick: Vieweg 1869, p. 260–267 <https://epdf.tips/universal-joints-and-driveshafts-analysis-design-applications.html>
4. Gruebler, M. F.: Getriebelehre (Theory of Kinematics). Berlin: Springer 1917, p. 6–39 2.4 <https://link.springer.com/book/10.1007/978-3-662-02746-2>
5. Steeds, W.: Universal Joints. Automob. Eng. 27 (1937) No. 354, p. 10–12 [https://books.google.ro/books?id=feckBgAAQBAJ&pg=PA77&lpg=PA77&dq=Steeds,+W.:+Universal+Joints.+Automob.+Eng.+27+\(1937\)+No.+354,+p.+10%E2%80%9312&source=bl&ots=7OocrDby_w&sig=ACfU3U2ap6uupTiNMum3slOhe0p_QfhBsQ&hl=fr&sa=X&ved=2ahUKEwiRxJmTv9qAAxUg1AIHHVJEClwQ6AF6BAgiEAM#v=onepage&q=Steeds%2C%20W.%3A%20Universal%20Joints.%20Automob.%20Eng.%2027%20\(1937\)%20No.%20354%2C%20p.%2010%E2%80%9312&f=false](https://books.google.ro/books?id=feckBgAAQBAJ&pg=PA77&lpg=PA77&dq=Steeds,+W.:+Universal+Joints.+Automob.+Eng.+27+(1937)+No.+354,+p.+10%E2%80%9312&source=bl&ots=7OocrDby_w&sig=ACfU3U2ap6uupTiNMum3slOhe0p_QfhBsQ&hl=fr&sa=X&ved=2ahUKEwiRxJmTv9qAAxUg1AIHHVJEClwQ6AF6BAgiEAM#v=onepage&q=Steeds%2C%20W.%3A%20Universal%20Joints.%20Automob.%20Eng.%2027%20(1937)%20No.%20354%2C%20p.%2010%E2%80%9312&f=false)
6. Balken, J.: Systematische Entwicklung von Gleichlaufgelenken (Systematic development of constant velocity joints). Diss. TU Munich 1981 [https://books.google.ro/books?id=GPdmft_cpKQC&pg=PA78&lpg=PA78&dq=6.%09Balken,+J.:+Systematische+Entwicklung+von+Gleichlaufgelenken+\(Systematic+development+of+constant+velocity+joints\).+Diss.+TU+Munich+1981&source=bl&ots=zsVpWS5BIO&sig=ACfU3U2FHQUzDPOvxyBRPchmYwgNmsvpeg&hl=fr&sa=X&ved=2ahUKEwjhu_Sgv9qAAxV70gIHHVvyqAiYQ6AF6BAgiEAM#v=onepage&q=6.%09Balken%2C%20J.%3A%20Systematische%20Entwicklung%20von%20Gleichlaufgelenken%20\(Sytematic%20development%20of%20constant%20velocity%20joints\).%20Diss.%20TU%20Munich%201981&f=false](https://books.google.ro/books?id=GPdmft_cpKQC&pg=PA78&lpg=PA78&dq=6.%09Balken,+J.:+Systematische+Entwicklung+von+Gleichlaufgelenken+(Systematic+development+of+constant+velocity+joints).+Diss.+TU+Munich+1981&source=bl&ots=zsVpWS5BIO&sig=ACfU3U2FHQUzDPOvxyBRPchmYwgNmsvpeg&hl=fr&sa=X&ved=2ahUKEwjhu_Sgv9qAAxV70gIHHVvyqAiYQ6AF6BAgiEAM#v=onepage&q=6.%09Balken%2C%20J.%3A%20Systematische%20Entwicklung%20von%20Gleichlaufgelenken%20(Sytematic%20development%20of%20constant%20velocity%20joints).%20Diss.%20TU%20Munich%201981&f=false)

7. Grashof, F.: Theoretische Maschinenlehre (Theoretical Engineering). Vol. 2: Theorie der Getriebe etc. (Theory of power transmission etc.) Leipzig: Voss 1883
[https://books.google.ro/books?id=iLyCAAQAQBAJ&pg=PA56&lpg=PA56&dq=Grashof,+F.:+Theoretische+Maschinenlehre+\(Theoretical+Engineering\).+Vol.+2:+Theorie+der+Getriebe+etc.+\(Theory+of+power+transmission+etc.\)+Leipzig:+Voss+1883&source=bl&ots=qVfguNvh0i&sig=ACfU3U2bNocOWAqbjixJk9cKP8FIjXuI9Q&hl=fr&sa=X&ved=2ahUKEwi_0ZHQv9qAAxWUHP0HHR8YD8AQ6AF6BAgIEAM#v=onepage&q=Grashof%2C%20F.%3A%20Theoretische%20Maschinenlehre%20\(Theoretical%20Engineering\).%20Vol.%202%3A%20Theorie%20der%20Getriebe%20etc.%20\(Theory%20of%20power%20transmission%20etc.\)%20Leipzig%3A%20Voss%201883&f=false](https://books.google.ro/books?id=iLyCAAQAQBAJ&pg=PA56&lpg=PA56&dq=Grashof,+F.:+Theoretische+Maschinenlehre+(Theoretical+Engineering).+Vol.+2:+Theorie+der+Getriebe+etc.+(Theory+of+power+transmission+etc.)+Leipzig:+Voss+1883&source=bl&ots=qVfguNvh0i&sig=ACfU3U2bNocOWAqbjixJk9cKP8FIjXuI9Q&hl=fr&sa=X&ved=2ahUKEwi_0ZHQv9qAAxWUHP0HHR8YD8AQ6AF6BAgIEAM#v=onepage&q=Grashof%2C%20F.%3A%20Theoretische%20Maschinenlehre%20(Theoretical%20Engineering).%20Vol.%202%3A%20Theorie%20der%20Getriebe%20etc.%20(Theory%20of%20power%20transmission%20etc.)%20Leipzig%3A%20Voss%201883&f=false)
8. Molly, H.: Bengisu, O.O Das Gleichgang-Gelenk im Symmetriespiegel (The constant velocity joint in the mirror of symmetry). Automob. Ind. 14 (1969) No. 2, p. 45–54
https://link.springer.com/chapter/10.1007/978-3-662-02746-2_2
9. Beyer, R.: Technische Kinematik (Engineering Kinematics). Leipzig: Barth 1931, p. 88, Fig. 176 [https://books.google.ro/books?id=iLyCAAQAQBAJ&pg=PA56&lpg=PA56&dq=Beyer,+R.:+Technische+Kinematik+\(Engineering+Kinematics\).+Leipzig:+Barth+1931,+p.+88,+Fig.+176&source=bl&ots=qVfguNvh7i&sig=ACfU3U01lgujj5L4CK11KbaDytlC86E1pg&hl=fr&sa=X&ved=2ahUKEwj5m9Hxv9qAAxWD_7sIHQsWCUUQ6AF6BAgeEAM#v=onepage&q=Beyer%2C%20R.%3A%20Technische%20Kinematik%20\(Engineering%20Kinematics\).%20Leipzig%3A%20Barth%201931%2C%20p.%2088%2C%20Fig.%20176&f=false](https://books.google.ro/books?id=iLyCAAQAQBAJ&pg=PA56&lpg=PA56&dq=Beyer,+R.:+Technische+Kinematik+(Engineering+Kinematics).+Leipzig:+Barth+1931,+p.+88,+Fig.+176&source=bl&ots=qVfguNvh7i&sig=ACfU3U01lgujj5L4CK11KbaDytlC86E1pg&hl=fr&sa=X&ved=2ahUKEwj5m9Hxv9qAAxWD_7sIHQsWCUUQ6AF6BAgeEAM#v=onepage&q=Beyer%2C%20R.%3A%20Technische%20Kinematik%20(Engineering%20Kinematics).%20Leipzig%3A%20Barth%201931%2C%20p.%2088%2C%20Fig.%20176&f=false)
10. Richtlinien VDI 2722 (VDI Directives): Homokinetische Kreuzgelenk-Getriebe einschließlich Gelenkwellen (Homokinetic universal jointed transmissions including driveshafts). Düsseldorf: VDI-Verlag 1978
<https://www.yumpu.com/en/document/view/7180412/universal-joints-and-driveshafts-hchrseherr-thoss-f-index-of>
11. d’Ocagne, M.: Cours de géométrie pure et appliquée de l’Ecole Polytechnique (Course of pure and applied geometry of the Ecole Polytechnique), vol. 2, Ch. VI Cinématique Appliquée (Applied Kinematics), No. 170–172 Joint universel de Cardan (Universal Cardan Joint), p. 52–57. Paris: Gauthier-Villars 1918
https://link.springer.com/chapter/10.1007/3-540-30170-4_1
12. Pahl, G., & Kuettner, K. H. (1990). Fundamentals (of design), in: Dubbel, Handbook of Mechanical Engineering, vol. 1. Berlin: Springer.
https://link.springer.com/chapter/10.1007/978-3-662-02746-2_5
13. F.Smeltz. (2006). Universal Joints and Driveshafts. Berlin: Springer,. <https://download.e-bookshelf.de/download/0000/0101/78/L-G-0000010178-0002343465.pdf>
14. A. Jante, Kraftfahrt-Mechanik, 3 Der Kraftschluß m. d. Fahrbahn (Motor vehicle mechanics, 3. Friction at the road surface). In: Bussien, R. (Publisher): Automobiltechnisches, 14, 1941.
https://books.google.ro/books?id=GPdmft_cpKQC&pg=PA246&lpg=PA246&dq=14.%0

[9A.+Jante,+Kraftfahrt-Mechanik,+3+Der+Kraftschlu%C3%9F+m.+d.+Fahrbahn+\(Motor+vehicle+mechanics,+3.+Friction+at+the+road+surface\).+In:+Bussien,+R.+\(Publisher\):+Automobiltechnisches,+14,+1941.&source=bl&ots=zsVpWS5FmJ&sig=ACfU3U0CSnxZx6VS0nM28PhYc_pENIBBxg&hl=fr&sa=X&ved=2ahUKewjiwJniwNqAAxVu1wIHHdIDCusQ6AF6BAgIEAM#v=onepage&q=14.%09A.%20Jante%2C%20Kraftfahrt-Mechanik%2C%203%20Der%20Kraftschlu%C3%9F%20m.%20d.%20Fahrbahn%20\(Motor%20vehicle%20mechanics%2C%203.%20Friction%20at%20the%20road%20surface\).%20In%203A%20Bussien%2C%20R.%20\(Publisher\)%203A%20Automobiltechnisches%2C%2014%2C%201941.&f=false](https://www.mdpi.com/2079-3197/9/12/145)

References Chapter 2

1. **Vasile, A.**, Bugaru, M., Nonuniformity of isometric properties of automotive driveshafts, *9 th International Conference on “Experiments/Process/System Modeling/Simulation/Optimization”*, **9 th IC-EpsMso**, Athens, Greece, 7-10 July **2021**, pp. 247-255, ISSN: 2241-9209, ISBN: 978-618-84028-2-9 <https://www.mdpi.com/2079-3197/9/12/145>
2. Patent Rzeppa. Available online: <https://worldwide.espacenet.com/patent/search/family/008989560/publication/FR628309A?q=pn%3DFR628309A>
3. Glaenzer-Spicer. Tripod Joint GI. European Patent No. 1.272.530, 4 July 1960.
4. Patent. Drive Shaft Tube and End Fitting Assembly and Method of Manufacturing Same. EP0685659A1, 1995. Available online: <https://patents.google.com/patent/EP0685659A1>
5. Patent. Vehicle Driveshaft. U.S. Patent 006279221 B1, 2001. Available online: https://www.google.com/search?q=USOO6279221B1&client=firefox-b-d&sxsrf=AoAemvJib3LZ507AICWIPBANx4VUsa9-Iw%3A1639040235249&ei=68SxYZH-De-C9u8Pq5mA4&ved=0ahUKewjRn_nXrNb0AhVvgf0HHauPCe8Q4dUDCA0&uact=5&oq=USOO6279221B1&gs_lcp=Cgnd3Mtd2l6EAM6BwgAEEcQsANKBAhBGABKB AhGGABQ5wlY5wlgRhdoAXACeACAAXaIAXaSAQMwLjGYAQCgAQKgAQHIAQjAAQE&scient=gws-wiz
6. Patent. Hybrid Driveshaft Based on Unidirectional and Fabric Composite Materials. U.S. Patent 20080045348 A1, 2008. Available online: <https://patents.google.com/patent/US20080045348>
7. Patent. Method of Manufacturing an Axially Collapsible Driveshaft Assembly. U.S. Patent 7080437 B2, 2006. Available online: <https://patents.google.com/patent/US7080437>

References Chapter 3

1. Grünwald, B. Theory, Computation and Design of Internal Combustion Engines for Automotive; Didactic & Pedagogical Publishing House: Bucharest, Romania, 1980. <https://www.google.com/search?q=Gr%C3%BCnwald%2C+B.+Theory%2C+Computati>

[on+and+Design+of+Internal+Combustion+Engines+for+Automotive%3B+Didactic+Vs+Pedagogical+Publishing+House%3A+Bucharest%2C+Romania%2C+1980&sca_esv=556587111&rlz=1C1GCEB_enRO1066RO1067&biw=1536&bih=747&ei=FELZZKyyB_aG9u8P_yciA0&ved=0ahUKEwisjJ7EwdqAAxV2g_0HHX8-B9EQ4dUDCA8&uact=5&oq=Gr%C3%BCnwald%2C+B.+Theory%2C+Computation+and+Design+of+Internal+Combustion+Engines+for+Automotive%3B+Didactic+Vs+Pedagogical+Publishing+House%3A+Bucharest%2C+Romania%2C+1980&gs_lp=Egxnd3Mtd2l6LXNlcnAingFHcsO8bndhbGQsIEIuIFRoZW9yeSwgQ29tcHV0YXRpb24gYW5kIERlc2lnbiBvZiBJbnRlcm5hbCBDdb21idXN0aW9uIEVuZ2luZXMgZm9yIEF1dG9tb3RpdmU7IERpZGFjdGljIFZzIFBIZGFnb2dpY2FsIFB1Ymxcpc2hpbmcgSG91c2U6IEJ1Y2hhcmVzdCwgUm9tYW5pYSwgMTk4MEgAUABYAHAAeACQAQCYAQCgAQCqAQC4AQPIAQD4AQHiAwQYACBB&sclient=gws-wiz-serp](https://www.scribd.com/document/235930186/Bolotin-VV-The-Dynamic-Stability-of-Elastic-Systems)

2. Bolotin, V.V. Dynamic Stability of Elastic Systems, 2nd ed.; US Military Report; Aerospace Corporation: El Segundo, CA, USA, 1962.
<https://fr.scribd.com/document/235930186/Bolotin-VV-The-Dynamic-Stability-of-Elastic-Systems>
3. Detroux, T.; Renson, L.; Masset, L.; Kerschen, G. The harmonic balance method for bifurcation analysis of large-scale nonlinear mechanical systems. *Comput. Methods Appl. Mech. Eng.* 2015, 296, 18–38.
<https://www.sciencedirect.com/science/article/abs/pii/S0045782515002297>
4. Bugaru, M. Dynamic Behavior of Geared System Transmission. Ph.D. Thesis, PhD-Granting by Auburn University & University Politehnica of Bucharest (Joint Ph.D. Program Romania-University POLITEHNICA of Bucharest/USA-Auburn University/Germany Technische Universitat Munich Based on Deuche Forschung Gemeinschaft-VDI), Auburn, AL, USA, Bucharest, Romania, 13 October 2004. Available online: <https://crescdi.pub.ro/#/profile/804>
5. Bugaru, M., Vasile, A., Model for torsional forced vibrations of automotive driveshafts, *9 th International Conference on “Experiments/Process/System Modeling/Simulation/Optimization”*, 9 th IC-EPSMSO, Athens, Greece, 7-10 July 2021, pp. 239-246, ISSN: 2241-9209, ISBN: 978-618-84028-2-9
<https://www.proquest.com/openview/2bad7bea3c810ac026b787e400e5c1a5/1.pdf?pq-origsite=gscholar&cbl=2032414>

References Chapter 4

1. Mitropolskii, Y.A. (1964), Problems of the Asymptotic Theory of Nonstationary Vibrations, Izdatel'stvo Nauka, Moscow, Russia. <https://www.abebooks.com/Problems-Asymptotic-Theory-Nonstationary-Vibrations-Mitropolskii/14804754982/bd>
2. Webber, H., Kaczmarczyk, S., Iwankiewicz, R.(2021) “Non-linear Response of Cable-mass-Spring System in High-Rise Buildings under Stochastic Seismic Excitation”, MDPI-Materials, <https://doi.org/10.3390/ma14226858>
3. Chan, K. T., Lai, K. F., Stephen, N. G., Young, K.(2011), “A new method to determine the shear coefficient of Timoshenko beam theory”, *Journal of Sound and Vibration*, Vol.

330, pp. 3488-3497.

<https://www.sciencedirect.com/science/article/abs/pii/S0022460X11001131>

4. Bugaru, M., **Vasile, A.**, Model for bending forced vibrations of automotive driveshafts, *9 TH International Conference on “Experiments/Process/System/Modeling / Simulation/Optimization”*, **9 TH IC-EPSMSO**, Athens, Greece, 7-10 July **2021**, pp. 231-238, ISSN: 2241-9209, ISBN: 978-618-84028-2-9 https://docs.upb.ro/wp-content/uploads/2022/10/Rezumat-Teza-Abilitare_Mihai_BUGARU.pdf

References Chapter 5

1. S. Li, Y. Wu, X. Zhang, “Analysis and Synchronization of a New Hyperchaotic System with Exponential Term”, in *Mathematics-MDPI*, vol. 9, no. 3281, Dec. 2021, pp. 1-16 <https://www.mdpi.com/2227-7390/9/24/3281>
2. M. Bugaru, “Chaotic Behavior of Helical Gear-Pair Systems Non-linear Parametrically Excited”, in *Romanian Journal of Acoustics and Vibration*, vol. 1, no.1, Dec. 2004, pp. 7–13. https://www.researchgate.net/publication/359985306_CHAOTIC_BEHAVIOR_OF_HELICAL_GEAR-PAIR_SYSTEMS_NON-LINEAR_PARAMETRICALLY_EXCITED
3. M. Bugaru, **A. Vasile**, Investigation of automotive driveshaft chaotic FBV 10th International Conference on “Experiments/Process/System Modeling/Simulation/Optimization” 10th IC-EPSMSO Loutraki, 5-8 July, 2023 ©LFME <https://10times.com/e15r-kgz5-ph35>